MODELS FOR BUS QUEUEING AT BUSY STOPS AND CORRIDORS, AND CONGESTION MITIGATION STRATEGIES

MINYU SHEN

PhD

The Hong Kong Polytechnic University

2020

The Hong Kong Polytechnic University

Department of Electrical Engineering

MODELS FOR BUS QUEUEING AT BUSY STOPS AND CORRIDORS, AND CONGESTION MITIGATION STRATEGIES

MINYU SHEN

A thesis
submitted in partial fulfilment of the requirements
for the degree of

Doctor of Philosophy

February 2020

CERTIFICATE OF ORIGINALITY

I hereby declare that this thesis is my own work and that, to the best of my knowledge and belief, it reproduces no material previously published or written, nor material that has been accepted for the award of any other degree or diploma, except where due acknowledgement has been made in the text.

_____ (Signed)

Minyu Shen (Name of student)

Abstract

Bus agencies often operate bus lines with high frequency to meet the ever-increasing demand. Problems that come along with high bus flow and patron demand include long bus queues and poor service reliability. This thesis develops analytical and simulation models for estimating capacities and key performance metrics (i.e., bus delays and headway variations) for congested bus stops and corridors.

At the stop level, built upon the previous analytical models for estimating isolated stops' bus-carrying capacities, this thesis develops analytical approximations to estimate the bus-carrying capacities at near- and far-side stops with one or multiple curbside berths. The approximations are derived using time-space diagrams of bus trajectories and probabilistic methods. They correctly account for the effects of key operating factors that were ignored or incorrectly addressed by previous methods. These factors include the signal timing and the distance between stop and signal. Comparison against computer simulation shows that our models furnish much more accurate estimates for near- and far-side stop capacities than previous methods in the literature. Numerical case studies are performed to examine how the stop capacity is affected by various operating factors. New findings and their practical implications are discussed.

Looking at the corridor level, buses form queues at stops along corridors when the number of berths in each stop is insufficient to serve its bus flows. Buses might discharge from these queued stops at headways that are smaller than scheduled. This tends to induce longer queues at downstream stops and higher variations in the bus headways entering them. A vicious cycle of growing bus delay thus propagates along the corridor. Patrons suffer as a result.

A simulation model is therefore developed in-house to jointly examine bus queueing dynamics and headway variability propagations in busy bus corridors shared by multiple bus lines. The model is used to examine two control strategies aimed at alleviating the vicious cycle in busy corridors. Both strategies hold buses at a corridor's upstream end. The first strategy does so to form bus convoys that are then released to traverse the corridor in unison. Though previously reported to be beneficial, present findings indicate that convoying generates greater headway variations and longer bus queues at stops than what occur under a do-nothing alternative. The second holding strategy releases buses into a corridor at fixed headways. This strategy performed surprisingly well, not only in regularizing headways, but

in reducing bus delays. The strategy was found to be especially beneficial for long corridors with many queued stops and high patron demands for travel. Practical implications of the findings are discussed. Discussion includes means of harnessing emerging technologies to enhance the headway-regularization strategy.

Acknowledgements

First, I would like to express my heart-felt gratitude to my supervisor, Dr. Weihua Gu, for his continuous guidance of my study and research. I have benefited enormously from his brilliant mind, rigorous attitude, and superior writing skill. Throughout my PhD life, he has done everything he could to help me develop research topics, make good judgement of research contribution, and improve my writing and presentation. More than that, he has also indulged my pursuit of interesting research topics, despite the few results obtained to date. He is and will always be my best role model as a researcher and mentor.

I would like to extend my sincere thanks to other PolyU faculty members: my co-supervisor Prof. Weinong Fu, Prof. Edward Chung, and Dr. Jinwoo Lee, for their warm encouragement and insightful discussions.

Acknowledgements must go to my good friends and office mates in transportation group of EE department, for the days and nights we were working together, and for all the fun we have had in HongKong. Among them, I would first like to express my thanks and respects to the faculty members from Mainland: Dr. Sangen Hu, Dr. Qiang Zeng, Dr. Wenbo Fan, Dr. Xin Li, and Dr. Yiming Bie. I am also indebted to Larry, Joy, Xiao Yang, Qiaolin Hu, Fangyi Yang, Fuliang Li, and all the other colleagues and friends who once worked in the group. Spontaneous and wide-ranging conversations with them are enjoyable and valuable. In particular, I want to thank Christine, for her continuous support and encouragement when I felt life sucks.

Thanks must also go to my best friends in dormitory 95018: Cheng Chen, Lingyu Ji, and Yuezhong Wu. They are my source of happiness every day and walk me through the dark side of the morning. I shall deliver the same thanks to Ruijie Li, Qihao Jia, Kun Liao and Dapeng Zhang, who make my life colorful.

Finally, I would like to thank my parents for their endless love and unconditional support. Words are inadequate to express how important they are for me.

Table of Contents

List of Figures

1 Introduction

Section 1.1 introduces the motivation for this thesis. Section 1.2 reviews the relevant studies. Section 1.3 summarizes the contributions of this thesis. The outline of this thesis is furnished in Section 1.4.

1.1 Motivation

Public transport is a promising means of mitigating growing traffic congestion in densely-populated cities, because the same amount of travel demand can be satisfied by using fewer vehicles that occupy less road space. Among all transit modes, the fixed-route bus system has been widely used due to its cost efficiency, flexibility, and short construction period. To meet the growing patron demand, transit agency often operates bus lines with high frequency. Real-world examples include: the BRS Presidente Vargas Corridor in Rio de Janeiro, Brazil, where peak-hour bus flow is 600 buses per hour (i.e., one bus per 6 seconds) in each direction; and the bus rapid transit corridor in Guangzhou, China, which serves 31 bus lines with a peak-hour demand of 27,000 patrons/h/direction (Global BRT Data, 2019). Problems that come along with high bus flow and patron demand include long bus queues and poor service reliability.

At a single stop, bus queues are often formed at the entry of busy stops due to the limited number of berths and the mutual blockages between buses serving there (Fang et al., 2012). Moreover, transit management agencies often place bus stops near signalized intersections to facilitate patrons' access via protected street crossings (Fitzpatrick et al., 1996). Thus, the stops' bus-carrying capacities will be further curbed by the neighboring traffic signal (Gibson, 1996; Tan and Yang, 2014). To avoid the ever-expanding bus queues, the transit agency needs to properly determine a stop's layout (including the number of berths) and location such that the maximum estimated bus arrival rate will not exceed the stop's bus-carrying capacity. To this end, models are needed to unveil the cause-and-effect relationships between key operating parameters (e.g., service time distribution, number of berths, signal timing, and distance between stop and signal) and stop capacity. These models will help practitioners in determining the appropriate stop designs and operating strategies.

Looking at the corridor level, patrons suffer from not only the long bus queues, but also irregular and unstable bus headways. This is because: the motions of delayed buses are further impeded by meeting larger numbers of boarding patrons

at downstream stops; while buses arriving earlier at a stop will meet fewer patrons and tend to travel faster (Newell and Potts, 1964). This adds to a patron's expected waiting time at her stop. Worse yet, a bus queue at a stop adds to variation in bus arrival times at stops downstream. Longer queues are therefore prone to form at downstream stops (Gu et al., 2011), which cause buses to fall further and further behind schedule as they traverse the corridor. This vicious cycle seems to have gone unreported in the literature. In light of the above, we need a new model to jointly examine the bus queueing dynamics and headway variability propagations in busy bus corridors shared by multiple bus lines. The new model can be used to assess effective control strategies for mitigating bus queues.

1.2 Literature review

Studies on bus queueing at a single stop are reviewed in Section 1.2.1. Section 1.2.2 describes studies on bus corridor operations.

1.2.1 Bus queueing at a single stop

For isolated bus stops, earlier works have focused on using microscopic simulations to estimate the stop capacity or bus queueing delay (Papacostas, 1982; Gibson et al., 1989; Fernández and Planzer, 2002). More recent studies have resorted to analytical methods, because they are capable of describing the causal relationships between the key input parameters and output performance metrics. For example, Markovian methods were often used to develop exact solutions to bus-stop queuing models with tandemly-deployed berths (Gu et al., 2012, 2015; Gu and Cassidy, 2013; Bian et al., 2019). Unfortunately, the above analytical methods cannot be extended to account for the influence of nearby signals, because bus queues formed at a near- or far-side stop integrate two types of servers: tandemly-deployed berths and the traffic signal, and the latter is not Markovian (Newell, 1965).

The best-known capacity formula for near- and far-side stops was first presented by the Highway Capacity Manual (HCM: TRB, 2000), and was later inherited by the Transit Capacity and Quality of Service Manual (TCQSM: Kittelson & Associates, Inc., 2013). The latest version of this formula (Equation 6-18 of TCQSM) is:

$$B_s = N_{el} f_{tb} \frac{3600(G/C)}{t_c + t_d(G/C) + Z c_v t_d}, \tag{1.1}$$

where B_s denotes the stop capacity (buses/hour); N_{el} the effective number of berths, which accounts for the mutual blockage between the buses dwelling in multiple,

tandemly deployed berths; f_{tb} the traffic blockage adjustment factor to account for the impacts of competing (right- or left-turning) traffic in the travel lane of buses; G/C the green ratio of the neighboring traffic signal with G being the green period (seconds) and C the cycle length (seconds); t_c is the clearance time (seconds), which includes a bus's movement time in and out of a berth and its "re-entry delay" for merging back to the general traffic from a bus bay; t_d a bus's dwell time (seconds) for loading and unloading patrons; and $Zc_v t_d$ the so-called "operating margin" (seconds) that accounts for the randomness in bus dwell time.

This formula is known to have a number of serious flaws, including the abuse of the empirical, site-specific values for N_{el} (see Exhibit 6-63 in TCQSM), and the fallacious derivation regarding the operating margin term. First, the N_{el} (see Exhibit 6-63 in TCQSM) is assumed to be independent of any other key operating factors, including the distribution of dwell times and the random bus arrival process. The values are only calibrated by empirical site-specific observation but are applied to general settings. Second, the derivation regarding the operating margin term is fallacious. The maximum bus discharging flow from the stop is achieved when the failure rate (FR) is 1, i.e., when there is always a queue present at the entrance (Gu, 2012). However, this formula unexpectedly estimates that the maximum capacity occurs at $FR = 0.5$. In fact, according to the calculation process in TCQSM, the Z-score corresponding to $FR = 1$ is negative. This indicates that the larger dwell time t_d, the larger stop capacity, which is intuitively wrong.

Moreover, the way for modeling the effect of the neighboring traffic signal in equation (1.1) is also questionable. First, the equation simply discounts both the numerator and the bus dwell time t_d in the denominator by the signal's green ratio. This oversimplified the effect of signal timing on the stop capacity, and ignored the effect of signal cycle length on the capacity given a fixed green ratio. (We will see momentarily in this thesis that cycle length has a significant impact on the stop capacity even when green ratio is fixed.) Second, the equation presumes that the effect of multiple berths on the stop capacity, represented by the coefficient N_{el}, is multiplicative and independent of the effect of signal. And lastly, the equation totally overlooked how the stop capacity would be affected by the distance between the stop and its neighboring signal. A recent modification of (1.1) was reported by Hisham et al. (2018), which still did not solve any of the above problems.

Critiques of the TCQSM formula described above have been widely reported in the literature and various models have been proposed to solve these problems. Some works proposed hypothetical models as replacement of (1.1); these models were

calibrated by either site-specific or simulation-generated data, and thus they are only applicable to a narrow range of sites (Alonso et al., 2013; Tan and Yang, 2014; Navarro et al., 2017). Other studies relied on either commercial software packages, e.g., ARENA and PARAMICS (Cortés et al., 2010a; Reilly and Aros-Vera, 2013), or self-developed simulation tools, e.g., IRENE and PASSION (Gibson, 1996; Fernández et al., 2007; Fernández, 2010). To their credit, these simulation models can account for more realistic features of bus stop operations. However, simulations are "blackboxes" that cannot readily reveal general insights on cause-and-effect relationship between key operating parameters and stop capacity. Many simulations are also computationally more demanding, and thus may not be suitable for investigating a large number of cases under various operating environments. In addition, practitioners always desire to have a simple formula, or recipe to be used conveniently. Such a formula or recipe cannot be obtained by regressing empirical or simulated data to some hypothetical function forms, because the stop capacity is a complicated function of several key input parameters, including the number of berths, the distance between stop and signal, the signal timing (cycle length and green ratio), and the distribution of bus dwell times.

There are also some studies on exploring how different operating strategies can mitigate bus queue at a single stop. For example, Gibson et al. (1989) and Fernández et al. (2007) proposed to split a multi-berth stop into multiple neighboring stops to reduce buses' mutual interference and improve the stop capacity. Furthermore, transit management agencies may pre-assign different bus lines into berths, and patrons will queue up after the specific berth for their target bus lines. Lu et al. (2010), Wu et al. (2011), and Tan et al. (2014) proposed some heuristic principles to optimize this line assignment problem, so as to reduce berth idleness and bus queueing delay.

1.2.2 Bus operations along a corridor

Bus queueing studies reviewed in the previous section have by-and-large focused on a single stop. In busy bus corridors, buses not only form queues at stops, but also exhibit poor reliability due to the random disturbances. Newell and Potts (1964) revealed that bus headway variation will grow as buses precede downstream of the corridor. An unexpectedly delayed bus will gradually become further delayed since it will meet more patrons at downstream bus stops; the subsequent bus then has fewer patrons to load and departs from those stops earlier than scheduled. This eventually leads to the notorious bunching phenomenon that is commonly observed by transit users.

Following this seminal work, various solutions have been proposed to address the bus bunching problem. These methods includes: allowing delayed buses to skip stops (Sun and Hickman, 2005; Cortés et al., 2010b), controlling travel speed between stops (Chandrasekar et al., 2002; Daganzo and Pilachowski, 2011), limiting boarding patrons (Delgado et al., 2009, 2012), prioritizing delayed buses at signalized intersections (van Oort et al., 2012; Anderson and Daganzo, 2020), and holding buses at select stops. Among the above strategies, schedule-based holding strategy is the most widely studied because they are simple to model and easy to implement in reality (Newell, 1974; Vandebona and Richardson, 1986; Adamski and Turnau, 1998; Eberlein et al., 2001; Hickman, 2001). To reduce the slack time required by the schedule-based method, Daganzo (2009) proposed an adaptive holding strategy where the holding times at control points are determined using the bus headways measured in real-time. The work was later extended to a wider range of headway-based strategies, including Daganzo and Pilachowski (2011); Bartholdi III and Eisenstein (2012); Andres and Nair (2017). Recently, some efforts were also made to study the bus bunching problem with multiple lines (Hernández et al., 2015; Schmöcker et al., 2016; Wu et al., 2017; Laskaris et al., 2018). More realistic features, such as common-line patrons, bus overtaking, and patron queue swapping among different lines, are explicitly modeled.

Regrettably, the above works on the strategies for preventing bus bunching seem to have assumed that no bus queue would ever occur at any stop, which is applicable to low-frequency bus systems only. Only a handful of studies have modeled bus corridors considering bus queues at busy stops, including Tirachini and Hensher (2011) and Tirachini (2014). However, in their works the bus queueing delays were predicted from a regression model, which was calibrated using simulated data of a single bus stop. Thus, the interactions between bus queues across consecutive stops were simply overlooked.

Commercial software packages such as PARAMICS and MISTRANSIT (Cortés et al., 2005, 2007) can model sufficient real-world operating details. However, they have a great number of parameters to calibrate, and are thus unsuitable for analyzing how key operating factors affect the bus system performance. In addition, their computational costs are high, which limit their applications for emulating congested bus corridors under a wide range of operating conditions.

A number of strategies were also proposed to improve bus commercial speed, including dedicated bus lane (Burinskiene et al., 2014) and signal priority strategies (Baker et al., 2002; Anderson and Daganzo, 2020). However, their overall effects on

bus queues and delays in a busy corridor were not modeled. Another strategy that was commonly believed to be able to reduce bus congestion in busy corridors is bus convoying (Yabe and Nakamura, 2005; Hidalgo et al., 2013). In this strategy, buses are held at a corridor's upstream end until a specified batch size is reached. Convoys are then released to traverse the corridor (and to enter and dwell in multi-berth stops) in unison. A field study of this strategy was conducted in Brazil (Szász et al., 1978; Germani and Szász, 1980; Meirelles, 2000). Convoying reportedly reduced bus delays and better regularized service. Notably, however, the above-cited field study observed the effects of convoying in combination with having expanded the number of bus berths in each stop along a corridor. The effects of these two factors were not disentangled; i.e., the study was not controlled to measure convoying's effects alone and free of confounding influences.

1.3 Overview of major contributions

Our first contribution is the development of analytical approximations for the bus-carrying capacities at near- and far-side stops with one or multiple curbside berths (where buses operate in a dedicated bus lane). The models are more accurate and general than the methods in previous studies and professional handbooks, because they explicitly account for the effects of key operating factors that were overlooked in the literature (e.g., the signal cycle length and the distance between stop and signal) and the characteristics of bus traffic (e.g., the move-up time and reaction time). The models can be conveniently used by practitioners to determine the appropriate design and location of a new bus stop for serving a predicted peak-hour bus flow, or to assess the performance of measures for mitigating bus congestion at an existing stop.

The second contribution is a set of findings drawn from the numerical analysis using the approximation models. Important ones include: i) the well-known TCQSM formula for bus stop capacity has large errors; (ii) ceteris paribus, a near-side stop produces higher capacity than a far-side one; and (iii) decreasing the signal cycle length while keeping the green ratio unchanged can increase a near- or far-side stop's capacity without reducing the general-purpose traffic's discharging capacity by much.

Our third contribution is the development of a new simulation model that describes multi-line bus operations and queues formed at a series of multi-berth stops in a corridor. The new model explicitly accounts for the patron boarding process, the mutual blockages between buses dwelling at stops, and the stop-to-stop headway

evolution process. Our simulation model is parsimonious, which allows us to efficiently simulate wide ranges of operating scenarios and highlight the effects of key operating parameters.

Built upon the simulation model, the fourth contribution comes from examining the effects of typical bus holding strategies on reducing bus queues and improving headway regularity in busy corridors. Strategies examined here include bus convoying and headway-regularization holding. Numerical analysis unveils a number of important findings that were not reported before. For example, we find that both bus queueing delays and headway irregularity at a stop grow as buses move downstream of a corridor. The conventional wisdom on bus convoying is wrong; i.e., it can neither reduce bus delay nor improve service reliability. However, the headway-regularization strategy performs unexpectedly well. It can both mitigate bus queues and improve service reliability under certain operating conditions.

1.4 Organization of the thesis

The thesis is organized as follows.

Chapter 2 presents the analytical capacity formulas for bus stops near signalized intersection. We first develop the capacity approximations for a single-berth near-side stop to illustrate the key idea of constructing the approximation. The single-berth stop approximation is then built upon to develop the approximation for multi-berth stops. The approximations for far-side stops are derived in similar ways as for near-side stops. Validation tests against the simulation are furnished, together with a comparison to the TCQSM formula. Numerical case studies are performed and insights stemming from our models are discussed.

Chapter 3 studies the corridor operations considering bus queues at busy stops. We first present the model setup for the bus corridor and the two holding strategies. Then we develop a simulation model for assessing the two strategies's performance in terms of two performance metrics: bus delay and headway variation. The strategies are then compared head-to-head and against a do-nothing alternative under various operating conditions. At last, managerial insights derived from the simulation results and their practical implications are discussed.

Chapter 4 concludes the thesis by summarizing our contributions, and discussing potential extensions of the present work.

2 Capacity Approximations for Near- and Far-side Bus Stops

We consider near- and far-side bus stops like those shown in Figures 2.1a and b; they are termed according to whether the stop is placed at the near-side (i.e. upstream side) or far-side (i.e. downstream side) of the intersection. The number of berths

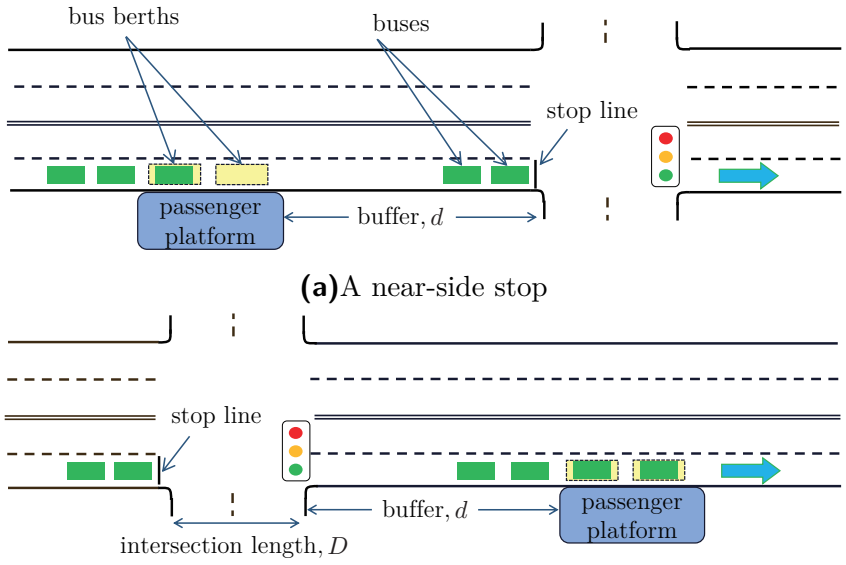

(a) A near-side stop

(b) A far-side stop

Figure 2.1: Curbside bus stops near signalized intersections.

is denoted by c. The land area between the stop and the intersection is termed as "buffer area", whose size is denoted by the (integer) number of buses that can reside within, d, as illustrated in the figures. If the buffer size is not an integer multiple of berth length, it will be rounded down to the nearest smaller integer since only an integer number of buses can be stored in the buffer. We further write d as the sum of an integer multiple of c and a non-negative residual: $d = nc + d_0$, where $n = 0, 1, 2, ...,$ and $0 \leq d_0 \leq c - 1$. We define a bus's dwell time, S, as the sum of: i) the time for loading and unloading patrons in a berth; ii) the time lost due to bus deceleration and acceleration; and iii) the time lost due to door opening and closing. We assume that dwell times of different buses are independent and identically distributed (i.i.d.) with mean μ_S and coefficient of variation C_S.[1] The signal cycle length and effective green period are denoted as C and G, respectively.

[1] One may also find more complicated bus dwell time models, which account for how patrons are loaded to and unloaded from a bus in, e.g., Jaiswal et al. (2010) and Fernández et al. (2008). However, for the simplicity of our modeling work, we adopt the present assumption that the bus dwell times are i.i.d. The same assumption has also been commonly used in the literature; see TCQSM (2013) and Gu et al. (2011, 2015).

Without loss of generality, we normalize all the time variables, unless otherwise specified, by setting the mean bus dwell time as the unit time, i.e., $\mu_S = 1$. We also normalized all the distance variables by setting the berth length (or equivalently, the bus jam spacing) as the unit distance. These normalizations will largely simplify the derivation of approximations.

For simplicity, we made the following assumptions:

(i) bus maneuvers are restricted within the curbside travel lane, which is dedicated to bus use only[2].

(ii) buses are not allowed to overtake each other at the stop or the intersection, or in any queue that forms upstream of the stop or intersection[3].

(iii) for a near-side stop, buses that are ready to depart the stop but are blocked by the red signal are all able to discharge during the following green phase.

(iv) for a far-side stop, the empty berths and the buffer space between stop and signal (see Figure 2.1b) can all be filled up by buses discharging through the intersection in a green phase, should a bus queue be always present upstream of the intersection[4].

Capacity is defined as the maximum rate that buses can discharge through a facility. To derive the capacities of near- and far-side stops, we treat the stop and the intersection as a whole. We specify that a bus queue is always present upstream of a near-side stop, or upstream of the intersection for the far-side stop case. The capacity of the near-side stop is the bus discharging rate from the intersection while

[2]At some busy stops not residing in a bus lane, bus operations may still enjoy a "de facto" exclusive right-of-way since other traffic often stay away from the neighborhood of those busy stops to avoid being blocked by the slow-moving and large-sized buses (Gibson et al., 1989; Fernández and Planzer, 2002). The models to be presented in this chapter can still be applied to those stops with caution.

[3]This assumption represents a common type of bus-stop operation rules (St. Jacques and Levinson, 1997; Kittelson & Associates, Inc., 2013). The same assumption was also made in other studies in this realm (Gu et al., 2011, 2015; Bian et al., 2015).

[4]Assumptions iii) and iv) are practically valid in general as explained below. For near- and far-side stops in the real world, the distance between the stop and the intersection is usually less than 100 meters and so can store at most 8 buses (suppose bus jam spacing is 12 meters). A stop located 100 meters away from the intersection can be regarded as a mid-block stop (Kittelson & Associates, Inc., 2013), on which the signal has a small impact. Moreover, stops with more than 4 berths are rare. Even for the extreme case of a 4-berth stop located 100 meters from the nearby intersection, to satisfy assumptions iii) and iv), the green period only needs to be long enough to discharge 12 buses consecutively. This requires a 42-second green period given a saturation headway of 3.5 seconds for discharging buses (Nguyen, 2013). A signal timing plan with more than 42 seconds green time is commonly used, especially at major intersections where neighboring stops are often congested.

for the far-side stop it is the bus discharging rate from the stop. With the persistent bus queues, assumptions iii) and iv) in the previous section mean that the green period is long enough for at least $d + c$ buses to discharge consecutively into the intersection, given that they are ready to discharge at the start of the green signal.

The approximation models for near-side stops are developed in Section 2.1. Those for far-side stops are developed in Section 2.2. Validation tests are furnished in Section 2.3, together with a comparison against the TCQSM formula. Numerical examples are discussed in Section 2.4. Insights stemming from our models and their practical implications are described in Section 2.5. The notations used in this chapter are summarized in Appendix A.

2.1 Near-side stop models

We first develop the capacity approximations for a single-berth near-side stop (Section 2.1.1) since in this simple case our key idea for constructing the approximation can be presented more clearly. The single-berth stop approximation is then built upon to develop the approximation for multi-berth stops in Section 2.1.2.

2.1.1 Capacity approximation for a single-berth near-side stop ($c = 1$ and $d = n$)

The downstream signal affects the stop's capacity only when a queue of buses formed at the intersection during a red period spills back to the berth, so that the berth cannot serve new buses. We denote T_B as the time during which the berth is blocked in a cycle. The single-berth near-side stop's capacity, Q_S, can then be written as:

$$Q_S = \frac{1}{1+\tau_m}\left(1 - \frac{E[T_B]}{C}\right), \tag{2.1}$$

where τ_m is a bus's movement time in and out of a berth (i.e., the clearance time t_c in equation (1.1) for curbside stops). The $\frac{1}{1+\tau_m}$ is the capacity of an isolated single-berth stop (i.e., a stop without neighboring signals), since the denominator is the sum of average dwell time (note $\mu_S = 1$ due to the normalization) and the average time a bus takes to move forward and fill the berth after the previous bus has left. The remaining work is on how to approximate $E[T_B]$.

To find $E[T_B]$, we first define the "extended red period" at the berth's location, during which buses can be served, but cannot discharge into the intersection. This extended red period is illustrated in the time-space diagrams of bus trajectories at

a single-berth near-side stop; see Figure 2.2 for the case of $d = n = 3$. Note that the extended red period is a constant when signal timing plan, buffer size, and bus traffic characteristics are specified. The solid lines with arrowheads in the figures represent trajectories of the *front* of buses, and the thicker, horizontal segments (labeled as S_1, S_2, S_3 and S_4) of these trajectories represent bus dwell times. In the interest of brevity, these trajectories are plotted as piecewise linear curves; see, e.g., Gu et al. (2013, 2014) for studies that also use piece-wise linear vehicle trajectories for analysis.

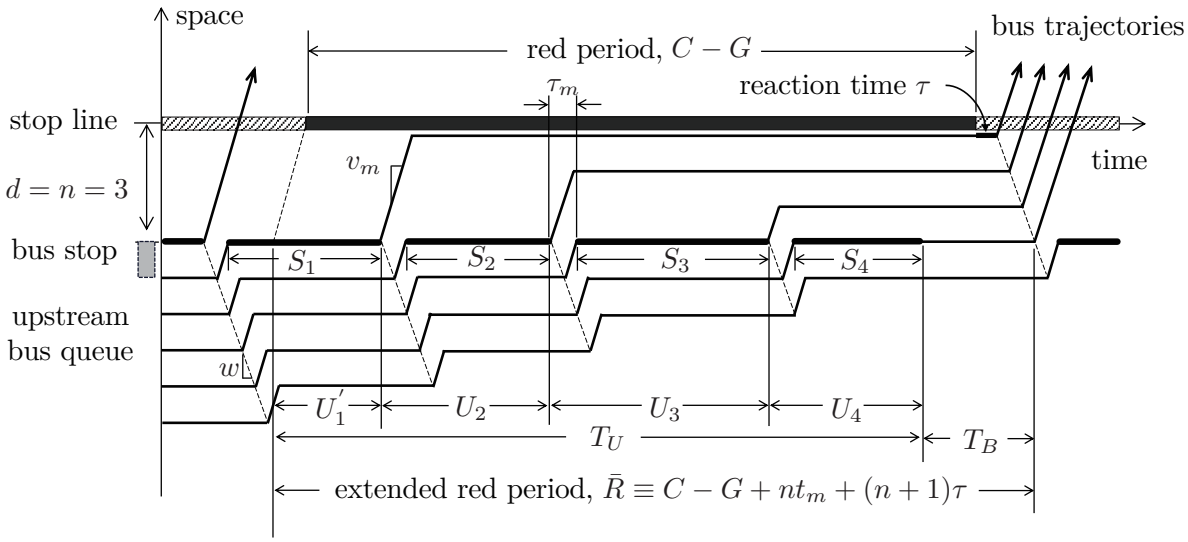

Figure 2.2: Time-space diagram of bus operations at a single-berth near-side stop ($d = n = 3$).

As illustrated in Figure 2.2, the extended red period starts $\frac{n}{v_m}$ earlier than a red period, and ends $\frac{n+1}{w}$ later than the same red period, where v_m is the bus's move-up speed when traveling through the queue, the berth and the buffer, and w is the backward wave speed of bus traffic.[5] For simplicity, we assume that v_m and w are the same for all the buses. For the convenience of description, we denote $\tau = \frac{1}{w}$ (which is termed the "reaction time" in some literature; see for example Menendez, 2006) and $t_m = \frac{1}{v_m}$. (Note that $\tau_m = \tau + t_m$.) Hence, the duration of extended red period is $\bar{R} \equiv C - G + nt_m + (n+1)\tau$, as shown in Figure 2.2. Note that assumption iii) ensures that $G \geq (c + d)\tau_m$, hence the extended red period will never exceed the cycle length.

The start time of extended red period is determined such that any bus that finishes service before this start time will be able to discharge into the intersection immedi-

[5]The backward wave speed is the speed at which the disturbances (in our case, the change of bus speed) propagate backwardly across the buses (Newell, 1993; Daganzo, 1994).

ately. On the other hand, the dwelling bus at this start time and all the following buses served during this extended red period will have to wait until the next green period to discharge; see Figure 2.2. The number of these trapped buses is no greater than the storage capacity of the berth and the buffer, i.e., $n+1$ ($= 4$ in Figure 2.2). The last trapped bus (regardless of the number of trapped buses) will depart the berth no earlier than $(n+1)\tau$ after the green start, and this time defines the end of the extended red period, as illustrated again in Figure 2.2. If $n+1$ buses are served in an extended red period, a blocked duration $T_B > 0$ may exist at the end of extended red period (see again the case of Figure 2.2); otherwise, the berth is busy throughout the extended red period and $T_B = 0$.

Figure 2.2 also shows that T_B can be calculated by:

$$T_B = max\{\bar{R} - T_U, 0\}, \tag{2.2}$$

where T_U denotes the sum of dwell times of the $n+1$ consecutive buses served in the extended red period plus their reaction and move-up times. From the time space diagram, it can be written as follows:

$$T_U = U_1^{'} + \sum_{j=2}^{n+1} U_j, \tag{2.3}$$

where $U_1^{'}$ denotes the portion of the first trapped bus's dwell time that is contained in the extended red period; and $U_j = S_j + \tau_m$ $(j = 2, 3..., n+1)$ (see again Figure 2.2). Note that $U_1^{'}$ is smaller than other U_j's because it starts service before the red period.

Due to the non-negativity of T_U, we can derive from equation (2.2) that:

$$E\left[T_B\right] = \int_{t=0}^{\bar{R}} (\bar{R} - t) f_{T_U}(t) dt, \tag{2.4}$$

where $f_{T_U}(t) = \left(f_{U_1'} * \underbrace{f_U * ... * f_U}_{n\ times} \right)(t)$ is the probability density function (PDF) of T_U; $f_{U_1'}$ and f_U are the PDFs of $U_1^{'}$ and U_j respectively, and the "$*$" is the convolution operator.

We now approximate T_U by a normal random variable with the same mean μ_T and variance σ_T^2. For large n's, this normal approximation is quite accurate thanks to the central limit theorem (CLT). But even for a relatively small n, the approximation can be fairly good. This is because: i) most of the components in the right hand side

of (2.3), i.e. the U_j's ($j = 2, 3, ..., n+1$) are i.i.d and usually exhibit a bell-shaped PDF in the real world; and ii) although U_1' has a different distribution from U_j, it is statistically smaller than U_j and thus has a small share in T_U if n is not too small. On the other hand, this CLT approximation may be less accurate if $n = 0$ or 1.

Applying the properties of normal distribution, we have:

$$\begin{aligned} E[T_B] &= \bar{R}F_{T_U}(\bar{R}) - \int_{t=0}^{\bar{R}} t f_{T_U}(t)dt \\ &= \bar{R}F_{T_U}(\bar{R}) - \int_{t=-\infty}^{\bar{R}} t f_{T_U}(t)dt \\ &\approx \bar{R}\Phi\left(\frac{\bar{R}-\mu_T}{\sigma_T}\right) - \left(\mu_T\Phi\left(\frac{\bar{R}-\mu_T}{\sigma_T}\right) - \sigma_T\phi\left(\frac{\bar{R}-\mu_T}{\sigma_T}\right)\right) \\ &= \sigma_T(r\Phi(r) + \phi(r)), \end{aligned} \tag{2.5}$$

where $F_{T_U}(\cdot)$ denotes the cumulative distribution function (CDF) of T_U; $\Phi(\cdot)$ and $\phi(\cdot)$ the CDF and PDF of a standard normal distribution, respectively; and $r = \frac{\bar{R}-\mu_T}{\sigma_T}$. The second equality in (2.5) holds because T_U is non-negative. The approximation step in (2.5) is obtained as follows: first approximate $f_{T_U}(t)$ by the PDF of a normal distribution with mean μ_T and variance σ_T^2 (the CLT approximation), and then apply the mean formula of a truncated normal distribution whose lower and upper truncated bounds are $-\infty$ and $\bar{R}$, respectively (see e.g., Greene, 2003).

Combining equations (2.1) and (2.5) furnishes an approximation of the single-berth stop's capacity, denoted as Q_{SA}:

$$Q_{SA} = \frac{1}{1+\tau_m}\left(1 - \frac{\sigma_T(r\Phi(r) + \phi(r))}{C}\right). \tag{2.6}$$

Finally, when S_j follows a gamma distribution[6], the mean μ_T and variance σ_T^2 of T_U are approximated as follows:

$$\begin{cases} \mu_T \approx n(1+\tau_m) + \dfrac{C_S^2 + (1+\tau_m)^2}{2(1+\tau_m)}; \\ \sigma_T^2 \approx \dfrac{5+8\tau_m}{12(1+\tau_m)^2} C_S^4 + (\dfrac{1}{2}+n) C_S^2 + \dfrac{(1+\tau_m)^2}{12}. \end{cases} \tag{2.7}$$

The derivation of (2.7) is relegated to Appendix B.

Approximation (2.6) exhibits high accuracy when n is large. But moderate errors may occur when n is rather small. Fortunately, our numerical results manifest that the error of (2.6) is less than 5% for most cases even when $d = 0$; see Section 2.3.1 for more details.

Significant errors may also occur when C_S is small, since (2.7) is derived using an assumption that U_1' is independent of signal phases (see Appendix B), which becomes invalid for small C_S. An extreme example where $C_S = 0$ (deterministic bus dwell time) is briefly discussed in Appendix B. More details regarding the accuracy of (2.6) are furnished in Section 2.3.

2.1.2 Capacity approximation for a multi-berth near-side stop ($c \geq 2$ and $d = nc + d_0$)

Since bus overtaking maneuvers are prohibited, the bus dwelling at the upstream-most berth of a multi-berth stop can depart only when all the downstream berths are vacated. Thus, in the absence of the traffic signal, queued buses will enter a c-berth curbside stop in convoys of size c (Gu et al., 2011), should a sufficiently long bus queue be present all the time. We denote U^p as the general service time of a c-bus convoy, which is defined as the total time the convoy spends at the c-berth stop for all of its buses to finish dwelling. Then a c-bus convoy served at a c-berth stop can be viewed as a hypothetical "bus" that spends a random "dwell time", U^p, at a "single-berth" stop. The distribution of U^p can be developed using the probability theory. Specifically, we find that the mean and variance of U^p can be

[6]Gamma distribution fits the real-world bus dwell times well (see, e.g., Ge, 2006), and is often used to model bus dwell times in the literature due to its non-negativity, parsimony and flexibility (Gu et al., 2011; Gu and Cassidy, 2013). However, our method can still be used if the bus dwell time is assumed to follow other commonly used distributions, e.g. the log-normal distribution (Wang et al., 2016, 2018).

approximated by the following functions (assuming S follows gamma distribution):

$$\begin{cases} E[U^p] \approx h(c, C_S) \equiv 0.7931 C_S \log(c) + 0.9911 + c\tau_m; \\ Var(U^p) \approx q(c, C_S) \equiv 0.6819 C_S^3 \arctan(c) + 0.5102 C_S^2. \end{cases} \tag{2.8}$$

The derivation of (2.8) is relegated to Appendix C. The appendix also includes a test of the accuracy of (2.8).

We now follow the logic in Section 2.1.1 to develop the approximate capacity; i.e., we consider that a c-berth stop's capacity ($c \geq 2$) is equal to the capacity of an isolated c-berth stop, multiplied by the fraction of time when the stop is not blocked by the queue arising from the signal. The blockage of the stop is again determined with the assistance of an extended red period, which is now defined at the location of the upstream-most berth with a duration of $\bar{R}^p \equiv C - G + (c+d-1)t_m + (c+d)\tau$; see Figure 2.3 for a 2-berth, 2-buffer stop as an example.

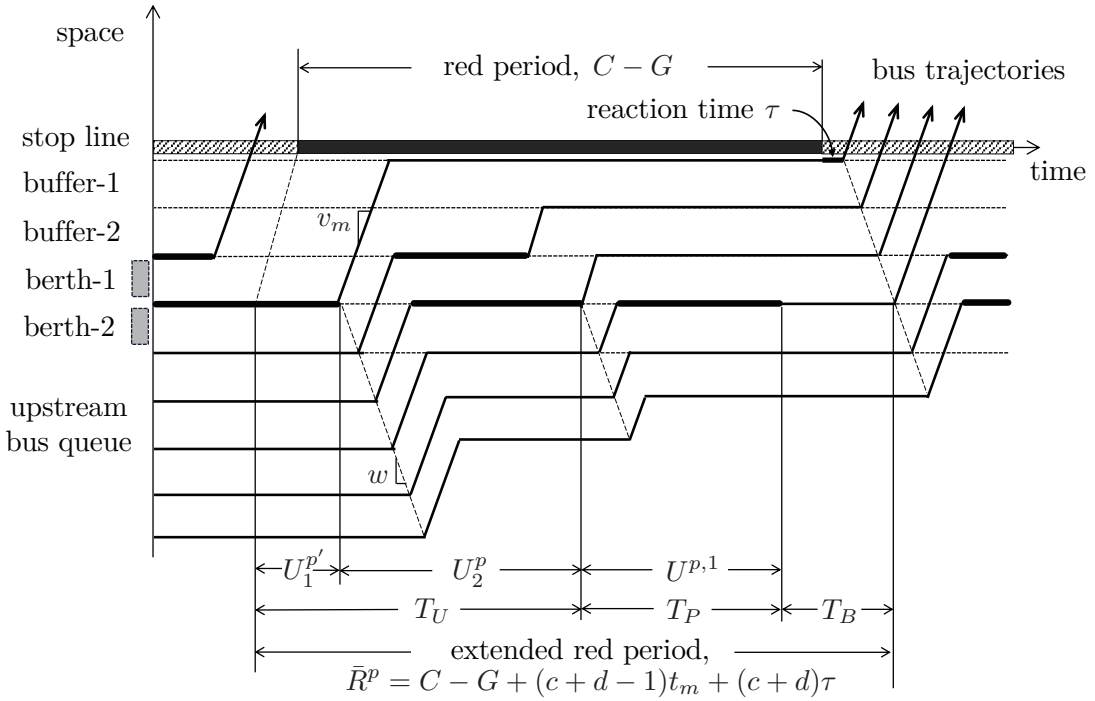

Figure 2.3: Time-space diagram of bus operations at a 2-berth, 2-buffer near-side stop.

For a multi-berth stop, the number of available buffer spaces near the end of an extended red period may be greater than 0 but less than c. In this case, only part of the c-bus convoy that is currently under service can proceed to the buffer after completing the services. The remaining buses in the convoy have to stay at the downstream berths of the stop. Consequently, the next bus convoy to be served by the stop would contain fewer than c buses. In the example shown in Figure

2.3, the last "convoy" served in the extended red period has only one bus. With a slight abuse of notation, we use the same symbol T_U (as in the single-berth case) to denote the part of extended red period for serving part of the first trapped convoy and all the *full*-size convoys. We denote T_P as the time for serving the last *small* convoy if any, and T_B as the time interval when all the berths are occupied by buses waiting for departure (i.e., when the stop is effectively idle). The T_U, T_P and T_B are illustrated in Figure 2.3. The stop's service rate is 0 during T_B, and is discounted by $1-\frac{N_P}{c}$ during T_P, where N_P is the number of buses in the small convoy. For simplicity, we further define the "effective service time of full-size convoys" as $T_U^{'} = T_U + \frac{N_P}{c}T_P$, and the "effective blockage time" as $T_B^{'} = max\{\bar{R}^p - T_U^{'}, 0\}$. We then write the approximate stop capacity as:

$$Q_{MA} \approx \left(\frac{c}{E[U^p]}\right)\left(1 - \frac{E[T_B^{'}]}{C}\right). \tag{2.9}$$

Note that (2.9) is an analog of (2.1) in the single-berth case. Following a derivation similar to the CLT approximation in Section 2.1.1, we have the approximate stop capacity:

$$Q_{MA} = \left(1 - \frac{\sigma_{T_U^{'}}(r\Phi(r) + \phi(r))}{C}\right)\left(\frac{c}{h(c, C_S)}\right), \tag{2.10}$$

where $r = \frac{\bar{R}^p - \mu_{T_U^{'}}}{\sigma_{T_U^{'}}}$, $\mu_{T_U^{'}}$ and $\sigma_{T_U^{'}}$ are mean and standard deviation of $T_U^{'}$.

Finally, $\mu_{T_U^{'}}$ and $\sigma^2_{T_U^{'}}$ are approximated by (again, assuming S follows gamma distribution):

$$\begin{cases} \mu_{T_U^{'}} \approx (n + \frac{1}{2})h(c, C_S) + \frac{q(c, C_S)}{2h(c, C_S)} + \frac{c + d_0 - E[M]}{c}h(c + d_0 - E[M], C_S); \\ \sigma^2_{T_U^{'}} \approx \frac{1}{12}h^2(c, C_S) + (n + \frac{1}{2})q(c, C_S) + \frac{5h(c, C_S) + 3\tau_m}{12h^2(c, C_S)(h(c, C_S) - c\tau_m)}q^2(c, C_S) \\ \qquad + \left(\frac{c + d_0 - E[M]}{c}\right)^2 q(c + d_0 - E[M], C_S). \end{cases} \tag{2.11}$$

Derivation of (2.11) is relegated to Appendix D.

2.2 Far-side stop models

The approximations for far-side stops are derived in similar ways as for near-side stops. The major difference lies in the calculation of the idle time period: a far-side stop becomes idle when the stop is starved by the upstream red signal, which

cuts off the bus inflow. We again present the approximation for single-berth stops first (in Section 2.2.1) to smooth the reading experience, and then for the more complicated multi-berth stops in Section 2.2.2. In both sections, we denote D as the length of intersection, i.e., the distance between stop line and the start of buffer; see Figures 2.1b, 2.4a and 2.4b.

2.2.1 Capacity approximation for a single-berth far-side stop ($c = 1$ and $d = n$)

We first define the extended red period, again at the berth's location, as shown by the example of a far-side single-berth stop with $d = 2$ (Figure 2.4a). It starts from the black dot on the left, which is $(n + 1)\tau$ ahead of the red start, and ends at the grey point on the right, which is $(D+n)t_m$ later than the following green start. The two dots are determined using the following logic. First, a bus whose dwell time extends from the green period to beyond the black dot is the first bus trapped in the extended red period. Figure 2.4a reveals that whenever a bus finishes its service and departs the stop on or before the black dot, another bus queued upstream of the signal can always cross the intersection and fill up the buffer before the signal turns red. On the other hand, the first queued bus that can cross the intersection in the following green period will arrive at the berth no earlier than τ_m after the grey dot. If $(n + 1)$ buses finish their services before the grey dot, the berth will be idle until the end of extended red period.

Hence, the duration of the extended red period for a single-berth far-side stop is $\bar{R}^F \equiv (n + 1)\tau + C - G + (D + n)t_m$, where the superscript F denotes the far-side stop case. Note that this is Dt_m longer than the extended red period for a single-berth near-side stop, and the difference is exactly the time needed for a bus to travel through the intersection.

Now we denote the period during which the berth is vacant as T_B^F, which can be calculated by:

$$T_B^F = \max\{\bar{R}^F - T_U^F, 0\}, \tag{2.12}$$

where $T_U^F = U_1^{'} + \sum_{j=2}^{n+1} U_j$ denotes the sum of dwell times, reaction times and move-up times of $n + 1$ consecutive buses served in the extended red period; $U_1^{'}$ and $U_j (j = 2, 3, ..., n + 1)$ are defined in similar ways as for near-side stops. The T_U^F is again approximated by a normal random variable with mean and variance given by equation (2.7). Consequently, the approximation of a single-berth far-side stop's capacity is calculated by (2.6) in which $r = \frac{\bar{R}-\mu_T}{\sigma_T}$ is replaced by $r = \frac{\bar{R}^F-\mu_T}{\sigma_T}$.

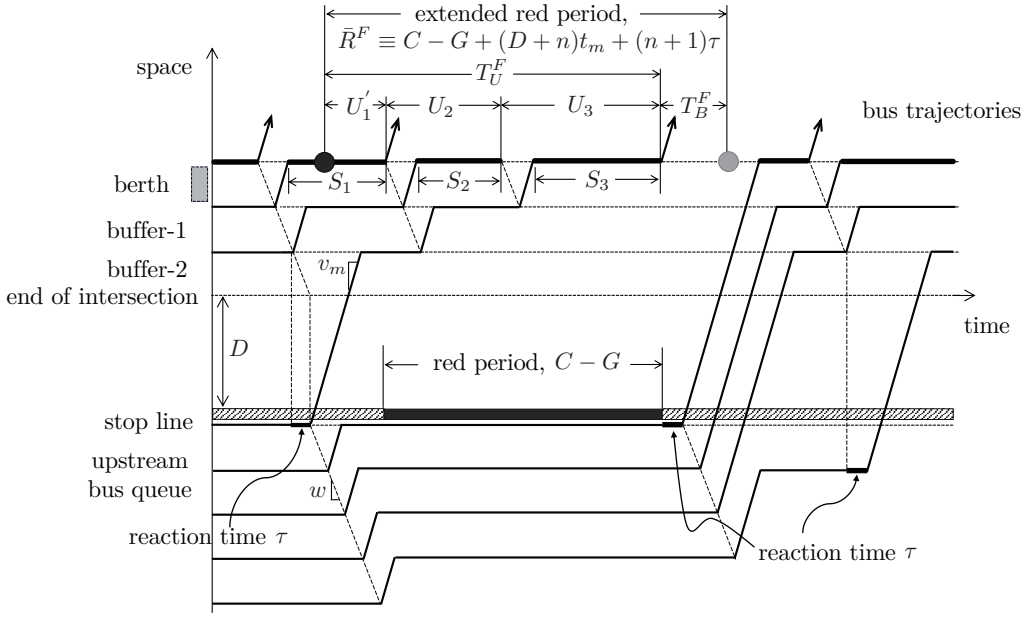

(a) $d = 2$

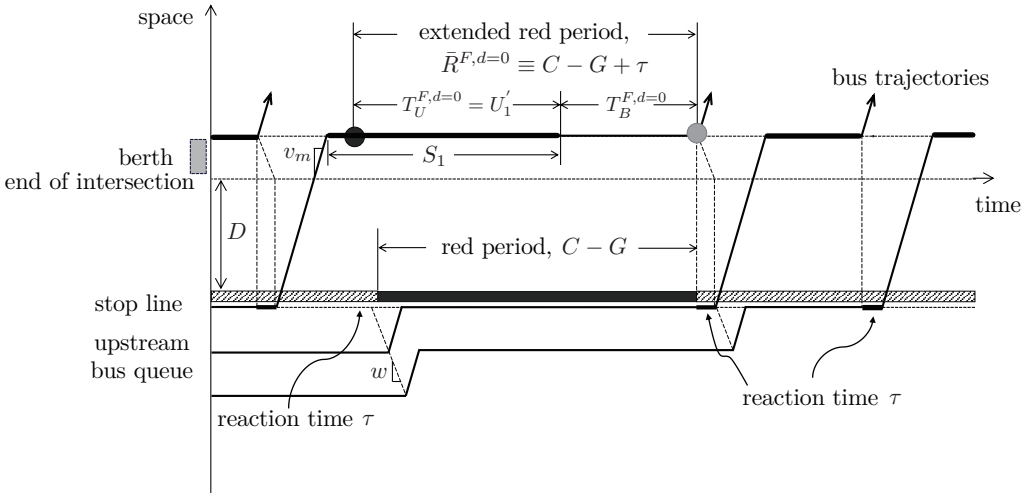

(b) $d = 0$

Figure 2.4: Time-space diagrams of bus operations at a single-berth far-side stop.

A special case arises when $d = n = 0$ (i.e., when the stop is placed immediately downstream of the intersection); see Figure 2.4b. In this case, a queued bus can discharge into the intersection only after seeing the berth becomes empty. Hence, the time gap between two consecutive buses' dwelling activities at the berth is now $\tau_m + Dt_m$ instead of τ_m in the case of $d > 0$. As a result, the duration of extended red period in this special case becomes $\bar{R}^{F,d=0} \equiv C - G + \tau$, because the first bus that crosses the intersection in the following green period should arrive at the berth

no earlier than $\tau_m + Dt_m$ after the end of extended red period; see Figure 2.4b for the illustration. Under this special case, the approximate capacity is:

$$Q_{SA}^{F,d=0} = \frac{1}{1+\tau_m+Dt_m}\left(1 - \frac{\sigma_T^{F,d=0}\left(r^{F,d=0}\Phi(r^{F,d=0}) + \phi(r^{F,d=0})\right)}{C}\right), \tag{2.13}$$

where $r^{F,d=0} = \frac{\bar{R}^{F,d=0} - \mu_T^{F,d=0}}{\sigma_T^{F,d=0}}$ and

$$\begin{cases} \mu_T^{F,d=0} \approx \dfrac{C_S^2 + (1+\tau_m+Dt_m)^2}{2(1+\tau_m+Dt_m)}; \\ \left(\sigma_T^{F,d=0}\right)^2 \approx \dfrac{5+8(\tau_m+Dt_m)}{12(1+\tau_m+Dt_m)^2}C_S^4 + \dfrac{1}{2}C_S^2 + \dfrac{(1+\tau_m+Dt_m)^2}{12}. \end{cases} \tag{2.14}$$

The increased time gap $\tau_m + Dt_m$ would render the single-berth far-side stop with $d = 0$ a very bad design, as we shall see in Section 2.4.2.

2.2.2 Capacity approximation for a multi-berth far-side stop ($c \geq 2$ and $d = nc + d_0$)

Again, we first define the extended red period. As illustrated in Figure 2.5 for a 2-berth, 3-buffer far-side stop, the extended red period is again defined at the location of the upstream-most berth (berth-2 in the figure). A black dot is marked on the timeline of that location at $\delta_1^L \equiv (d+1)\tau + (c-1)\tau_m$ earlier than the red start. If a c-bus convoy completes service by the black dot, another c-bus convoy will discharge through the intersection to fill up the buffer before the present green period ends (which is the case shown in the figure). On the other hand, if the c-bus convoy completes service after $\delta_2^L \equiv (d+1)\tau$ ahead of the red start (not shown in the figure), then no additional bus is able to fill up the vacant space in the buffer before the green end. When the c-bus convoy completes service after δ_1^L, but before δ_2^L ahead of the red start, a *small* convoy of less than c buses will proceed to fill part of the vacancies in buffer. To simplify the modeling work, however, we ignore the possibility of having small convoys and define the extended red period's start time from an expectation perspective, i.e., at $\delta^L \equiv \frac{1}{2}(\delta_1^L + \delta_2^L) = (d+1)\tau + \frac{1}{2}(c-1)\tau_m$ before the red start.

The gray dot in Figure 2.5, which is located $\delta^R \equiv (D+d)t_m$ after the following green start, marks the end of extended red period. This is because the gray dot is τ_m ahead of the earliest time that a bus from the upstream queue can arrive at the

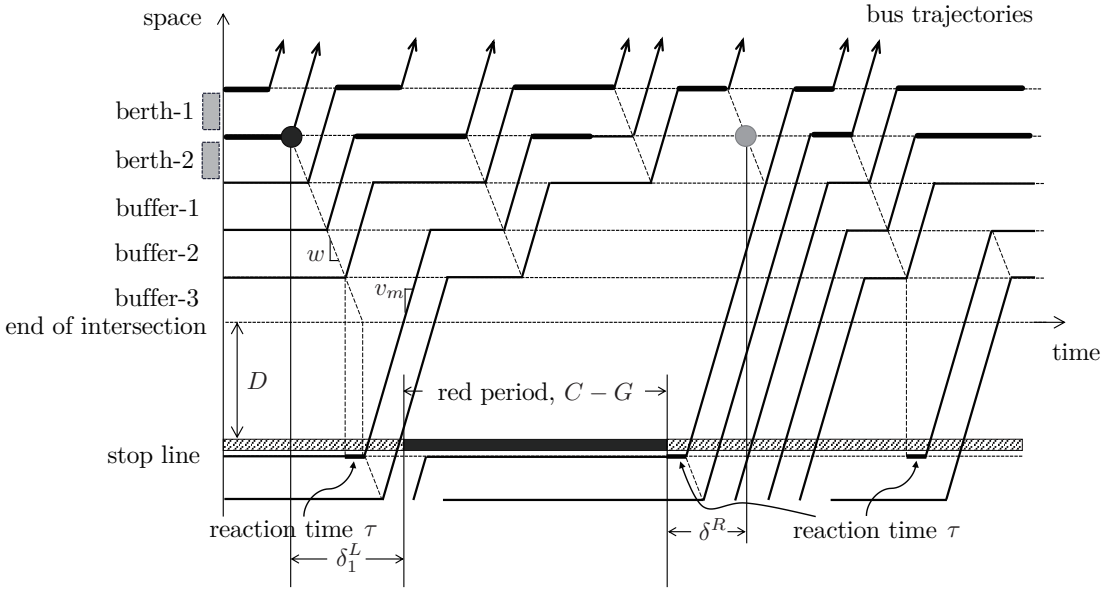

Figure 2.5: Time-space diagram of bus operations at a 2-berth, 3-buffer far-side stop.

upstream-most berth in the following green period. Hence, the length of extended red period is $\bar{R}^{Fp} \equiv C - G + \delta^L + \delta^R = C - G + (d + \frac{c+1}{2})\tau + (D + d + \frac{c-1}{2})t_m$.

We denote T_U^F as the total time for serving all the convoys but the last smaller one (if any) in the extended red period; T_P^F as the time for serving that last small convoy, during which the service rate is discounted by $\frac{c-d_0}{c}$ (if this small convoy does not exist, $T_P^F = 0$); and T_B^F as the time when all the berths are vacant. These three variables are illustrated in Figure 2.6 for a 2-berth, 3-buffer far-side stop. For simplicity, we define the effective service time of full-size convoys as $T_U^{F'} \equiv T_U^F + \frac{d_0}{c} T_P^F$ and the effective idle time as $T_B^{F'} \equiv max\{\bar{R}^{Fp} - T_U^{F'}, 0\}$. The $T_U^{F'}$ can be expressed by:

$$T_U^{F'} = U_1^{p'} + \sum_{j=2}^{n+1} U_j^p + \frac{d_0}{c} U^{p,d_0}. \tag{2.15}$$

Similar to the near-side stop case, the mean $E[U^p]$ and variance $Var(U^p)$ of U_j^p are given by (2.8). The $E[U_1^{p'}]$ and $Var(U_1^{p'})$ can be found in (D.6) of Appendix D as functions of $E[U^p]$ and $Var(U^p)$. When $d_0 \neq 0$, the $E[U^{p,d_0}]$ and $Var(U^{p,d_0})$ are obtained by substituting d_0 for some c in (2.8):

$$\begin{cases} E[U^{p,d_0}] \approx 0.7931 C_S \log(d_0) + 0.9911 + c\tau_m; \\ Var(U^{p,d_0}) \approx 0.6819 C_S^3 \arctan(d_0) + 0.5102 C_S^2. \end{cases} \tag{2.16}$$

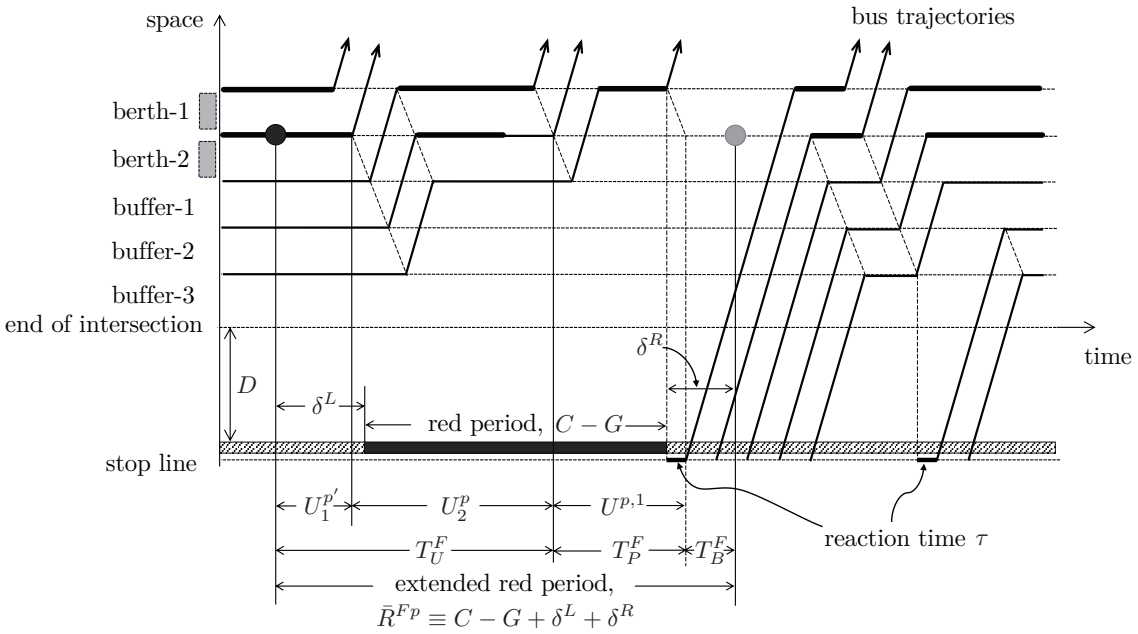

Figure 2.6: Time-space diagram of bus operations at a 2-berth, 3-buffer far-side stop where all the buffered buses are served within the extended red period.

Hence, $\mu_{T_U^{F'}}$ and $\sigma^2_{T_U^{F'}}$ can be determined as follows:

$$\begin{cases} \mu_{T_U^{F'}} \approx E[U_1^{p'}] + nE[U^p] + \dfrac{d_0}{c} E[U^{p,d_0}]; \\ \sigma^2_{T_U^{F'}} \approx Var(T_1^{p'}) + nVar(U^{p'}) + \left(\dfrac{d_0}{c}\right)^2 Var(U^{p,d_0}). \end{cases} \tag{2.17}$$

The approximation of a multi-berth far-side stop's capacity is calculated by (2.10) where $\sigma_{T_U^{F'}}$ substitutes for $\sigma_{T_U'}$ and $r = \frac{\bar{R}^{Fp} - \mu_{T_U^{F'}}}{\sigma_{T_U^{F'}}}$. Note that this approximation only applies for the case of $d \geq 1$.

For the special case of $d = 0$, the time gap between two consecutive convoys becomes $c\tau_m + Dt_m$, and the extended red period becomes $\bar{R}^{Fp,d=0} \equiv C - G + (\frac{c+1}{2})\tau + (\frac{c-1}{2})t_m$. Thus the approximate capacity becomes:

$$Q_{MA}^{F,d=0} = \left(1 - \frac{\sigma_{T_U'}^{F,d=0}(r_p^{F,d=0}\Phi(r_p^{F,d=0}) + \phi(r_p^{F,d=0}))}{C}\right)\left(\frac{c}{h(c, C_S) + Dt_m}\right), \tag{2.18}$$

where $r_p^{F,d=0} = \frac{\bar{R}^{Fp,d=0} - \mu_{T_U'}^{F,d=0}}{\sigma_{T_U'}^{F,d=0}}$ and

$$\begin{cases} \mu_{T_U'}^{F,d=0} \approx \dfrac{(h(c,C_S)+Dt_m)^2 + Var(U^p)}{2(h(c,C_S)+Dt_m)}; \\ \left(\sigma_{T_U'}^{F,d=0}\right)^2 \approx \dfrac{(5h(c,C_S)+8Dt_m+3\tau_m)q^2(c,C_S)}{12(h(c,C_S)+Dt_m)^2(h(c,C_S)-c\tau_m)} + \dfrac{q(c,C_S)}{2} + \dfrac{(h(c,C_S)+Dt_m)^2}{12}. \end{cases} \tag{2.19}$$

The $q(c, C_S)$ and $h(c, C_S)$ are given by (2.8).

2.3 Model validation via simulation

In this section, we use computer simulation to examine the accuracy of the proposed approximations for near- and far-side stops. We develop event-based simulation programs for near- and far-side stops under the assumption that a bus queue is always present upstream of both the stop and the intersection. The operation logic in the simulation is the same as the analytical model. This is a common approach used in queueing theory literature to verify the analytical model. To be true, it would be better to conduct a field study for validation. But in reality it is generally hard to find a very busy stop operating very close to the capacity for a sufficiently long time. We leave it as one of our future works.

The pseudocode is furnished in Appendix E, and the detailed program code can be downloaded from: https://github.com/Minyu-Shen/Simulation-for-bus-stops-near-signalized-intersection. We also develop a program to visualize bus motions in the simulation. This program is used to validate the simulation. The visualization code is also provided in the above web link.

The parameter values used in the simulation are listed in Table 2.1. Stops with

Table 2.1: Parameter values for simulation validation and numerical analysis.

Category	Parameter	Physical value	Normalized value
Bus stop design	c	1∼4	–
	d	0∼4	–
Bus operations	μ_S	25 s	1
	C_S	0.3∼1	–
Bus traffic characteristics	s_j	12 m	1
	w	25 km/h	14.47
	v_m	20 km/h	11.57
Signalized intersection	C	80∼240 s	3.2∼9.6
	D	24∼48 m	2∼4
	G/C	0.3∼0.7	–

less-varied dwell times, i.e., those with $C_S \in [0, 0.3)$, are not examined here since they are rare in reality. For each instance with specific values for C_S, c, d, C, G/C and D, 300,000 buses are simulated to ensure that the average bus discharge rate converges to the steady-state capacity. To facilitate the readers' understanding of the numerical cases discussed in the following sections, the normalized capacity values obtained from our models were converted back to the actual physical values in the unit of "buses per hour".

Select validation results of the approximations are furnished in Section 2.3.1. Section 2.3.2 compares the simulated and approximate capacities against the TCQSM capacity formula (1.1).

2.3.1 Validation of the approximations

We first plot the approximate capacity and the simulated capacity against C as dashed and solid curves, respectively, in Figures 2.7a-d. The four figures illustrate the results for four near-side stops with $c \in \{1, 2\}$ and $C_S \in \{0.3, 0.8\}$, respectively. We assume $G/C = 0.5$ in all the figures, and examine three values of d in each figure: $d = 0, 2$, and 4. Stops with 3 or more berths exhibit similar results, which are omitted here in the interest of brevity.

Comparison between approximation and simulation results unveils that the approximation is quite accurate for most of the cases illustrated by the figures. The error is almost negligible for single-berth stops, and is consistently small for various values of C and d. It grows as c increases since great error is brought by the various approximation steps used in the multi-berth model (see Section 2.1.2). Moreover, for 2-berth near-side stops with large C_S (Figure 2.7d), the approximation consistently underestimates the capacity. This is partly due to the overestimation of the intermediate variable M in Appendix D. Finally, the error is larger for 2-berth stops with small C_S (Figure 2.7c), because the approximation model fails to capture the high sensitivity of capacity to C when C_S is small. A brief explanation of this large error is that when C_S is small, the service time of the first trapped convoy (or bus) is highly correlated with the signal timing (see the end of Section 2.1.1 and Appendix B). A more detailed explanation of the high sensitivity of capacity to C is furnished below by using an extreme example of a 2-berth near-side stop with no buffer ($d = 0$), $G/C = 0.5$, and deterministic dwell time ($C_S = 0$). This stop's simulated capacity is plotted as the solid curve in Figure 2.8.

Note the first declining segment on the solid capacity curve for $80\,\text{s} \leq C < 134.6\,\text{s}$. For any C in this range, only 4 buses are served per cycle (one 2-bus convoy in the

red period and another convoy in the green). This is because $G = \frac{C}{2} < 67.3\,\text{s} = (\tau + 2\tau_m) + \mu_S + 2\tau_m + \mu_S$. The validity of the above inequality can be verified using the following parameter values: $\tau = s_j/w = 1.73\,\text{s}$, $t_m = s_j/v_m = 2.16\,\text{s}$, $\tau_m = \tau + t_m = 3.89\,\text{s}$, and $\mu_S = 25\,\text{s}$ (see Table 2.1). The reader can also verify by drawing a simple time-space diagram that $(\tau + 2\tau_m) + \mu_S + 2\tau_m + \mu_S$ is the minimum time needed for a 5th bus to discharge in a green period. Thus, as $C > 134.6\,\text{s}$, the stop capacity jumps to a higher value. (i.e., now 5 buses are served per cycle; see the small solid declining segment for $134.6\,\text{s} \leq C \leq 142.4\,\text{s}$ in Figure 2.8.) The 6th bus (which is in the same convoy as the 5th bus when entering the berths) will still be blocked by the red signal until $C > 142.4\,\text{s}$ (i.e., $G = \frac{C}{2} > 71.2\,\text{s} = (\tau+2\tau_m)+\mu_S+2\tau_m+\mu_S+\tau_m)$. Hence we observe another capacity jump at $C = 142.4\,\text{s}$, beyond which 6 buses will be served per cycle. Consequently, the capacity curve exhibits a "sawtooth" shape, which is an intuitive result since when the bus dwell time is deterministic, the number of buses that can be served in a green period "jumps" as the green duration exceeds certain thresholds.

The "sawteeth" in the curve would be gradually smoothed as C_S increases, as illustrated by the dotted, dashed, and dash-dot curves in Figure 2.8, which represent the cases of $C_S = 0.1$, 0.2, and 0.3, respectively. The fluctuations also diminish as C or d increases, because a larger C (and thus a larger G when G/C is fixed) means more buses will be served in each green period, and a larger d means more buses can potentially be served in each red period. In both cases, the "capacity jumps" created by serving one additional bus per cycle will be diluted. We also see by comparing Figures 2.7a and c that the capacity fluctuations are larger for a large c. This is because a larger convoy size c will render the convoy dwell time U^p (see equation (C.1) in Appendix C) less varied; i.e., the coefficient of variation $\frac{\sqrt{Var(U^p)}}{E[U^p]}$ will decrease with c.

Finally, the above capacity fluctuations are not captured by our models, which rely on the CLT approximation. Hence the approximations would be inaccurate when C_S is very small. Fortunately, this issue is of lesser practical concern since in the real world C_S is usually no less than 0.4 (St. Jacques and Levinson, 1997; Levinson and St. Jacques, 1998; Bian et al., 2015).

The accuracy of our approximation is further examined by box plots of the percentage approximation error, $|\frac{Q_{\text{appx}} - Q_{\text{sim}}}{Q_{\text{sim}}}|$, where Q_{appx} is the approximate capacity and Q_{sim} is the simulation result. These box plots are shown in Figures 2.9a-c for near-side stops with $c = 1, 2, 3$, respectively; each figure displays the results for $C_S \in \{0.3, 0.55, 0.8\}$ and $d \in \{0, 1, 2, 3, 4\}$. Each error box represents the distribu-

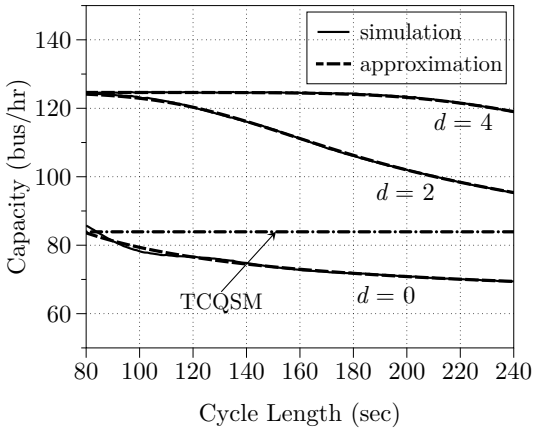

(a) $c = 1, C_S = 0.3$, near-side

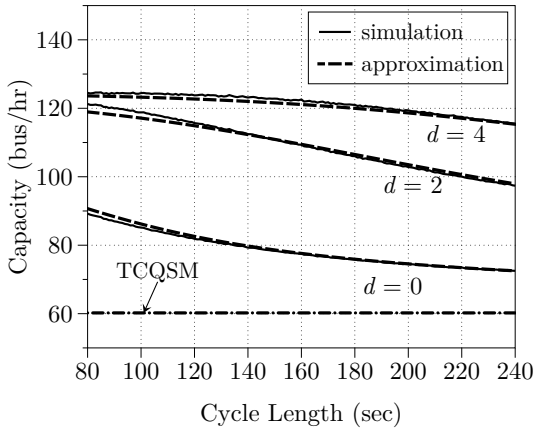

(b) $c = 1, C_S = 0.8$, near-side

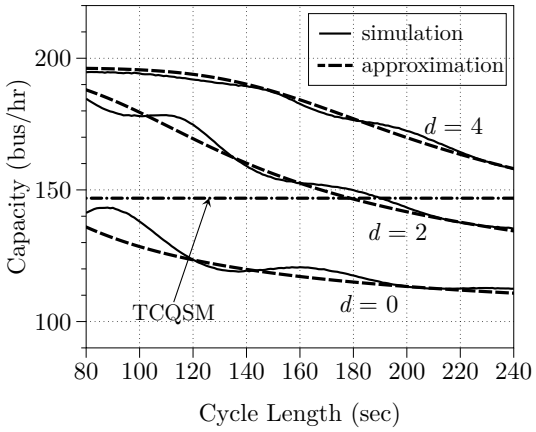

(c) $c = 2, C_S = 0.3$, near-side

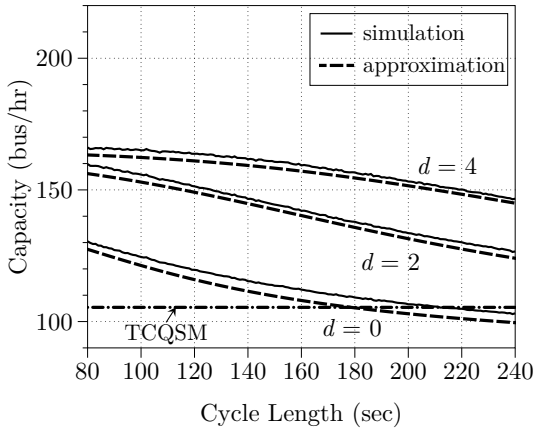

(d) $c = 2, C_S = 0.8$, near-side

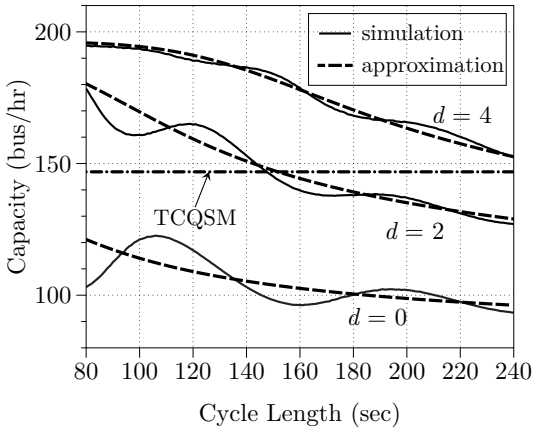

(e) $c = 2, C_S = 0.3$, far-side, $D = 3$ (normalized)

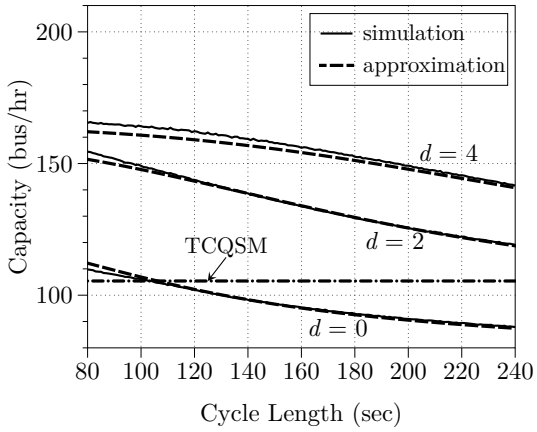

(f) $c = 2, C_S = 0.8$, far-side, $D = 3$ (normalized)

Figure 2.7: Validation of the approximations.

tion of the percentage errors for a set of C values ranging from 80 s to 240 s and a fixed $G/C = 0.5$. Specifically, each box spans the range from the first quartile to the third quartile of the error distribution; the band inside each box indicates the

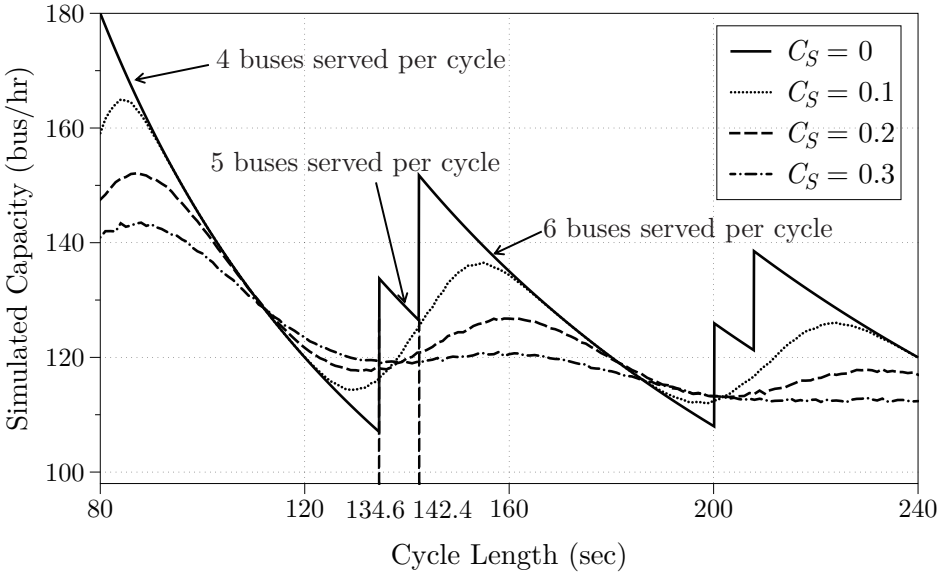

Figure 2.8: Sensitivity of capacity to C when $C_S \leq 0.3$ ($c = 2$, $d = 0$, near-side stop).

median; and the whiskers above and below each box indicate the maximum and minimum errors (save for the outliers if any), respectively.

First note that most errors are less than 1% for single-berth stops (Figure 2.9a), 3% for 2-berth stops (Figure 2.9b), and 5% for 3-berth stops (Figure 2.9c). The errors increase with c because: i) the multi-berth model incorporates more approximation steps than the single-berth model; and ii) for a fixed d and C, a larger c means fewer convoys will be served in an extended red period, which will render the CLT approximation less accurate.

For a given c, the largest error always occurs with the smallest C_S and $d = 0$ (see the outliers on top of the left-most box plot in each figure). This is mainly due to the uncaptured high sensitivity of capacity to C when C_S is small (see the explanation above).

It is also observed in Figures 2.9b and c that for a fixed C_S and c, the error generally diminishes with d. The reason is simple: a larger d means more convoys can potentially be served in an extended red period, thus rendering a more accurate CLT approximation. This effect is not observed in Figure 2.9a since for single-berth stops the error is already very small regardless of the value of d, and other factors may be dominating as d grows. Nevertheless, in all the cases examined here, the CLT approximation is quite good even when $d = 0$, which is a little surprising to us. This maybe partly due to the bell-shaped distributions used for bus dwell times, which are similar to the shape of normal PDFs.

Similar findings are obtained when comparing the approximation against simulation results for far-side stops; see Figures 2.7e and f for a 2-berth far-side stop with $D = 3$ and $C_S = 0.3$ and 0.8, respectively, and Figures 2.10a-c for box plots of approximation errors for far-side stops with $D = 3$, $C_S \in \{0.3, 0.55, 0.8\}$, $d \in$

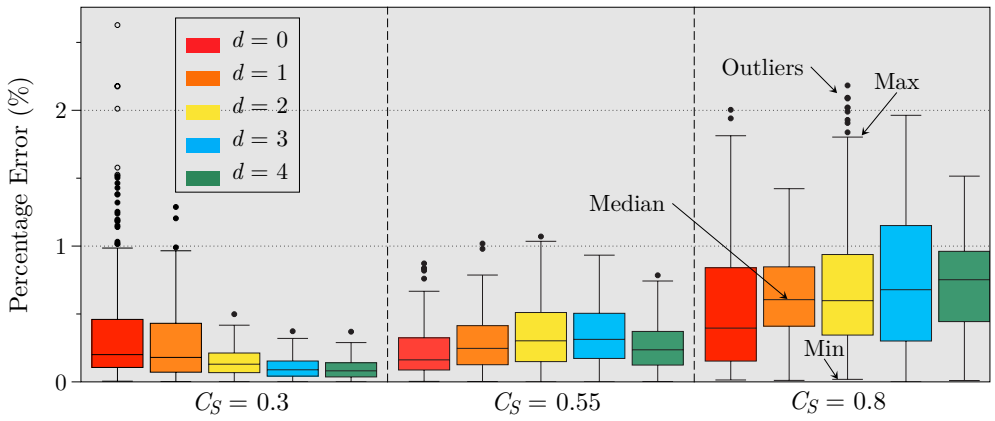

(a) $c = 1$

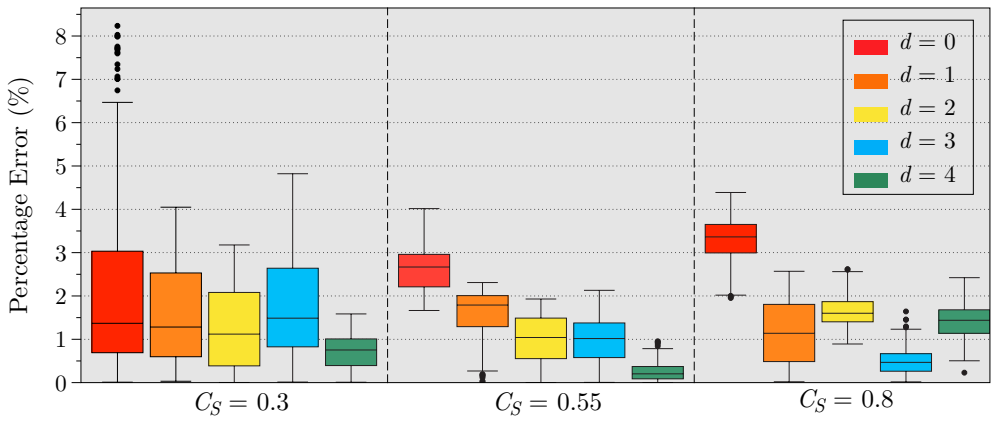

(b) $c = 2$

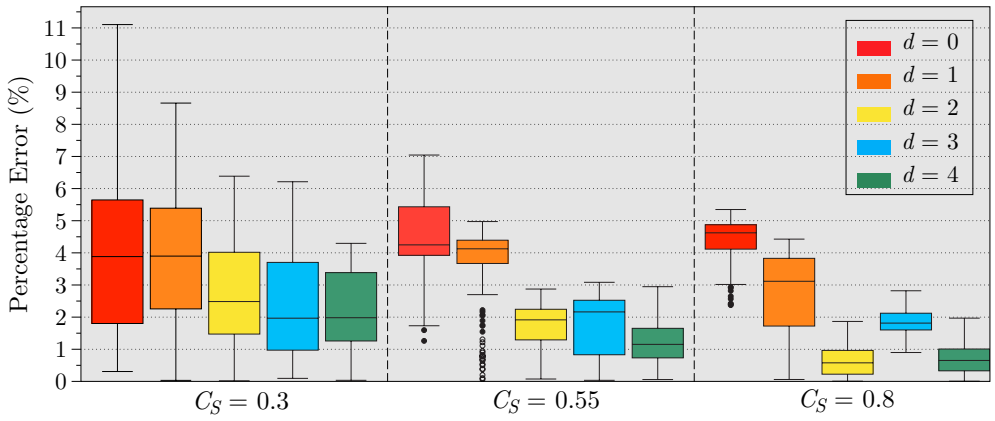

(c) $c = 3$

Figure 2.9: Box plots of percentage error between approximations and simulation results for near-side bus stops.

$\{0, 1, 2, 3, 4\}$, and $c = 1, 2, 3$, respectively. Comparisons between Figures 2.7c and e and between Figures 2.9a-c and Figures 2.10a-c unveil that the far-side stop models have larger errors when C_S is small, due to the greater sensitivity of far-side stop capacity to C. When C_S is large and $c = 2$ and 3, however, the far-side stop models

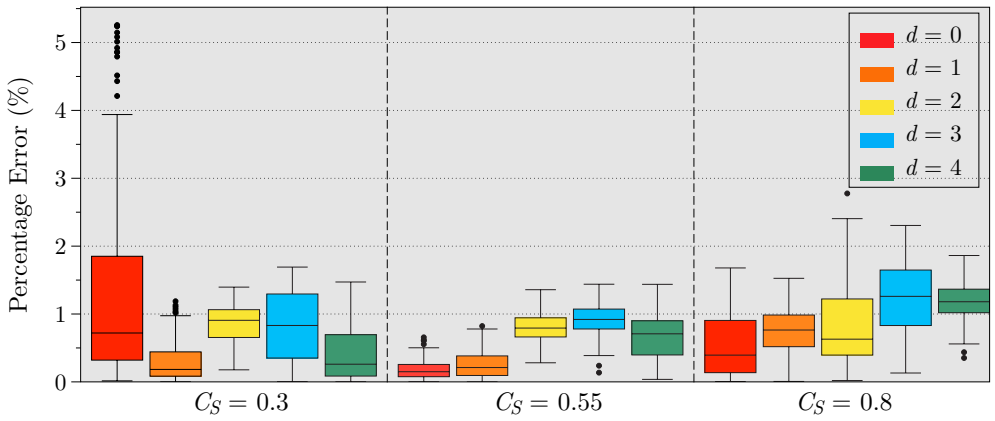

(a) $c = 1$

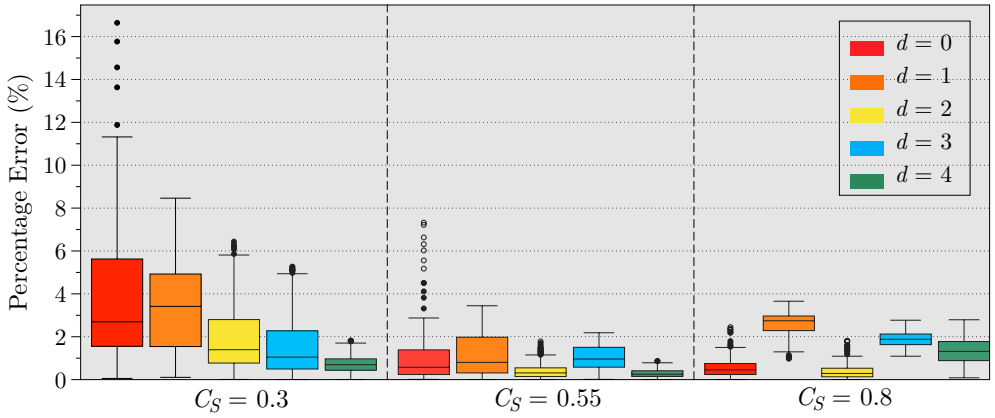

(b) $c = 2$

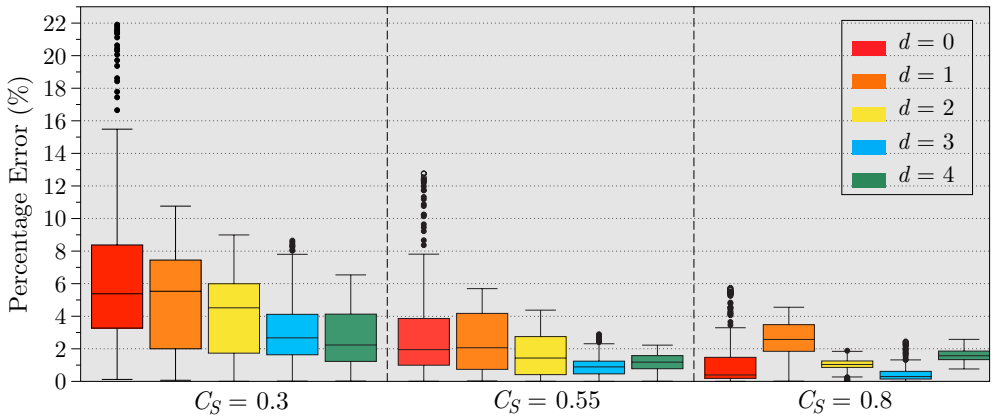

(c) $c = 3$

Figure 2.10: Box plots of percentage error between approximations and simulation results for far-side bus stops.

exhibit smaller errors than the near-side ones. This is mainly due to the larger error that occurs when estimating M in the multi-berth near-side stop model (see Appendix D).

Though only the results for $c = 1\sim3$ are shown here, our approximation also performs fairly good for $c = 4$, where the errors in most cases are far below 10%. For $c = 5$ and 6, however, errors between 10% and 20% appear more frequently, mainly because the convoy dwell time U^p has a very small coefficient of variation.

2.3.2 Comparison against the TCQSM capacity formula

We now use the same simulation results to validate the TCQSM formula (1.1), and compare its accuracy with our approximation. The capacity calculated from (1.1) is plotted as the dash-dot line in each of Figures 2.7a-f. The parameters in (1.1) take the following values: the effective berth number N_{el} is set to 1 and 1.75 for single and double-berth stops, respectively, according to Exhibit 6-63 in TCQSM (Kittelson & Associates, Inc., 2013); $f_{tb} = 1$ since we assume the bus operations are not affected by other traffic; the clearance time t_c is equal to τ_m since the re-entry delay is zero for bus stops located in dedicated lanes; the operating margin coefficient, Z, is set to 0.675 since TCQSM claims that this value would yield the maximum capacity of the stop; the mean dwell time $t_d = \mu_S$; and the coefficient of variation in dwell time $c_v = C_S$. The TCQSM formula is independent of the buffer size d and the cycle length C (given a fixed green ratio G/C). Hence, only one horizontal line is plotted in each of Figures 2.7a-f.

Comparison between the dash-dot curve and the solid curves unveils how far the TCQSM estimate is from the ground truth. Note first how the simulated capacity varies with C and d, and that these effects are totally ignored by the TCQSM formula. Even for the case of $d = 0$ (under which it is believed that the TCQSM formula is developed), the TCQSM formula's error is above 10% for most cases, and can be up to 50% (see Figure 2.7c). This is because the operating margin term in (1.1), Zc_vt_d, is too sensitive to c_v. Closer examination of the solid curves in these figures unveils that the ratio between the capacities of a 2-berth stop and a single-berth stop (given other parameter values are equal), i.e., the "effective number of berths" for a 2-berth curbside stop, is not a constant. In fact this ratio varies with all the relevant parameters examined here: C, d and C_S. Finally, the TCQSM formula treats the near- and far-side stops in the same way, while in reality a near-side stop produces a higher capacity than its far-side counterpart. (The reason of

this and more comparisons between near- and far-side stops are furnished in Section 2.4.2.)

2.4 Numerical analysis

We now examine broader ranges of numerical instances using the approximation models, i.e., equations (2.6), (2.10), (2.13) and (2.18), and discuss their practical implications. Section 2.4.1 examines the discounting effect of the neighboring signal on the stop's capacity, and how this effect depends on various operating factors, especially the buffer size d. Section 2.4.2 discusses which side of the intersection to better place a stop at, when the objective is to improve the bus-carrying capacity. We still use the parameter values in Table 2.1 in the following sections.

2.4.1 Capacity discounting effect of the signal

From equations (2.1) and (2.9), we see that the percentage capacity loss caused by the signal can be simply expressed by $\frac{E[T_B]}{C}$ for a single-berth stop and $\frac{E[T_B^{'}]}{C}$ for a multi-berth stop. Figures 2.11a and b plot this percentage capacity loss against the red period duration for instances with $C_S = 0.4$ and 0.8, respectively. Each figure contains 12 curves representing 12 scenarios with $c \in \{1, 2, 3\}$ and $d \in \{0, 1, 2, 3\}$. We use different line types to mark curves with different c: solid for $c = 1$, dotted for $c = 2$, and dashed for $c = 3$; and different colors to mark curves with different d: black for $d = 0$, red for $d = 1$, blue for $d = 2$, and green for $d = 3$. We choose red period duration as the horizontal axis because the numerators of percentage capacity loss, $E[T_B]$ and $E[T_B^{'}]$, are functions of red period duration only, and are independent of C. The scaling effect of C on the percentage capacity loss can thus be isolated from other factors, and be simply illustrated by using different vertical axes, one for each value of C. (Three vertical axes for $C = 100\,\text{s}$, $130\,\text{s}$ and $160\,\text{s}$, respectively, are used in the figures.)

In each figure, comparing the curves of the same line type unveils that the capacity loss drops rapidly as d grows. For example, note how the capacity loss drops from 55% to 3% when d increases from 0 to 3 for a single-berth stop with $C = 100\,\text{s}$ and a red period of $70\,\text{s}$, as marked by the four black dots in Figure 2.11a. For a larger c, the capacity loss drops with the increase of d at a slower speed. This is intuitive because more buffer spaces are needed to mitigate the signal's negative impacts on the capacity of a large stop. Similar results are also observed for far-side stops, which are omitted here in the interest of brevity.

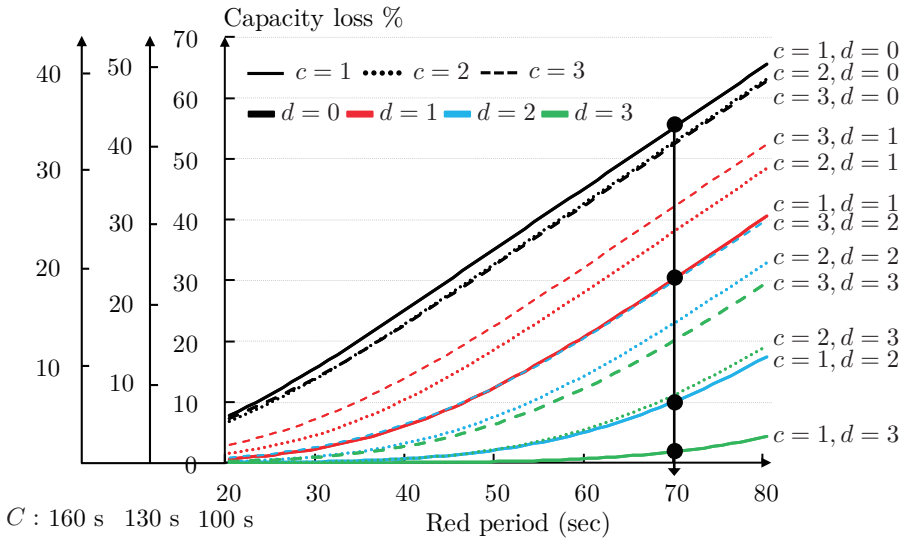

(a) $C_S = 0.4$

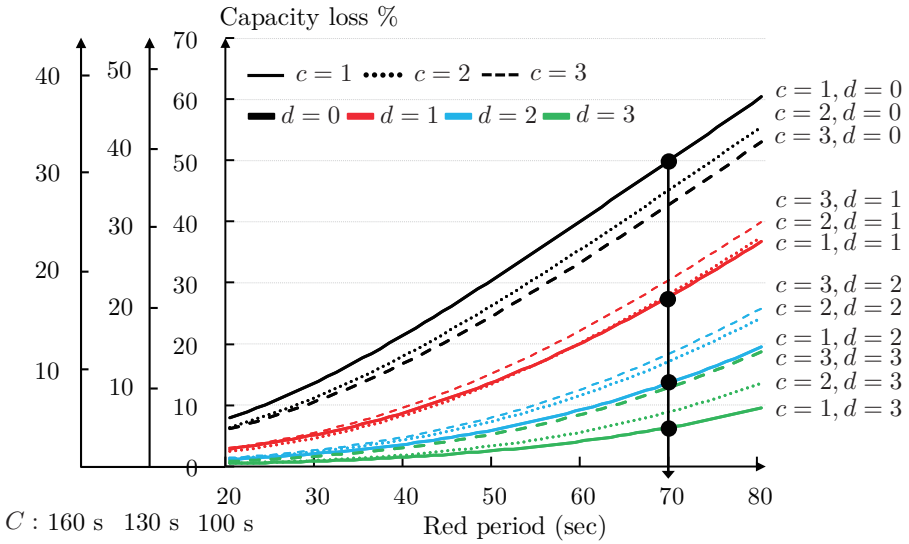

(b) $C_S = 0.8$

Figure 2.11: Percentage capacity loss resulting from the signal for near-side stops.

The above results can be used to determine how far from the intersection a stop should be placed to achieve a certain percentage, θ, of an isolated stop's capacity. This is useful in practice because transit agencies often prefer to place a stop in the proximity of the intersection to facilitate patrons' access and transfers, and to reduce the number of unprotected street crossings (Fitzpatrick et al., 1996). The buffer size d required to achieve a target percentage θ is a function of c, C_S, C, and G/C, which can be calculated numerically from (2.6) and (2.13) for single-berth stops, and (2.10) and (2.18) for multi-berth stops. Some tabulated values of the critical d for near-side stops when $\theta = 95\%$ are furnished in Appendix F.

The effect of c on the capacity loss is a little more complicated. When $d = 0$, the capacity loss decreases as c grows. This is because only one convoy is served in an extended red period, and a larger convoy will increase the utilization of the red period. On the other hand, the capacity loss increases with c for any $d > 0$, since in this case the number of convoys that can be served in an extended red period drops as c grows. Lastly, comparison between Figures 2.11a and b unveils that for multi-berth stops, the damage done by the signal is smaller for a larger C_S. This is because a larger C_S renders a longer convoy service time, and thus more of an extended red period will be utilized for serving the convoys. However, this is not true for single-berth stops.

2.4.2 Comparison between near- and far-side stops

There has been a long debate on which side of the intersection is better for the placement of a bus stop (Terry and Thomas, 1971; Fitzpatrick et al., 1996). Factors that may affect this decision include safety reasons, potential conflicts between dwelling buses and turning traffic, patron accessibility, etc. (Fitzpatrick et al., 1996). There exist a number of studies that quantified and compared the benefits and costs of near- and far-side stops. But most of them have significant limitations because they relied on simulation of specific stop layouts or empirical data collected from specific sites (Zhao et al., 2007; Li et al., 2012; Diab and El-Geneidy, 2015; Cvitanić, 2017). On the other hand, computationally efficient analytical models that can be used to examine the general cases are rare. The latter kind of models include Furth and SanClemente (2006) and Gu et al. (2014). However, these two works focused on comparing the bus and car delays at near- and far-side stops where at most one bus would arrive in each signal cycle. Thus they said nothing about busy bus stops where bus queues are often present.

Using our approximation models, we plot in Figure 2.12a the percentage of difference in capacity between near- and far-side stops, $\frac{Q_{\text{ns}}-Q_{\text{fs}}}{Q_{\text{ns}}}$, where Q_{ns} and Q_{fs} denote the capacities of near-side and far-side stops, respectively. Four curves are plotted in the figure for $D = 2, 3, 4, 5$ (normalized), respectively, and for $c = 2$, $d = 2$, $G/C = 0.5$ and $C_S = 0.5$. All the four curves are above 0, which indicates that a near-side stop always produces a higher bus-carrying capacity than its far-side counterpart, should other conditions be the same. This is mainly because a far-side stop's extended red period is longer than that of a near-side stop due to the extra term of Dt_m; see the equations of $\bar{R}$ in Section 2.1.1, $\bar{R}^p$ in Section 2.1.2, $\bar{R}^F$ in Section 2.2.1, and $\bar{R}^{Fp}$ in Section 2.2.2. The term Dt_m is added because at a far-side stop buses queued upstream have to travel across the intersection to reach the stop. This also explains

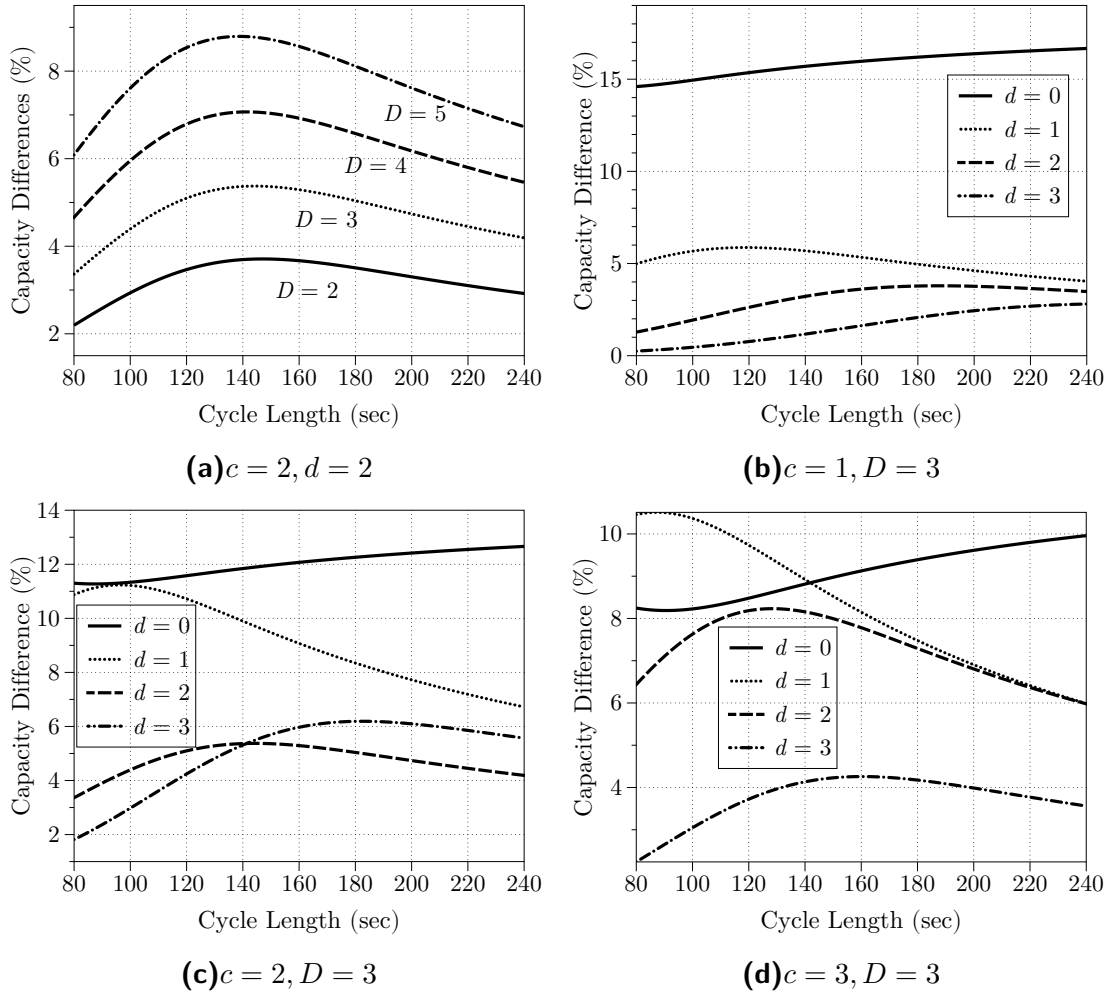

Figure 2.12: Capacity comparison between near- and far-side stops with $G/C = 0.5$ and $C_S = 0.5$.

why the capacity difference diminishes as D decreases, as shown in the figure. Hence, a bus stop should be placed at the near side of an intersection, if the bus-carrying capacity is the major concern. Interestingly, this is on the contrary to the finding in Gu et al. (2014), which states that far-side stops are more favorable since they produce less bus delay than near-side ones. Note again that the above-cited work applies only to stops with low to medium bus traffic.

We further plot the percentage capacity differences against C for $c = 1, 2, 3$ in Figures 2.12b-d, respectively, where D is assumed to be 3. Each figure contains four curves representing the cases of $d = 0, 1, 2, 3$, respectively. The figures show that the advantage of near-side stops by-and-large diminishes as d increases. This is also intuitive because when d is sufficiently large, the capacities of near- and far-side stops both approach that of an isolated stop. Figure 2.12b also shows that a single-berth far-side stop is particularly unproductive when $d = 0$ (over 15% capacity

difference for $d = 0$ versus less than 6% for $d = 1$). This can also be explained using our models: note in this case that the time gap between two consecutive buses increases from τ_m to $\tau_m + Dt_m$ (see Section 2.2.1). In Figures 2.12c and d, however, the gap between the capacity differences for $d = 0$ and $d = 1$ becomes smaller. This is because, for far-side stops with $c > 1$, a convoy will discharge through the intersection together, which dilutes the negative effect of the extra term Dt_m.

2.5 Summary

This chapter develops analytical approximations for single- and multi-berth curbside stops located in dedicated bus lanes and near signalized intersections. The approximations are derived using time-space diagrams of bus trajectories and probabilistic methods. The approximations have closed-form formulas, except for the standard normal CDF (i.e. $\Phi(r)$), which itself has several good closed-form approximations in the literature (e.g. Vazquez-Leal et al., 2012). The models explicitly account for the effects of key operating factors that were overlooked in the literature (e.g., the signal cycle length and the buffer size) and the characteristics of bus traffic (e.g., the move-up time and reaction time). Extensive simulation tests manifest that in most cases the approximation error is within 5%. Larger approximation errors may arise when C_S is small, c is large, and d is small.

Practical implications of this work are discussed in Section 2.5.1. Section 2.5.2 justify the necessity of analytical models. Section 2.5.3 introduces the potential extensions of this work.

2.5.1 Practical implications

Our accurate and computationally-efficient approximations can be conveniently used by practitioners to replace the flawed capacity formulas of curbside bus stops in the professional handbooks. They can be used, e.g., to determine the appropriate design and location of a new bus stop for serving a predicted peak-hour bus flow, or to assess the performance of measures for mitigating bus congestion at an existing stop. Measures to be considered would include adding berths and increasing the distance between stop and intersection (recall that our models can furnish critical distances needed to reduce or eliminate the capacity discounting effect of neighboring signals; see again Appendix F). Strategies that can reduce the mean and variance of bus dwell times (e.g., using wider bus doors, low-floor buses, and off-board fare collection) can also be assessed by our models for near- and far-side stops. In addition, practitioners may also consider to decrease the signal cycle length while

keeping the green ratio unchanged. This would reduce the red period duration and thus significantly increase a near- or far-side stop's capacity (see again Figures 2.7 and 2.11) without affecting the general-purpose (GP) traffic's discharging capacity at the intersection by much. (Note that this measure would be deemed to have no effect if the TCQSM formula (1.1) is used.) Finally, a congested far-side stop can be relocated to the near-side of intersection to gain up to 15% of additional capacity (see again Figures 2.12a-d), although this capacity gain diminishes as d increases.

2.5.2 Advantages of analytical model

Admittedly, many numerical results presented in this chapter can also be generated through simulation. Still, our analytical approach is useful due to the following reasons:

1. Some general insights can be immediately inferred from the capacity formulas or from our analytical derivation, but would be difficult to obtain directly from simulation. For example, equations (2.1) and (2.9) show that the percentage capacity loss due to the signal ($\frac{E[T_B]}{C}$ or $\frac{E[T_B^{'}]}{C}$) is inversely proportional to cycle length; and the formulas for $E[T_B]$ and $E[T_B^{'}]$ (e.g. equation (2.5)) reveal that this percentage capacity loss is a non-linear function of red period duration. Hence the effect of signal on bus-stop capacity is not as simple as described in the TCQSM formula (1.1). Built upon these insights, we further conclude that stop capacity can be increased by reducing red period duration (or cycle length) while keeping the green ratio unchanged. These insights also inspire us to create diagrams similar to Figures 2.11a and b, where the effects of cycle length and red period duration are clearly illustrated for stops with various sizes and locations. Note how these diagrams can be used by practitioners in the design of near- and far-side stops.

   As another example, note how the formulas of extended red periods reveal the significant differences between capacities of near-side and far-side stops, given that other conditions are equal. Capacity formulas for far-side stops with no buffer ($d = 0$) further unveil why this is a very bad design in terms of stop capacity. Note that it would be difficult to reveal and confirm these general findings using simulation results, since there are numerous scenarios to simulate under various operating parameters.

2. The analytical approach can help us better understand the cause-and-effect relationships behind the key factors affecting bus-stop capacity. Many findings from the numerical results can thus be explained; please refer to Section 3.2

for details. Understanding of these findings is very useful for practitioners to make appropriate design decisions under diverse operating environments. On the other hand, simulations are "black boxes" that usually cannot furnish straightforward explanations of those causal relations.

3. Parsimonious analytical models are always desirable for their convenience in practical use. This is why simple formulas or procedures described in professional handbooks (e.g. TCQSM and HCM) are still embraced by practitioners despite their well-known flaws, and despite the fact that commercial simulation tools become more and more powerful today. In addition, simulation is often much more time-consuming than applying analytical formulas (even if the latter may require some numerical computation, like in our case). In practice, an accurate analytical model can be used in the initial stage of a design project to identify a few promising options, and the more detailed and realistic simulation can be employed to select from those few design options and fine-tune the final design.

2.5.3 Potential extensions

To be sure, our approximations are limited in that they apply only to scenarios where: i) an exclusive bus lane is present; ii) the green period is long enough to discharge all the queued buses for a near-side stop, or to fill up the vacant buffer and berths of a far-side stop; and iii) bus overtaking maneuvers are prohibited. Potential extensions of the present work to address some of the above limitations are discussed as follows.

In reality, buses discharging from a near-side stop may compete against right-turning GP traffic for the buffer space. For this case, the distribution of buffer spaces occupied by right-turning vehicles can be approximated using right-turning vehicles' arrival process and the bus discharge rate into the buffer. This distribution can then be incorporated into our stop capacity approximation to account for the impact of right-turning traffic. A similar approach can be used to account for the impact of (through-moving) GP vehicle queues on the capacity of a near-side bus bay stop, where exiting buses have to merge back to the GP traffic lanes. For far-side bus bay stops without bus lane, exiting buses may be blocked when they are waiting for a sufficient gap in the GP traffic to merge back. This effect can be estimated by incorporating a stochastic merge model into the approximation.

For a near-side stop, if the green period is too short to discharge $c + d$ queued buses, residual bus queues may exist in the buffer at the end of some green peri-

ods. This case is difficult to model since bus operations in neighboring cycles are highly correlated. One potential approach is to model the residual queue lengths by a Markov chain, but closed-form approximations of stop capacity would not be available. Fortunately, such a case is rare in reality (see Footnote 4). On the other hand, a far-side stop with a short green period is equivalent to a far-side stop with a smaller buffer, for which our present approximations can be directly applied.

3 Simulation Assessments of Bus-Holding Strategies for Busy Corridors

This chapter evaluates both, bus convoying and headway regularization for busy corridors with bus queues at stops. The effectiveness in reducing bus queues is tested for wide-ranging cases involving homogeneous corridors where each stop has the same number of berths and patron demand. The strategies are compared head-to-head and against the do-nothing alternative. Experiments are controlled to eliminate confounding factors.

In that queueing dynamics in bus corridors render analytical models intractable[1], present evaluations were performed using simulation. Existing simulation models either: were developed for a single bus stop (Gibson et al., 1989; Fernández, 2010); fail to account for bus queues at stops (Wu et al., 2017); or require calibration of numerous parameters (Cortés et al., 2005, 2007). The latter concern can make it difficult to evaluate wide-ranging conditions, and can obscure factors that contribute most to a holding strategy's effectiveness. A parsimonious simulation model of multi-line bus operations was therefore developed in-house and used for the present analysis.

Simulation experiments confirm that queues and variability in headways grow as buses progress along a corridor. Contrary to previous reports, convoying buses was found to increase bus delay and headway variability. In contrast, the headway-regularizing strategy reduced these negative outcomes.

Present means of abstracting and simulating corridor operations with and without the bus-holding strategies are detailed in Section 3.1. Parametric analyses of the strategies and their comparisons head-to-head and against a do-nothing alternative are presented in Section 3.2. Practical implications of the findings, particularly in regard to the deployment of headway regularization are described in Section 3.3. Included there is discussion on how technologies might advance real-world deployments.

[1]To appreciate this intractability, note that a corridor with multiple bus stops is a queueing network (Shortle et al., 2018), and that each node (i.e., each multi-berth stop) is a polling system that itself is difficult to solve (e.g., Takagi, 1988).

3.1 The Corridor Model

Our abstractions of the corridor and its bus operations are presented in Section 3.1.1. The two control strategies, including the means of holding and releasing buses, are discussed in Section 3.1.2. The performance metrics for the strategies and the do-nothing alternative are presented in Section 3.1.3. Issues concerning simulation development and experiments are discussed in Section 3.1.4. Notations are defined when introduced, and are presented again in Appendix A for the reader's convenience.

3.1.1 Abstractions

Consider a corridor serving L bus lines. The lines may originate at different locations upstream, and merge onto the corridor, as in the example shown in Figure 3.1. The lines run through N multiple-berth stops inside the corridor and diverge downstream. Assume that: each stop has the same number of berths, denoted c; and each line has the same service frequency, $\frac{f}{L}$, where f is the corridor's bus flow across all lines combined. The scheduled bus headway on each line, H, is therefore $\frac{L}{f}$. Denote as $a^0_{l,j}$ the arrival time of bus j on line l ($l \in \{1, 2, ..., L\}, j \in \{1, 2, ...\}$) at the corridor's upstream end. Assume $a^0_{l,j}$ is a Gaussian random variable with mean jH and standard deviation $C_H H$, where C_H is a coefficient of specified value.[2]

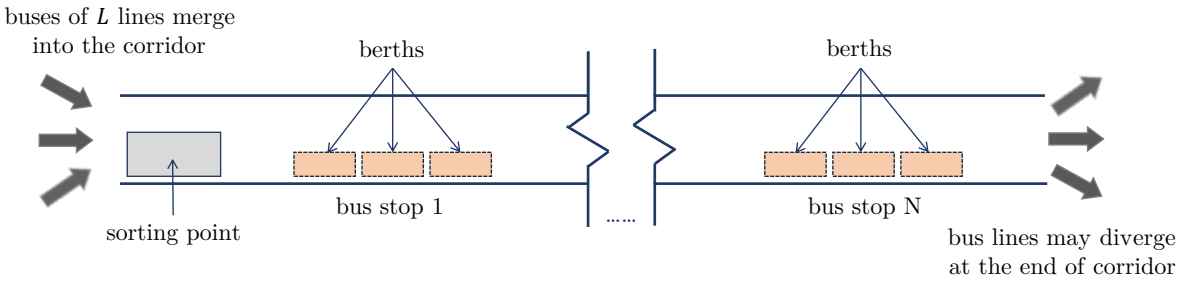

Figure 3.1: Corridor layout ($c = 3$).

At each stop along the corridor, buses enter and exit berths in first-in-first-out fashion, meaning that overtaking maneuvers are prohibited, as in Gu et al. (2011, 2015) and Shen et al. (2019). An arriving bus must therefore enter a queue if the stop's upstream-most berth is occupied. The delay imposed by this queue at stop s to bus j on line l is denoted $q^s_{l,j}$. When a bus finishes loading and unloading its patrons, it may be blocked by another bus occupying a downstream berth in the

[2] Our simulation tests found that using other distributions for $a^0_{l,j}$ produces only marginal differences in outcomes.

same stop. The ensuing in-berth delay is denoted $b^s_{l,j}$. A bus's departure time from a stop is therefore:

$$d^s_{l,j} = a^s_{l,j} + q^s_{l,j} + S^s_{l,j} + b^s_{l,j}, l \in \{1, 2, ..., L\}, j \in \{1, 2, 3, ...\}, s \in \{1, 2, ..., N\}, \quad (3.1)$$

where $a^s_{l,j}$ and $d^s_{l,j}$ denote the arrival and departure times, respectively, at stop s for bus j on line l; and $S^s_{l,j}$ the bus's dwell time for loading and unloading patrons. Assume that the bus queues that form at a stop are not affected by queues from other nearby bottlenecks, e.g., traffic signals. The two delay terms, $q^s_{l,j}$ and $b^s_{l,j}$, will be determined dynamically in the simulation.

Assume that $S^s_{l,j}$ is dictated by the number of boarding patrons[3]; i.e.,

$$S^s_{l,j} = \alpha + \beta p^s_{l,j}, l \in \{1, 2, ..., L\}, j \in \{1, 2, 3, ...\}, s \in \{1, 2, ..., N\}, \quad (3.2)$$

where $p^s_{l,j}$ denotes the number of boarding patrons for bus j of line l; α the lost time due to bus acceleration and deceleration at a stop; and β the boarding time per patron. Making this assumption allows us to model the propagations of bus queue and headways along the corridor. If we just assume the dwell time of each bus to be a random variable following some distributions like in Chapter 2, correlations between bus queues at neighboring stops would be neglected.

To estimate the $p^s_{l,j}$, note that a boarding patron may take more than one bus line if her destination stop is served by multiple lines (Cominetti and Correa, 2001; Schmöcker et al., 2016; Laskaris et al., 2018). These common-line trips are modeled by dividing the L bus lines into n line groups, each consisting of $\frac{L}{n}$ lines[4] that share a certain proportion of common-line patrons, $\gamma\,(0 \leq \gamma \leq 1)$. Patrons are assumed to arrive at a stop at constant rate λ, and are divided into n equally-sized demand groups. Assume that patrons in each of the n demand groups will take only buses that belong to a specific line group; i.e., no patron can take two lines that belong to different groups. Thus, common-line patrons arrive at a line group at rate $\gamma \cdot \frac{\lambda}{n}$, and can take any of the $\frac{L}{n}$ lines in that group. Non-common-line patrons arrive at the line group at rate $(1-\gamma)\frac{\lambda}{n}$. Those patrons are further divided into $\frac{L}{n}$ equally-sized subgroups, and patrons in each subgroup can only take a specified line in that group. The arrival rate of non-common-line patrons for a specific line is thus $(1-\gamma)\frac{\lambda}{L}$. Further assume that the number of berths at each stop matches

[3]The assumption has previously been used to simplify analysis (e.g., Daganzo, 2009).

[4]This implies that L is an integer multiple of n. We judge this simplification to be acceptable, since our aim is to examine how bus operations are affected by a few key factors.

the number of line groups, i.e., $c = n$. This assumption simplifies the simulation of bus convoying, as we shall see momentarily.

To illustrate the above ideas, consider a corridor that serves $L = 6$ lines that are divided into $n = 3$ line groups. Suppose $\gamma = 0.3$. Then for each of the 3 line groups, common-line patrons arrive at rate $\gamma \cdot \frac{\lambda}{n} = 0.1\lambda$, and non-common-line patrons arrive at each bus line at rate $(1-\gamma)\frac{\lambda}{L} = \frac{7}{60}\lambda$.

Three more assumptions are used to describe the patron boarding process:

(i) a bus arriving at a berth will admit all common- and non-common-line patrons who can take this bus, including those who arrive while the bus is dwelling;

(ii) if two buses belonging to the same line group are dwelling simultaneously at a stop, their common-line patrons will divide themselves into two equally-sized batches, with one batch heading for each bus; and

(iii) a bus has sufficient patron-carrying capacity, such that no patron is left behind.[5]

With the above assumptions, $p^s_{l,j}$ can be simulated for each bus at any stop. Note that the above abstractions simplify the modeling work and can highlight the effects of key parameters (i.e., c and γ) on bus queueing.

Finally, a bus's arrival time at stop $s+1$ is determined by:

$$a^{s+1}_{l,j} = d^s_{l,j} + t^s_{l,j}, l \in \{1, 2, ..., L\}, j \in \{1, 2, 3, ...\}, s \in \{1, 2, ..., N\}, \tag{3.3}$$

where $t^s_{l,j}$ denotes the inter-stop travel time of bus j of line l from stop s to stop $s+1$. The $t^s_{l,j}$ is assumed to follow a Gaussian distribution[6] with mean μ_T and variance σ^2_T, i.e., $t^s_{l,j} \sim \mathcal{N}(\mu_T, \sigma^2_T)$. The variance parameter σ^2_T indicates the level of disturbance to bus travel times between stops. For example, a lower σ^2_T may occur where a dedicated bus lane or signal priority schemes are deployed.

[5] This assumption is made to keep our model parsimonious. It allows us to simulate bus operations without knowing the full patron OD information. The same assumption was also made in Osuna and Newell (1972), Daganzo (2009), and Schmöcker et al. (2016). We have also performed simulation tests where buses have a finite patron-carrying capacity. Results show that the findings presented in this thesis still hold under the finite capacity constraint.

[6] We have also performed simulation tests where inter-stop travel times follow other bell-shaped distributions like log-normal. They produce only marginal differences in outcomes.

3.1.2 Holding strategies

For the two strategies examined, buses are held, sorted and dispatched at a sorting point located at the corridor's upstream end; see again Figure 3.1. The sorting point contains c dedicated bus lanes, each serving a line group. Arriving buses of any line group will first queue in the assigned lane. Bus departures from a sorting point are controlled by signals installed at the downstream end of each lane.

Figure 3.2 illustrates a sorting point for a case of $L = 6$ and $n = c = 3$. (Similar layout structure can be found in the Sao Paulo pilot project (Szász et al., 1978) when the convoying strategy was first implemented.) Among the three line groups, line group A consists of lines 1 and 4, line group B lines 2 and 5, and line group C lines 3 and 6. The two strategies hold and release buses in the following two ways.

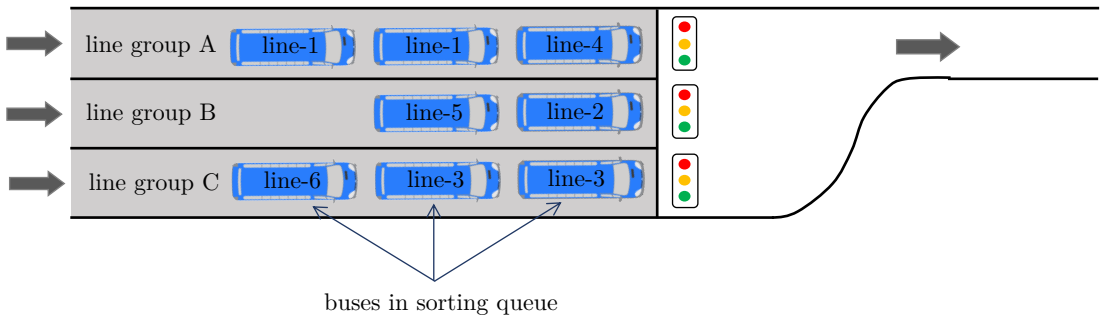

Figure 3.2: Layout of a sorting point ($L = 6, c = 3$).

The scheme presently used to convoy buses is similar to the one in Szász et al. (1978). Upon consolidating at the sorting point, one bus from each of the c line groups is released into the corridor as a single convoy. For the example shown in Figure 3.2, the three downstream-most buses (on lines 4, 2 and 3) are dispatched together. They arrive and depart all of the corridor's stops in unison. Convoy size (three in the present example) equals the number of berths in each stop, and each bus in a convoy is uniquely assigned to a berth. The distribution of a convoy's travel time between stops is dictated by its head bus and is $\mathcal{N}(\mu_T, \sigma_T^2)$.

Under the headway-regularizing strategy, buses are held at the sorting point[7] until a headway between consecutive bus departures from the same line group reaches $\frac{c}{L}H = \frac{c}{f}$. With Figure 3.2 again as the example, the departure headways between any two buses in the same line group would be no less than $\frac{H}{2}$. A bus arriving to an

[7] Thus, there is only one control point in our headway-regularizing strategy.

empty line group at a time greater than $\frac{c}{L}H$ since the group's previous departure is released into the corridor immediately.

Under either strategy, a sorting delay, denoted $w^0_{l,j}$, is incurred to bus j on line l. Assume for simplicity that travel time between the sorting point and stop 1 is zero. Hence, bus j on line l's arrival time to stop 1 is calculated as:

$$a^1_{l,j} = a^0_{l,j} + w^0_{l,j}, l \in \{1, 2, ..., L\}, j \in \{1, 2, 3, ...\}. \tag{3.4}$$

Under a do-nothing scheme, $w^0_{l,j}$ is set to 0 in the above equation.

3.1.3 Performance metrics

For both strategies and the do-nothing alternative, the following performance metrics are derived from the simulation:

(i) average bus delay at each stop s, given by:

$$w^s = E_{l\in\{1,2,...,L\},j\in\{1,2,...\}}[d^s_{l,j} - a^s_{l,j} - S^s_{l,j}], s \in \{1, 2, ..., N\}, \tag{3.5}$$

where $E_{l\in\{1,2,...,L\},j\in\{1,2,...\}}[\cdot]$ is the mean operator over all the buses from L lines;

(ii) average cumulative delay per bus upon departure from stop s, given by:

$$W^s = E_{l\in\{1,2,...,L\},j\in\{1,2,...\}}[w^0_{l,j}] + \sum_{i=1}^{s} w^s, s \in \{1, 2, ..., N\}; \tag{3.6}$$

(iii) average coefficient of variation in the buses' entry headways at stop s for any bus line. The entry headway is measured between two consecutive buses of the same line, and is given by:

$$C^s_E = E_{l\in\{1,2,...,L\}}\left[\frac{\sqrt{V_{j\in\{1,2,...\}}[a^s_{l,j+1} + q^s_{l,j+1} - a^s_{l,j} - q^s_{l,j}]}}{E_{j\in\{1,2,...\}}[a^s_{l,j+1} + q^s_{l,j+1} - a^s_{l,j} - q^s_{l,j}]}\right], \tag{3.7}$$

where $a^s_{l,j+1} + q^s_{l,j+1} - a^s_{l,j} - q^s_{l,j}$ is the entry headway at stop s between buses j and $j + 1$ of line l; $E_{l\in\{1,2,...,L\}}[\cdot]$ is the mean operator over all the L lines; and $V_{l\in\{1,2,...,L\}}[\cdot]$ is the variance operator over all the L lines. (Note that bus indices will be swapped if overtaking occurs between two buses of the same line on an interlink between stops.) This third metric is a proxy for bus

headway regularity at stop s. Entry headway was chosen because it is directly perceived by patrons waiting at the stop.

3.1.4 Simulation issues

A discrete-time simulation program was developed using C++ to emulate the corridor's bus operations. The program consists of four modules that describe operations: (1) at a sorting point; (2) on an inter-stop link; (3) at a bus stop; and (4) under patron boarding. These modules are executed sequentially at each time step. The program's entire logic is illustrated by the flowchart in Figure 3.3. A visualization tool of bus motion was also developed, which takes simulation outcomes as its inputs. The tool was used to examine potential programming errors. The program code can be downloaded from: https://github.com/Minyu-Shen/corrior-simulation.

Each simulation run starts with a 1-hour warm-up period, during which time patron arrival rate, λ, was set to a low value of 100 patrons/h/stop, and no bus holding was implemented. This warm-up time mimics an off-peak period when bus queues might appear occasionally, and only at some stops. This was followed by a 6-hour simulation period of a corridor's bus operations at a specified λ. Simulations were performed on a MacBook Pro 2015 with 2.2 GHz Intel Core i7 processor and 16 GB 1600 MHz DDR3 memory. A simulation run took 0.2 s on average to complete.

For each set of inputs, the simulation was repeated a certain number of times to ensure that the average performance metrics derived in Section 3.1.3 converged. The number was selected so that the estimated variances of w^s and C_E^s were not greater than 5×10^{-4} min^2 and 1×10^{-3}, respectively. One can refer to Section 11.7 of Ross (2014) for the calculation of this number. For illustration, Figure 3.4 plots the average w^{10}, w^{11}, and w^{12} for a 12-stop corridor against the number of repetitive runs under a do-nothing alternative with: $f = 100$ buses/h, $\lambda = 600$ patrons/h/stop, $\sigma_T = 10$ sec, $L = c = 3$, and $C_H = 0.4$. Note how the average bus delays converge when the number of runs exceeds 150.

3.2 Parametric Analysis

This section begins by exploring the impacts of the two bus-holding strategies under a range of patron demand for travel. Comparisons offered in Section 3.2.1 show that convoying is virtually always inferior to the do-nothing alternative. In contrast, the headway-regularization strategy is shown to outperform the do-nothing case on high-demand corridors that are long enough to contain at least 5 or 6 stops. Convoying is

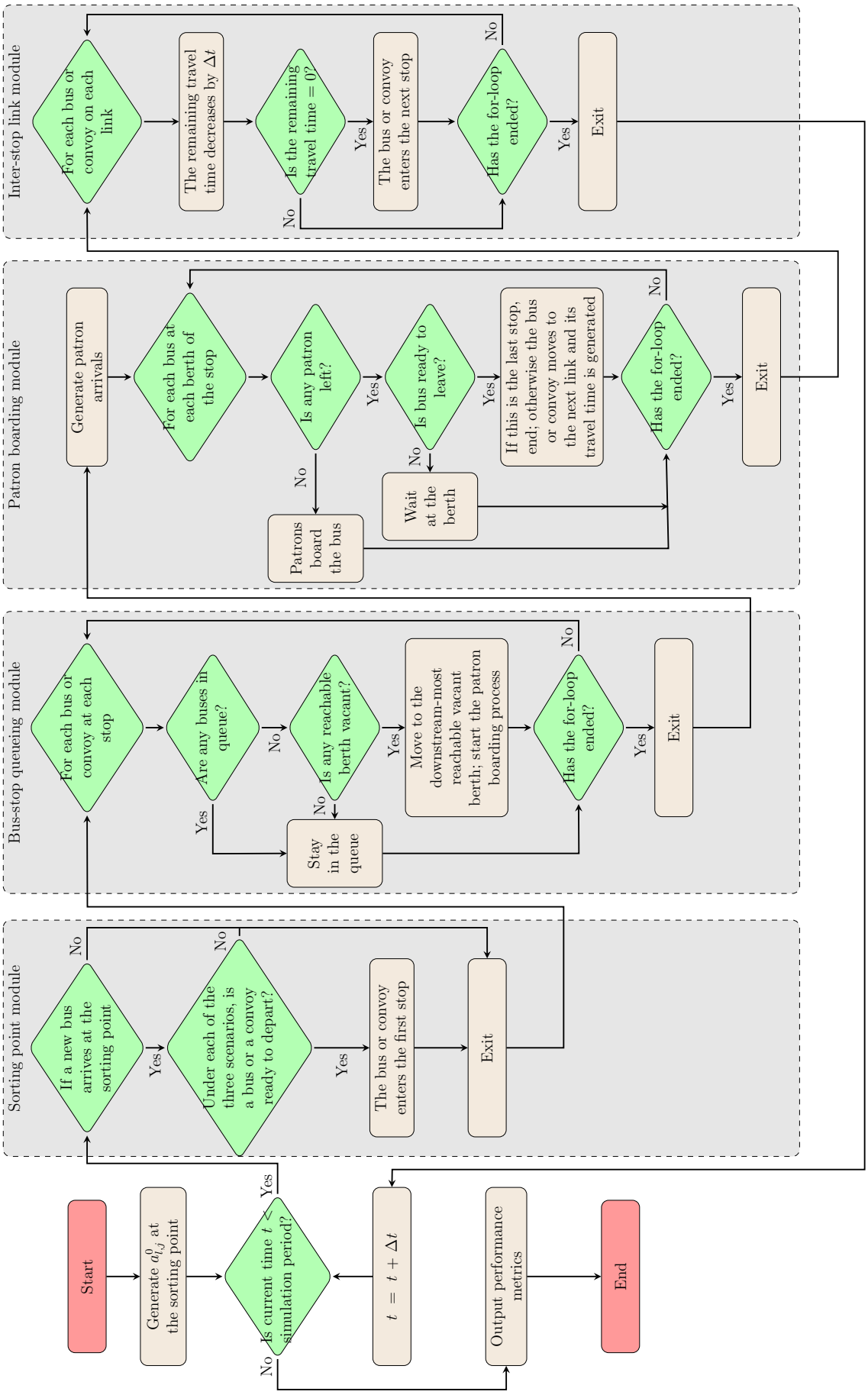

Figure 3.3: Flowchart of simulation.

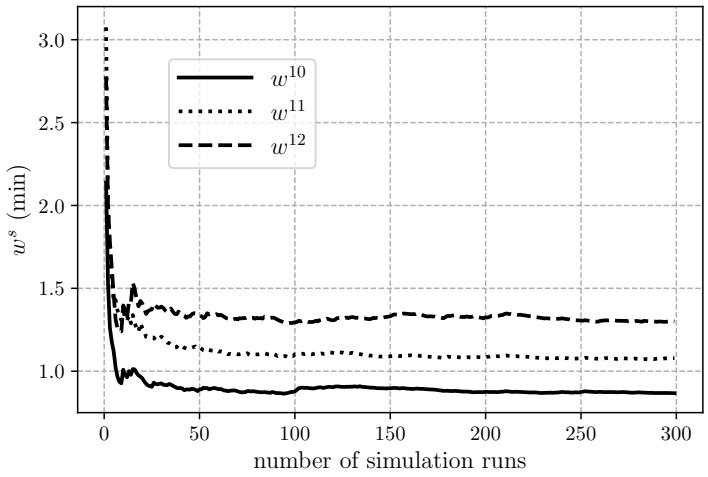

Figure 3.4: Convergence of average bus delays.

removed from further consideration in light of these findings. Sections 3.2.2-3.2.7 are instead dedicated to examining headway-regularization and the do-nothing option in parametric fashion. Comparisons in these latter sections are drawn for ranges of C_H, σ_T, f and other factors.

3.2.1 Demand effects

Discussion starts with Figures 3.5 and 3.6. Their graphs present curves of average and cumulative bus delays, w^s and W^s, respectively, at each of $N = 12$ stops along a corridor. Outcomes are collectively displayed for three patron demands: $\lambda \in \{300, 600, 800\}$ patrons/h/stop. In all cases, $f = 100$ buses/h; $L = c = 3$; $C_H = 0.4$; $\sigma_T = 10$ s; and $\mu_T = 4\sigma_T$[8]. The $\alpha = 8$ s and $\beta = 4$ s/patron, as in El-Geneidy and Surprenant-Legault (2010).

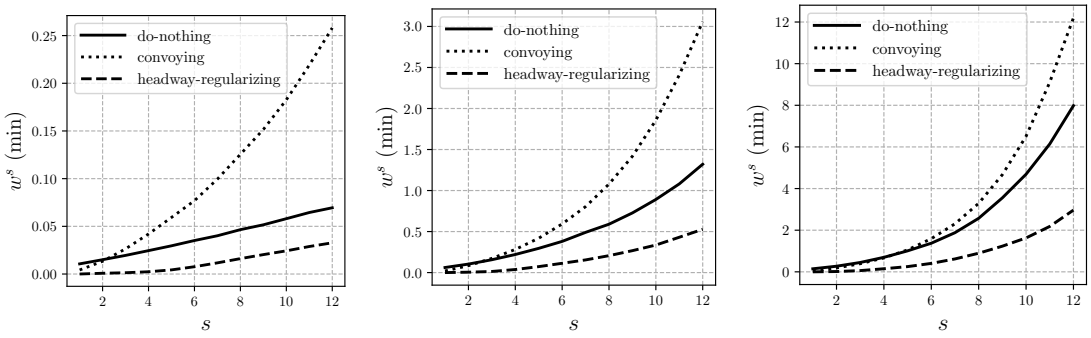

(a) $\lambda = 300$ patrons/h/stop **(b)** $\lambda = 600$ patrons/h/stop **(c)** $\lambda = 800$ patrons/h/stop

Figure 3.5: Comparison of strategies in terms of w^s.

[8]The μ_T was set to $4\sigma_T$ to ensure non-negative inter-stop trip times, but were excluded from analysis to focus instead on bus delays.

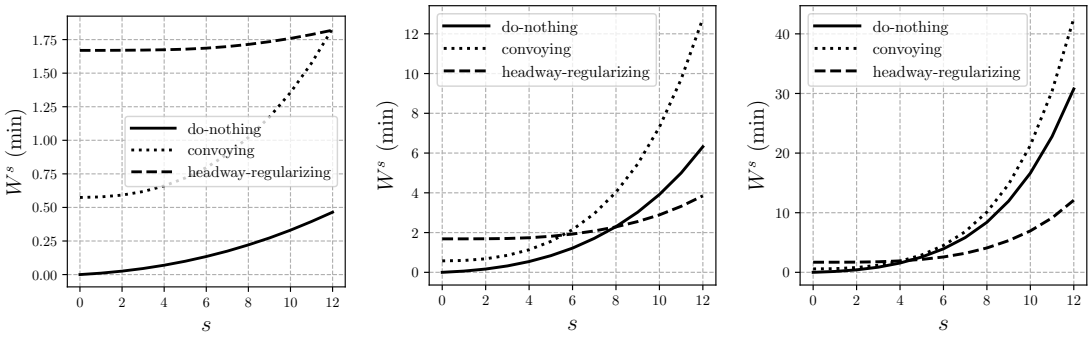

(a) $\lambda = 300$ patrons/h/stop **(b)** $\lambda = 600$ patrons/h/stop **(c)** $\lambda = 800$ patrons/h/stop

Figure 3.6: Comparison of strategies in terms of W^s.

Note from the curves how w^s and W^s always rise with stop number, s. This confirms that buses accrue more delay as they travel along a corridor.[9]

By visually comparing the dotted and solid curves in Figures 3.5 and 3.6, we further see that convoying generates greater bus delays than what occurs by doing nothing, irrespective of demand. Convoying's poor performance is at odds with previous reports; see for example Szász et al. (1978). It occurs because an entire convoy waits for all its constituent buses to be sorted, and waits again at each stop downstream for all its buses to complete their boardings and alightings. In light of this outcome, convoying is removed from further consideration.

Headway regularization is a different story. Turning now to the dashed and solid curves in Figures 3.5a-c, we see that for $s \geq 1$, headway regularization always produces lower w^s than that of doing nothing.

Of course, this second holding strategy creates bus delays at sorting points, and this is captured in the W^s shown in Figures 3.6a-c. One can view the W^s-curves as corridor-wide delays on corridors of specified N. This being the case, comparison of the dashed and solid curves shows that headway regularization saves corridor-wide delay in higher-demand cases with sufficient N. For demand $\lambda = 600$ patrons/h/stop, headway regularization is desirable on corridors with $N \geq 8$; see Figure 3.6b. For higher $\lambda = 800$ patrons/h/stop, an $N \geq 5$ is needed to justify the headway-regularizing strategy.

[9]The coefficient of variation in entry headways at s, C_E^s, was also found to increase with s, though evidence is omitted in the interest of brevity.

3.2.1.1 Closer look at headway regularization

The following two observations help explain the favorable impacts of headway regularization.

Observation 1 Regularizing headways at a corridor's upstream end diminishes headway variations at stops downstream; and

Observation 2 as a consequence of the first observation, buses encounter less delay in the queues that form at those stops.

Evidence and further discussion of these observations are furnished in Appendix G.

In light of its favorable performance, further tests of headway regularization are presented in the remainder of this section. The tests consist of: varying parameters one by one relative to the baseline conditions used in Section 3.2.1; and comparing bus delays against do-nothing alternatives with identical parameter values. Except where otherwise noted, tests feature $\lambda = 800$ patrons/h/stop, since headway regularization has shown itself suitable for corridors with high demands such as this.

3.2.2 Arrival deviations

The curves in Figure 3.7 display the savings in W^s achieved by headway regularization relative to the do-nothing alternative. One curve is presented for each of two values used for the deviation in bus arrival headways at a sorting point: $C_H \in \{0.2, 0.6\}$. Recall that $\lambda = 800$ patrons/h/stop, and that all other parameter values equal those used in Section 3.2.1.

By diminishing the headway variations that buses would otherwise exhibit as they begin traversing a corridor, headway regularization can diminish bus delays at stops downstream. Study of Figure 3.7 confirms that on corridors with sufficient N ($N \geq 5$ in the present cases), the value of headway regularization grows when buses have greater tendency to deviate from schedules.

3.2.3 Deviations in inter-stop trip times

Variation in trip times between stops naturally creates variation in the headways that buses exhibit in arriving at those stops. The effectiveness of headway regularization therefore diminishes as σ_T grows large.

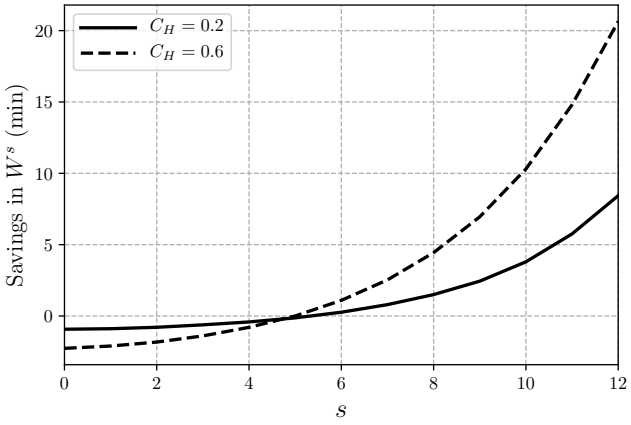

Figure 3.7: Effect of C_H.

This is confirmed via Figure 3.8. Its delay-savings curves were constructed using rather extreme values of $\sigma_T \in \{0, 30\}$ s. Note the smaller savings in W^s for the larger σ_T.

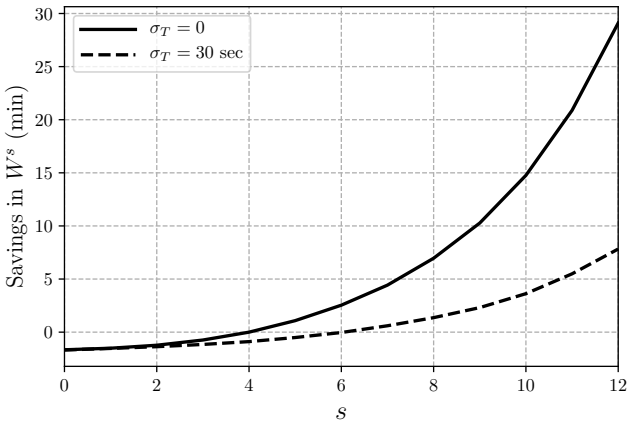

Figure 3.8: Effect of σ_T.

3.2.4 Bus flows

All else equal, larger bus headways (i.e., smaller bus flows, f) increase not only the average numbers of patrons boarding and alighting at a stop, but also the variances in these patron counts. This, in turn, increases the variability of bus dwell times at stops, and thus the variation in headways downstream.

This is unveiled in Figure 3.9, with its distinct curves for $f \in \{100, 200\}$ buses/h. Note how headway regularization can be especially effective under the lower f.

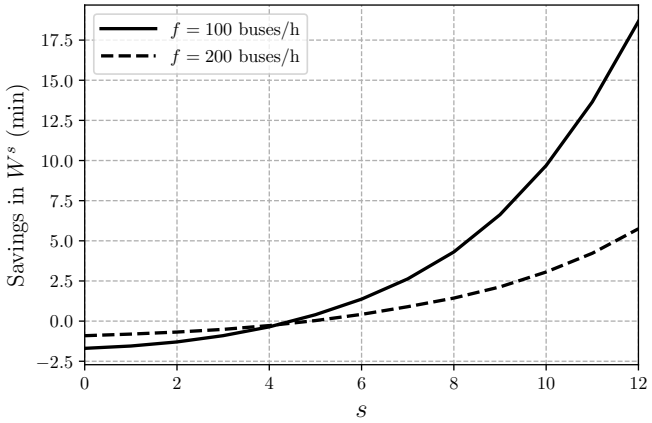

Figure 3.9: Effect of f.

3.2.5 Common-line patrons

We set a corridor's number of lines, $L = 6$; and its number of line groups, n, and berths per stop c, both at 3. We examine the effects of common-line patrons by setting $\gamma \in \{0.5, 1\}$. The latter value of γ describes a case in which all patrons are common-line ones, which is equivalent to a case in which $L = c = 3$, just as in Section 3.2.1.

With the larger portion of common-line patrons, a delayed bus will serve greater numbers of patrons at a stop, which only adds to the bus's delay. These unstable conditions can trigger bus bunching; e.g., see Schmöcker et al. (2016). Note from Figure 3.10 how delay savings are as a result larger for $\gamma = 1$.

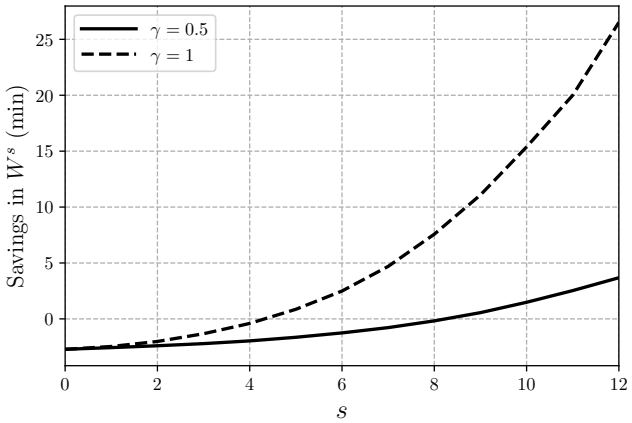

Figure 3.10: Effect of γ.

3.2.6 Number of lines

We set $L \in \{6, 9\}$; $c = 3$; $\gamma = 0.8$; and all other parameters, including f, to the baseline case. The impacts of headway regularization are only moderately sensitive

to f, as shown in Figure 3.11. If f instead increased proportionally with L, such that $\frac{f}{L}$ was constant, the regularization strategy would be less effective for reasons given in Section 3.2.4. If λ increased proportionally with L, the strategy would be more effective, as seen in Section 3.2.1.

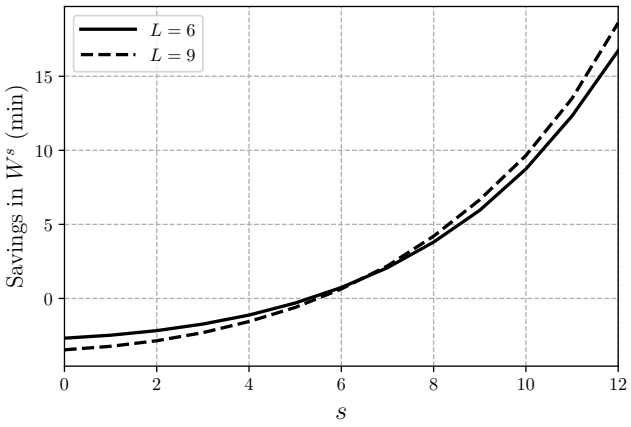

Figure 3.11: Effect of L.

3.2.7 Number of berths in a stop

We set berth size, $c \in \{3, 5\}$. To examine $c = 3$, we set: $f = 100$ buses/h; $\lambda = 800$ patrons/h/stop; and $L = 3$ so that each line group has only a single bus line. For $c = 5$, we set $f = \frac{500}{3}$ buses/h and $\lambda = \frac{4000}{3}$ patrons/h/stop, so that line frequency, $\frac{f}{L}$, and demand per line, $\frac{\lambda}{L}$, are kept the same as in the examination of $c = 3$.[10] In similar fashion, we set $L = 5$ so that the number of bus lines per line group is kept the same across both examinations.

Delay savings can be greater with larger c (i.e., $c = 5$), as evident in Figure 3.12 . Although c in this case increased proportionally with f and λ, bus delays at queued stops were larger with larger c, owing to the prohibition on overtaking maneuvers inside each stop; see Gu et al. (2015). Once again, headway regularization is seen to be especially effective when congestion grows large.

3.3 Summary

Present tests confirm that buses can encounter worsening conditions as they proceed through corridors with queued stops. Tests also show that this vicious cycle can become worse by dispatching buses in convoys. Previous studies that reported

[10] Holding f and λ fixed instead would have made for a trivial examination, since the larger c in that case would have obviously reduced bus queueing, and thus the benefit of headway regularization.

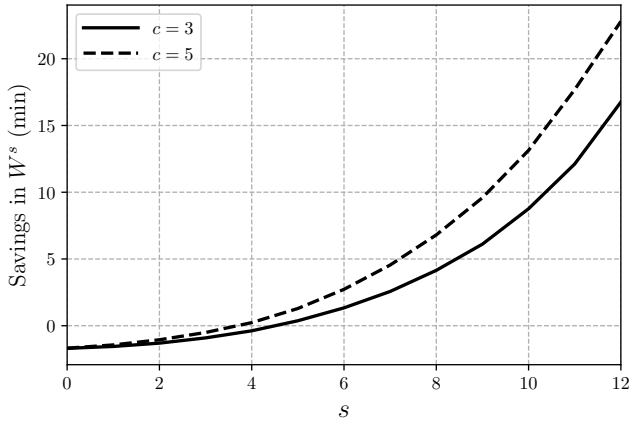

Figure 3.12: Effect of c.

otherwise were evidently plagued by a confounding factor: the addition of bus berths to a corridor's stops. Convoying itself is not an antidote to growing bus queues and delays.

In certain circumstances, headway regularization was found to be an effective remedy. Past studies have reported that delays inherent in regularizing bus entries into corridors are not offset by any savings incurred downstream. But those studies assumed a corridor's stops are free of bus queues. In the presence of these queues, we find that the delays at an upstream sorting point can be smaller than the delays saved downstream, provided that the corridor contains a sufficiently larger number of stops.

The findings unveil where and how to deploy headway regularization in real settings. Firstly, our parametric tests show that the strategy's advantages grow with diminishing bus flows and growing patron demands for travel. The busiest bus corridors would therefore seem the best settings. Tests also show how the effectiveness of headway regularization improves when buses' inter-stop trip times are less varied. This speaks to the potential value of deploying dedicated bus lanes (e.g., Burinskiene et al., 2014 or signal priority schemes (e.g., Baker et al., 2002) together with headway regularization. The strategy was also found to be more effective when bus lines share large proportions of common-line patrons who can reach their destinations via any one of multiple lines. Therefore, bus lines that serve distinct patron groups might best be assigned to distinct line groups at sorting points.[11]

[11] Headway regularization does not require that the number of line groups equal the number of berths in each stop. This is required only for convoying. The equality was preserved in the present work so as to draw fair comparisons across the two bus-holding strategies.

Even with the regularization strategy, headway variations and bus queueing will to some extent still grow stop-by-stop. On especially long corridors with many stops, buses might therefore be held (and headways regularized) at multiple, regularly-spaced sorting points. To minimize resulting delays to patrons on board, efforts can go to locating these points where onboard occupancies tend to be smallest.

The above findings came via a simulation model developed in-house. Its relatively simple logic and parsimonious structure can be used for other kinds of corridor studies; e.g., to determine a suitable number of berths per stop. Moreover, the model can be readily extended to accommodate a bus's patron-carrying capacity constraint, or corridors with inhomogeneous geometry and demand pattern; or to explore other more sophisticated headway-regularizing schemes, such as Daganzo and Pilachowski (2011) and Argote-Cabanero et al. (2015).

3.3.1 Implications in the era of connected and autonomous vehicles (CAVs)

For better or worse, the emergence of CAVs may spark renewed interest in bus convoying. After all, convoying trucks and other vehicles holds a promise of higher travel speeds (Liu et al., 2019), improved fuel efficiency (Mersky and Samaras, 2016) and reductions in other operating costs as well (Dai et al., 2020). Still, the present findings call into question whether benefits like these might outweigh the downside of convoying buses in busy corridors.

In contrast, CAV technologies could give a welcomed boost to the headway regularization of buses. For example, the technology might eliminate need for any sorting point by enabling bus-to-bus communication to control corridor entries and departures as well as travel speeds. The technologies might also advance the use of cooperative bus-control measures such as adaptive holding (Muñoz et al., 2013; He et al., 2019) and novel signal priority schemes (Estrada et al., 2016; Anderson and Daganzo, 2020).

4 Conclusions

Section 4.1 summarizes this dissertation's contributions. Section 4.2 discusses possible extensions of the current work.

4.1 Contributions

Analytical approximations are developed for estimating the bus-carrying capacities at near- and far-side stops under various operating conditions. Our approximations correct the flaws of the TCQSM formula by properly accounting for the effects of previously-overlooked key operating factors on stop capacity. Validations via self-developed simulation show that the approximations exhibit quite good accuracy. A number of managerial insights are also unveiled from extensive numerical case studies. For example, we find that, all else equal, a congested near-side stop can produce more capacity (up to 15%) than a far-side one, and a far-side stop with no buffer is a very bad design in terms of stop capacity. It is because at a far-side stop buses queued upstream have to travel across the intersection to reach the stop. Moreover, stop capacity can be increased by reducing red period duration (or cycle length) while keeping the green ratio unchanged. The fixed green ratio can ensure that the general-purpose traffic's discharging capacity will not be reduced by much.

The approximation models can be conveniently used by practitioners to determine a near- or far-side stop's bus-carrying capacity with several key input parameters, including the number of berths, the distance between stop and signal, the signal timing (cycle length and green ratio), and the distribution of bus dwell times. Inversely, practitioners can use the models to determine the number of berths and the critical distance needed for serving a predicted peak-hour bus flow; e.g., Appendix F furnishes some tabulated values of the critical distances that eliminate the capacity discounting effect of neighboring signals. Practitioners can also use these models to assess the performance of strategies for mitigating bus congestion at an existing stop. These strategies include means to reduce the mean and variance of bus dwell times (e.g., using wider bus doors, low-floor buses, and off-board fare collection) and signal timing plan.

At the corridor level, a parsimonious simulation model is developed to emulate multi-line bus operations in a congested corridor with multi-berth stops. The model accounts for the patron boarding process and mutual blockage between buses dwelling at curbside stops, and outputs the average bus queueing delays and coefficients of

variation in bus headways at each stop. The model is used to examine how the bus delays and headway variations vary along the corridor, and two bus-holding strategies that aim to mitigate bus queues. Due to its parsimonious nature, the simulation model is computationally efficient and thus enables us to draw general insights under various operating environments. Important findings include: (i) buses can encounter worsening conditions as they proceed through corridors with queued stops; (ii) the convoying strategy, which was believed to be beneficial by conventional wisdom, would actually render greater bus delays and headway variations. These reported benefit of convoying may actually come from the addition of berths; and (iii) past studies have reported that delays inherent in regularizing bus entries into corridors are not offset by any savings incurred downstream. But those studies assumed a corridor's stops are free of bus queues. In the presence of these queues, we find that the delays at an upstream sorting point can be smaller than the delays saved downstream, provided that the corridor contains a sufficiently larger number of stops. Key factors affecting the performance of the headway-regularizing strategy include the inter-stop travel time variations and common-line patron ratios.

The findings have practical implications. For example, when improving a corridor's overall capacity, the bus agency may consider building wider stops, and deploy passing lanes in the corridor's downstream segment. Moreover, to preserve the benefit of holding, buses may need to operate in a dedicated bus lane or adopt bus signal priority scheme. They can not only increase bus travel speed, but also reduce travel time variations. Under appropriate conditions, buses can also be held a second time in the middle of a corridor, so that bus delays and headway variations can be further reduced for downstream stops. Finally, bus lines that are associated with different demand groups should be assigned to different line groups for holding.

4.2 Future work

In addition to those potential extensions discussed at the end of Chapters 2 and 3, we also plan to conduct the following work in the future:

(i) At busy stops, transit agencies may pre-assign different bus lines into berths so that patrons can queue up after the specific berth for their target lines. The aim is to avoid chaos and conflict between the waiting queues. The simulation model in Chapter 3 can be adapted to quantify the impact of different berth allocation plan on the stop performance. Simulation-based

heuristic algorithm can then be designed to find the optimal plan that yields minimum bus queueing delay.

(ii) Develop smarter, adaptive holding strategies that may have better performance than the simple one investigated in Chapter 3. We will explore whether adaptive holding control schemes that are similar to Daganzo (2009) and Argote-Cabanero et al. (2015) can better improve both the bus travel speed and the service reliability. Particularly, we expect to identify a strategy that can efficiently combat large disturbances that may occur in buses' inter-stop travel. This strategy can be designed in a cooperative way such that the buses from different lines can communicate with each other for sharing the real-time position. This idea is currently being explored.

(iii) Extend the corridor simulation model in Chapter 3 to study the bus route design optimization, particularly for a BRT corridor shared by multiple lines. Previous studies on this topic either failed to incorporate the delays caused by the interaction between buses or used an over-simplified queueing delay model (e.g., Tirachini and Hensher, 2011). The decision variables include the bus frequency of each line, the number of berths of each stop, the stop spacings, and skip-stop schemes. The system performance metrics include queueing time, patron waiting time and in-vehicle travel time. The efficient simulation model in this thesis enables us to conduct simulation-based optimization for a wide range of operating conditions.

Appendix

A Tables of notation

Table A.1: List of notations used in Chapter 2

Notation	Description
Input parameters	
c	Number of berths
C	Cycle length
C_S	Coefficient of variation in bus dwell time
d	Number of buffer spaces
D	Length of signalized intersection
G	Green period duration
n, d_0	Parameters satisfying $d = nc + d_0$ when $n = 0, 1, 2, ...,$ and $0 \leq d_0 < c$
s_j	Jam spacing / berth length
t_m	Time for a bus to travel forward through one berth
τ	Reaction time of a bus
μ_S	Mean of bus dwell time
v_m	Bus's move-up speed
w	Backward wave speed of bus traffic
Other parameters and variables	
δ^L, δ^R	Start and end time of extended red period, respectively, for a multi-berth far-side stop
M	Number of buses in a multi-berth near-side stop at the start of an extended red period
$\bar{R}, \bar{R}^F$	Extended red periods for single-berth near- and far-side stops, respectively
$\bar{R}^p, \bar{R}^{Fp}$	Extended red periods for multi-berth near- and far-side stops, respectively
$\bar{R}^{F,d=0}, \bar{R}^{Fp,d=0}$	Extended red periods for single- and multi-berth far-side stops with $d = 0$, respectively
T_B, T_B^F	Times during which the stop is fully blocked for near-side stops or vacant for far-side stops, respectively

$T_B^{'}, T_B^{F'}$	Effective blockage time for a near-side stop and effective vacant time for a far-side stop, respectively
T_P, T_P^F	Times of serving the last small convoy (if any) for multi-berth near- and far-side stops, respectively
T_U, T_U^F	Total times for serving $n+1$ consecutive buses in an extended red period for single-berth near- and far-side stops, respectively; and total times for serving all the full-size convoys in an extended red period for multi-berth near- and far-side stops, respectively.
$T_U^{'}, T_U^{F'}$	Effective service time of full-size convoys for near- and far-side stops, respectively
$U_1^{'}, U_1^{p'}$	Portions of times for serving the first trapped bus (for single-berth stops) and convoy (for multi-berth stops) in the extended red period, respectively
U_j	Sum of dwell time, reaction time and move-up time of j-th bus.
U_j^p	Total time for serving the j-th convoy
$U^{p,x}$	Time for serving the last small convoy of size x in the extended red period
μ_T, σ_T^2	Mean and variance of T_U, respectively
$\mu_{T_U^{'}}, \sigma_{T_U^{'}}^2$	Mean and variance of $T_U^{'}$, respectively
$\mu_{T_U^{F'}}, \sigma_{T_U^{F'}}^2$	Mean and variance of $T_U^{F'}$, respectively

Table A.2: List of notations used in Chapter 3

Notation	Description
$a_{l,j}^0$	Arrival time of the j-th bus of line l to the corridor's start point
$a_{l,j}^s$	Arrival time of the j-th bus of line l to stop s
α	Time lost due to bus deceleration and acceleration, and door opening and closing at a stop
β	Boarding time per patron
$b_{l,j}^s$	In-berth delay of the j-th bus of line l at stop s
c	Number of berths
C_H	Coefficient of bus arrival time deviation at the corridor's start point.
C_A^s	Average coefficient of variation in the buses' arrival headways at stop s for any line
C_D^s	Average coefficient of variation in the buses' departure headways at stop s for any line

C_E^s	Average coefficient of variation in the buses' entry headways at stop s for any line
$d_{l,j}^s$	Departure time of the j-th bus of line l from stop s.
f	Total bus flow
γ	Ratio of common-line patrons shared by bus lines in a line group
H	Scheduled service headway within any bus line
λ	Total patron arrival rate per stop
L	Number of bus lines
μ_T	Mean bus travel time between two consecutive stops
n	Number of line groups
N	Number of stops in the corridor
$p_{l,j}^s$	Number of boarding patrons for the j-th bus of line l at stop s
$q_{l,j}^s$	Queueing delay of the j-th bus of line l at stop s.
σ_T	Standard deviation of bus travel time between two consecutive stops
$S_{l,j}^s$	Dwell time of the j-th bus of line l at stop s
$t_{l,j}^s$	Inter-stop travel time of the j-th bus of line l from stop s to stop $s+1$
$w_{l,j}^0$	Sorting delay of the j-th bus of line l at the sorting point
w^s	Average bus delay at stop s
W^s	Average cumulative delay per bus from the sorting point to stop s

B Derivation of approximations (2.7)

First, we have $E[U_j] = 1 + \tau_m$ and $Var(U_j) = Var(S_j) = C_S^2$. Due to the mutual independence between $U_1^{'}$ and U_j's, μ_T and σ_T^2 can be obtained as follows:

$$\begin{cases} \mu_T = n(1+\tau_m) + E[U_1^{'}]; \\ \sigma_T^2 = nC_S^2 + Var(U_1^{'}). \end{cases} \tag{B.1}$$

The $E[U_1^{'}]$ and $Var(U_1^{'})$ are derived by assuming that the start of the extended red period is a *random incidence* within a renewal process of consecutive bus departures from the stop. By the definition of random incidence (Larson and Odoni, 1981), the renewal interval that contains the random incidence, W, has the following PDF:

$$f_W(t) = \frac{t f_U(t)}{E[U]} = \frac{t f_S(t-\tau_m)}{1+\tau_m}, \tau_m \le t \le \infty, \tag{B.2}$$

where f_U is the PDF of $U_j = S_j + \tau_m (j = 1, 2, ..., n+1)$, and f_S is the PDF of S_j.

Conditioning on W, $U_1^{'}$ is uniformly distributed in $[0, W]$. Thus, we have:

$$E[U_1^{'}] = E\left[E[U_1^{'} \mid W]\right] = E\left[\frac{1}{2}W\right] = \frac{1}{2}\int_{\tau_m}^{\infty} t \cdot \frac{t f_S(t-\tau_m)}{1+\tau_m} dt$$
$$= \frac{1}{2(1+\tau_m)}\int_0^{\infty} (u+\tau_m)^2 \cdot f_S(u) du = \frac{E[S^2] + 2\tau_m + \tau_m^2}{2(1+\tau_m)}.$$

$$Var(U_1^{'}) = E\left[U_1^{'2}\right] - (E[U_1^{'}])^2 = E\left[E[U_1^{'2} \mid W]\right] - (E[U_1^{'}])^2 = E\left[\frac{1}{3}W^2\right] - (E[U_1^{'}])^2$$
$$= \frac{1}{3(1+\tau_m)}\int_0^{\infty} (u+\tau_m)^3 \cdot f_S(u) du - (E[U_1^{'}])^2$$
$$= \frac{E[S^3] + 3\tau_m E[S^2] + 3\tau_m^2 + \tau_m^3}{3(1+\tau_m)} - (E[U_1^{'}])^2.$$

Since S_j follows a gamma distribution with mean 1, by using its moment generating function, we can calculate that $E[S^2] = C_S^2 + 1$ and $E[S^3] = 2C_S^4 + 3C_S^2 + 1$. Thus, we have:

$$E[U_1^{'}] = \frac{C_S^2 + (\tau_m + 1)^2}{2(1+\tau_m)}; \tag{B.3}$$

$$Var(U_1^{'}) = \frac{5 + 8\tau_m}{12(1+\tau_m)^2} C_S^4 + \frac{1}{2} C_S^2 + \frac{(1+\tau_m)^2}{12}. \tag{B.4}$$

Plugging (B.3) and (B.4) into (B.1), we have:

$$\begin{cases} \mu_T \approx n(1+\tau_m) + \dfrac{C_S^2 + (1+\tau_m)^2}{2(1+\tau_m)}; \\ \sigma_T^2 \approx \dfrac{5 + 8\tau_m}{12(1+\tau_m)^2} C_S^4 + (\dfrac{1}{2} + n) C_S^2 + \dfrac{(1+\tau_m)^2}{12}. \end{cases} \tag{2.7}$$

The above approximations rely on the hypothetical uncorrelation between $U_1^{'}$ and signal timing. Their performance would be poor if C_S is small. For example, in the deterministic case where $C_S = 0, \tau_m = 0$ and $C - \bar{R} = 2.99$, we have $U_1^{'} = 0.01$, while (B.3) gives $E[U_1^{'}] = 0.5$. But if $C - \bar{R}$ increases slightly from 2.99 to 3.01, we would have $U_1^{'} = 0.99$ while (B.3) still gives $E[U_1^{'}] = 0.5$. Hence the distribution of $U_1^{'}$ and the stop capacity can be highly sensitive to signal timing when C_S is small. Note that if $C_S > 0$, the correlation between $U_1^{'}$ and signal phases diminishes as green duration increases, and so does the sensitivity of stop capacity to signal timing.

C Derivation of approximation (2.8)

Figure C.1 shows the bus trajectories of a 3-bus convoy dwelling at a 3-berth stop. From the figure, we have:

$$U^p = max\{S_1, S_2, ..., S_c\} + c\tau_m, \tag{C.1}$$

where $S_j (j = 1, 2, ..., c)$ denotes the dwell time of the j-th bus in the convoy. From

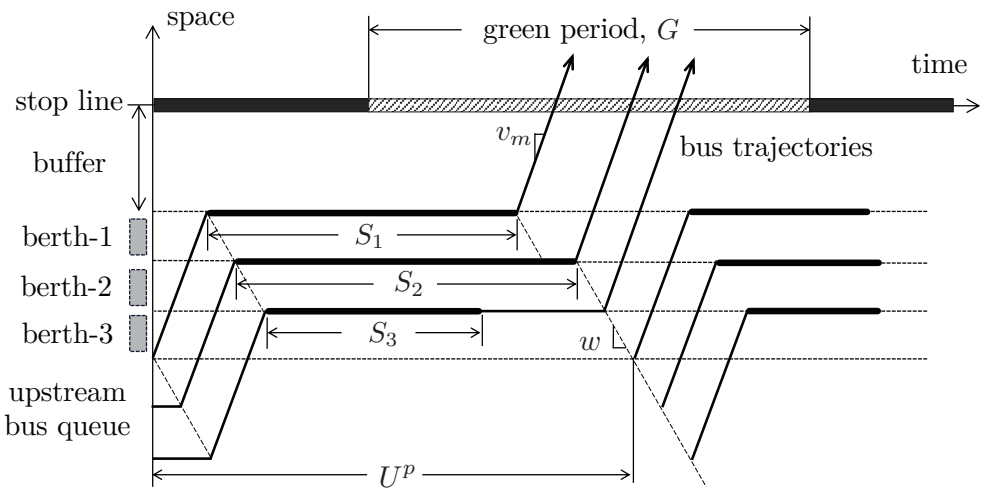

Figure C.1: Time-space diagram of bus operations at a 3-berth near-side stop.

(C.1), we can obtain the CDF of U^p as follows:

$$F_{U^p}(t) = (F_S(t - c\tau_m))^c \quad \text{for} \quad t \geq c\tau_m, \tag{C.2}$$

where F_S is the CDF of S_j. Since S_j is a non-negative continuous random variable, we have:

$$E[U^p] = c\tau_m + \int_0^\infty (1 - (F_S(t))^c)\, dt. \tag{C.3}$$

Similarly,

$$Var(U^p) = 2\int_0^\infty t\,(1 - (F_S(t))^c)\, dt - \left(\int_0^\infty (1 - (F_S(t))^c)\, dt\right)^2. \tag{C.4}$$

The two integrals in equations (C.3) and (C.4) are the first and second raw moments of the order statistic $max\{S_1, S_2, ..., S_c\}$; see David and Nagaraja (2004) for the detailed derivations. Unfortunately, there is neither closed-form expressions nor good approximations for these moments, save for a few very special cases (David and Nagaraja, 2004). In light of this, we here fit least squares models to tabulated

values of these moments when S_j follows a gamma distribution with $C_S \in [0.2, 1]$ and $1 \leq c \leq 6$. (Note that the above parameter ranges have covered most of the curbside stops in the real world; for example, Levinson and St. Jacques (1998) concluded from empirical data that $C_S \in [0.4, 0.8]$, and stops containing more than 6 berths are also rare in the real world.) The tabulated values were furnished by Gupta (1960) and Prescott (1974). Our best-fitted models selected from numerous candidates with various mathematical forms are:

$$\begin{cases} E[U^p] \approx h(c, C_S) \equiv 0.7931 C_S \log(c) + 0.9911 + c\tau_m; \\ Var(U^p) \approx q(c, C_S) \equiv 0.6819 C_S^3 \arctan(c) + 0.5102 C_S^2. \end{cases} \tag{2.8}$$

The goodness-of-fit of (2.8) is illustrated in Figure C.2a for $E[U^p]$ and Figure C.2b for $Var(U^p)$ for the realistic ranges of c and C_S, where the dashed curves represent the fitted models and the solid curves represent the tabulated values furnished by the literature. The root-mean-square error (RMSE) of the above models are 0.0125 and 0.0131, respectively; and the R-squared values are 0.9984 and 0.9992, respectively.

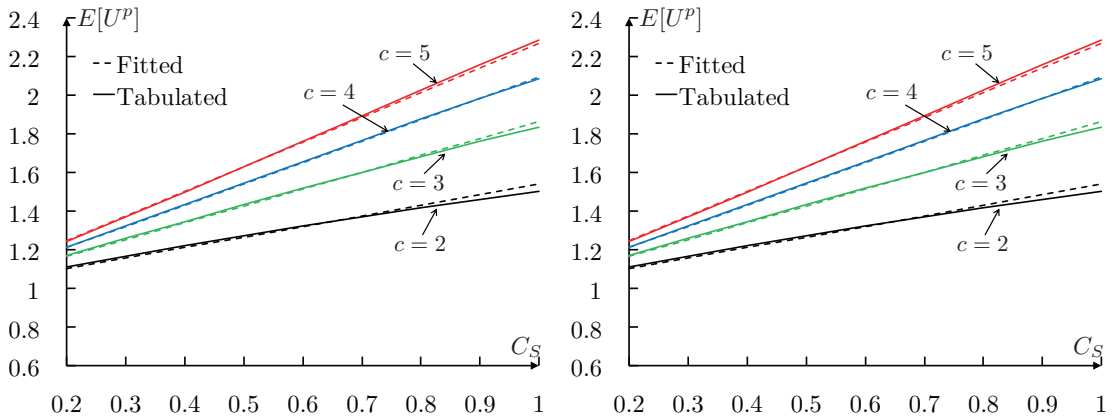

Figure C.2: Goodness-of-fit for (2.8).

D Derivation of approximations (2.11)

The T_U' depends on T_U, N_P, and T_P, which all depend upon the number of buses in the stop at the start of the extended red period. We denote this number as M ($1 \leq M \leq c$). (Note that some of these M buses may have completed their services, but they are blocked by buses residing in the downstream berths.) Depending on the value of M, the following three cases may arise:

1. If $M < d_0$, $(n+1)$ full-size convoys can be served following the first convoy in the extended red period. The $(n+3)$-th convoy would be a small one with only $d_0 - M$ buses. Thus we have:

$$\begin{cases} T_U = U_1^{p'} + \sum_{j=2}^{n+2} U_j^p; \\ N_P = d_0 - M; \\ T_P = U^{p,d_0-M}, \end{cases} \tag{D.1}$$

   where $U_1^{p'}$ denotes the portion of the first convoy's service time that is contained in the extended red period; U_j^p $(j = 2, 3, ..., n+2)$ the time for serving the j-th (full-size) convoy; and U^{p,d_0-M} the time for serving the small convoy of $d_0 - M$ buses.

2. If $M = d_0$, we have:

$$\begin{cases} T_U = U_1^{p'} + \sum_{j=2}^{n+2} U_j^p; \\ N_P = 0; \\ T_P = 0. \end{cases} \tag{D.2}$$

3. If $d_0 < M \leq c$, only n full-size convoys can be served following the first one, and the $(n+2)$-th convoy would be a small one with $c + d_0 - M$ buses. Thus,

$$\begin{cases} T_U = U_1^{p'} + \sum_{j=2}^{n+1} U_j^p; \\ N_P = c + d_0 - M; \\ T_P = U^{p,c+d_0-M}. \end{cases} \tag{D.3}$$

The $E[T_U^{'}]$ and $Var(T_U^{'})$ can be derived given the distribution of M, which depends upon c and the bus dwell time distribution. Unfortunately, the distribution of M is very difficult to derive analytically, even for special (e.g. gamma) distributions of bus dwell times. Hence we again seek an approximation to solve this issue.

We find by extensive numerical experiments for bus stops with $c \leq 6$ that, if the start of the extended red period is treated as a random incidence in the first convoy's service time (similar to the assumption made in Appendix B for single-berth stops), and if the bus dwell times follow a gamma distribution with $C_S \in [0.1, 1]$, then $M \geq c - 1 \geq d_0$ for 85.8% of the time. This is also intuitive: while some buses of the convoy may have completed their services earlier, they may not be able to

depart the stop as long as there is one bus still dwelling at a downstream berth. We henceforth ignore the above case 1 and consider cases 2 and 3 only. Cases 2 and 3 can be further combined into one case described by the following equation:

$$T_U^{'} \approx U_1^{p'} + \sum_{j=2}^{n+1} U_j^p + \frac{c + d_0 - M}{c} U^{p,c+d_0-M}. \tag{D.4}$$

We further use the following approximations:

$$\begin{cases} \mu_{T_U^{'}} \equiv E[T_U^{'}] \approx E[U_1^{p'}] + nE[U^p] + E[\frac{c + d_0 - M}{c} U^{p,c+d_0-M}] \\ \qquad\qquad \approx E[U_1^{p'}] + nE[U^p] + \frac{c + d_0 - E[M]}{c} E[U^{p,c+d_0-E[M]}]; \\ \sigma^2_{T_U^{'}} \equiv Var(T_U^{'}) \approx Var(U_1^{p'}) + nVar(U^p) + Var(\frac{c + d_0 - M}{c} U^{p,c+d_0-M}) \\ \qquad\qquad \approx Var(U_1^{p'}) + nVar(U^p) + \left(\frac{c + d_0 - E[M]}{c}\right)^2 Var(U^{p,c+d_0-E[M]}). \end{cases} \tag{D.5}$$

The mean and variance of $U_1^{p'}$ are obtained by the following approximations in which the start of the extended red period is treated as a random incidence:

$$\begin{cases} E[U_1^{p'}] \approx \dfrac{E^2[U^p] + Var(U^p)}{2E[U^p]}; \\ Var(U_1^{p'}) \approx \dfrac{5E[U^p] + 3\tau_m}{12E^2[U^p](E[U^p] - c\tau_m)} Var^2(U^p) + \dfrac{Var(U^p)}{2} + \dfrac{E^2[U^p]}{12}. \end{cases} \tag{D.6}$$

Section D.1 presents the derivation of (D.6).

We also have $E[U^{p,c+d_0-E[M]}] \approx h(c + d_0 - E[M], C_S)$ and $Var(U^{p,c+d_0-E[M]}) \approx q(c + d_0 - E[M], C_S)$; see equations (2.8). Finally, the value of $E[M]$ is again approximated by a fitted least-square model as follows (with RMSE = 0.061 and $R^2 = 0.9974$):

$$E[M] \approx 0.9617c - 0.1899 \cdot c \cdot C_S. \tag{D.7}$$

Plugging (2.8), (D.6) and (D.7) into (D.5) and simplifying, we have (2.11).

D.1 Derivation of (D.6)

We again use the random incidence assumption adopted in Appendix B. In addition, we approximate $S^p \equiv \max\{S_1, S_2, ..., S_c\}$ as a gamma-distributed random variable with the same mean $E[S^p]$ and variance $Var(S^p)$. Using the moment gener-

ating function of gamma distribution, we find that $E[S^{p2}] = E^2[S^p] + Var(S^p)$ and $E[S^{p3}] = E^3[S^p] + 3E[S^p]Var(S^p) + \frac{2Var^2(S^p)}{E[S^p]}$. The renewal interval that contains the random incidence, W, has the following PDF:

$$f_W(t) = \frac{t f_{U^p}(t)}{E[U^p]} = \frac{t f_{S^p}(t - c\tau_m)}{E[S^p] + c\tau_m}, c\tau_m \leq t \leq \infty. \tag{D.8}$$

Conditioning on W, $U_1^{p'}$ is uniformly distributed in $[0, W]$. So,

$$\begin{aligned} E[U_1^{p'}] &= E\left[\frac{1}{2}W\right] = \frac{1}{2(E[S^p] + c\tau_m)} \int_0^\infty (u + c\tau_m)^2 \cdot f_{S^p}(u)du \\ &= \frac{(E[S^p] + c\tau_m)^2 + Var(S^p)}{2(E[S^p] + c\tau_m)} = \frac{E[U^p]}{2} + \frac{Var(U^p)}{2E[U^p]}. \end{aligned} \tag{D.9}$$

$$\begin{aligned} Var(U_1^{p'}) &= E\left[\frac{1}{3}W^2\right] - (E[U_1^{p'}])^2 \\ &= \frac{1}{3(E[S^p] + c\tau_m)} \int_0^\infty (u + c\tau_m)^3 \cdot f_S(u)du - (E[U_1^{p'}])^2 \\ &= \frac{E[S^{p3}] + 3c\tau_m E[S^{p2}] + 3(c\tau_m)^2 E[S^p] + (c\tau_m)^3)}{3(E[S^p] + c\tau_m)} - (E[U_1^{p'}])^2 \\ &= \frac{5E[U^p] + 3c\tau_m}{12E^2[U^p](E[U^p] - c\tau_m)} Var^2(U^p) + \frac{Var(U^p)}{2} + \frac{E^2[U^p]}{12}. \end{aligned} \tag{D.10}$$

E Simulation algorithms in Chapter 2

The following notation is used in this simulation:

B_i — The number of berth in which the i-th bus dwells, counting from the downstream-most berth, which is numbered berth 1;

F_i — The number of buffer space at which the i-th bus waits, counting from the downstream-most buffer space, which is numbered buffer 1; $F_i = 0$ means that the bus is not in any buffer; $F_i > d$ means that the bus is blocked immediately after service;

LQ_i — Time when the i-th bus leaves the upstream queue;

ES_i — Time when the i-th bus finishes service;

WB_i — The i-th bus's waiting time in the berth after service;

LB_i — The i-th bus's departure time from the berth;

WF_i — The i-th bus's waiting time in the buffer due to the red signal (for near-side stops only);

FT_i — The number of moves that the i-th bus makes in the buffer area before

entering a berth (for far-side stops only);

LFN_i — The time when the i-th bus leaves the buffer and discharges into the intersection (for near-side stops only).

$LFF_{i,j}$ — The time when the i-th bus makes the j-th move in the buffer area (for far-side stops only; $j \in [1, 2, ..., FT_i]$).

Algorithm 1: Simulation of bus operations at a near-side bus stop.

Generate the service times according to a given distribution with μ_S and C_S;
Set states of the first bus: $LQ_1 \leftarrow 0$, $B_1 \leftarrow 1$, $ES_1 \leftarrow LQ_1 + ct_m + S_1$, $LB_1 \leftarrow ES_1$;
if $mod(LB_1 + dt_m, C) \leq G$ **then**
    $F_1 \leftarrow 0$, $WF_1 \leftarrow 0$;
else
    $F_1 \leftarrow 1$, $WF_1 \leftarrow C - mod(LB_1 + dt_m, C) + \tau$, $LFN_1 \leftarrow WF_1 + LB_1 + dt_m$;
foreach *simulated bus* $i \geq 2$ **do**
    if $B_{i-1} < c$ **then**
        $LQ_i \leftarrow LQ_{i-1} + \tau_m$, $B_i \leftarrow B_{i-1} + 1$;
    else
        if $F_{i-1} < d + c$ **then**
            if $F_{i-1} < d$ **then**
                $B_i \leftarrow 1$;
            else
                $B_i \leftarrow F_{i-1} - d + 1$;
            $LQ_i = LQ_{i-1} + (c - B_{i-1} + 1)t_m + S_{i-1} + WB_{i-1} + \tau$;
        else
            $B_i \leftarrow 1$, $LQ_i = LFN_{i-1} + \tau$;
    $ES_i \leftarrow LQ_i + (c - B_i + 1)t_m + S_i$;
    $WB_i \leftarrow max(0, LB_{i-1} + \tau - ES_i)$, $LB_i \leftarrow ES_i + WB_i$;
    if $F_{i-1} = 0$ **or** $F_{i-1} = d + c$ **then**
        if $RM_i \leftarrow mod(LB_i + (B_i + d - 1)t_m, C) \leq G$ **then**
            $F_i \leftarrow 0$, $WF_i \leftarrow 0$, $LFN_i \leftarrow LB_i$;
        else
            $F_i \leftarrow 1$, $WF_i \leftarrow C - RM_i + \tau$, $LFN_i \leftarrow LB_i + (B_i + d - 1)t_m + WF_i$;
    else
        if $LFN_{i-1} + \tau \leq LB_i + (B_i + d - F_{i-1} - 1)t_m$ **then**
            if $RM_i \leftarrow mod(LB_i + (B_i + d - 1)t_m, C) \leq G$ **then**
                $F_i \leftarrow 0$, $WF_i \leftarrow 0$, $LFN_i \leftarrow LB_i$;
            else
                $F_i \leftarrow 1$, $WF_i \leftarrow C - RM_i + \tau$, $LFN_i \leftarrow LB_i + (B_i + d - 1)t_m + WF_i$;
        else
            $F_i \leftarrow F_{i-1} + 1$, $WF_i \leftarrow LFN_{i-1} + \tau - LB_i - (B_i + d - F_i)t_m$,
            $LFN_i = LFN_{i-1} + \tau$;

Algorithm 2: Simulation of bus operations at a far-side bus stop.

Generate the service times according to a given distribution with μ_S and C_S;
Set states of the first bus: $LQ_1 \leftarrow 0$, $F_1 \leftarrow 0$, $FT_1 \leftarrow 0$, $B_1 \leftarrow 1$, $ES_1 \leftarrow LQ_1 + (c+d+D)t_m + S_1$, $WB_1 \leftarrow 0$, $LB_1 \leftarrow ES_1$;
foreach *simulated bus* $i \geq 2$ **do**
    if $F_{i-1} = 0$ **then**
        if $B_{i-1} = c$ **then**
            if $d = 0$ **then**
                $B_i \leftarrow 1$, $F_i \leftarrow 0$; **if** $temp \leftarrow mod(LB_{i-1} + \tau, C) \leq G$, **then** $LQ_i \leftarrow LB_{i-1} + \tau$, **else**, $LQ_i \leftarrow C - temp + LB_i + \tau$; **endif**
                $LB_i = ES_i \leftarrow LQ_i + (c+d+D)t_m + S_i$;
            else
                if $mod(LQ_{i-1} + \tau_m, C) \leq G$ **then**
                    $LQ_i \leftarrow LQ_{i-1} + \tau_m$, $F_i = B_i = FT_i \leftarrow 1$, $LFF_{i,1} \leftarrow LB_{i-1} + \tau$, $LB_i = ES_i \leftarrow LFF_{i,1} + ct_m + S_i$;
                else if $temp \leftarrow C - mod(LQ_{i-1}, C) + LQ_{i-1} + \tau < LB_{i-1} + \tau$ **then**
                    $F_i = B_i = FT_i \leftarrow 1$, $LFF_{i,1} \leftarrow LB_{i-1} + \tau$, $LB_i = ES_i \leftarrow LFF_{i,1} + ct_m + S_i$;
                else
                    $LQ_i = temp$, $FT_i = F_i \leftarrow 0$, $B_i \leftarrow 1$, $LB_i = ES_i \leftarrow LQ_i + (c+d+D)t_m + S_i$;
        else
            $F_i \leftarrow 0$; **if** $mod(LQ_{i-1} + \tau_m, C) \leq G$ **then**
                $LQ_i \leftarrow LQ_{i-1} + \tau_m$, $B_i \leftarrow B_{i-1} + 1$, $ES_i \leftarrow LQ_i + (c+d-B_i+1+D)t_m + S_i$, $LB_i \leftarrow ES_i + max(0, LB_{i-1} + \tau - ES_i)$;
            else if $temp \leftarrow C - mod(LQ_{i-1} + \tau_m, C) + LQ_{i-1} + \tau_m + \tau < LB_{i-1} + \tau$ **then**
                $LQ_i \leftarrow LB_{i-1} + \tau$, $B_i \leftarrow B_{i-1} + 1$, $LB_i = ES_i \leftarrow LQ_i + (d+c-B_i+1+D)t_m + S_i$;
            else
                $LQ_i \leftarrow temp$, $B_i \leftarrow 1$, $LB_i = ES_i \leftarrow LQ_i + (c+d+D)t_m + S_i$;
    else if $F_{i-1} < d$ **then**
        if $mod(LQ_{i-1} + \tau_m, C) \leq G$ **then**
            $LQ_i \leftarrow LQ_{i-1} + \tau_m$, $F_i \leftarrow F_{i-1} + 1$, $B_i \leftarrow \text{Berth}(F_i)$;
        else
            $LQ_i \leftarrow LQ_{i-1} + C - mod(LQ_{i-1}, C) + \tau$, Which-buffer-berth();
        When-leave-buffer-berth();
    else
        if $mod(LFF_{i-1,1} + \tau, C) \leq G$ **then**
            $LQ_i \leftarrow LFF_{i-1,1} + \tau$, Which-buffer-berth();
        else
            $LQ_i \leftarrow LFF_{i-1,1} + \tau + C - mod(LFF_{i-1,1} + \tau, C) + \tau$, Which-buffer-berth();
        When-leave-buffer-berth();

```
Function Berth(x):
    if mod(x, c) = 0 then
        return c;
    else
        return mod(x, c);
Function Which-buffer-berth():
    flag ← 0;
    for k = 1 : 1 : FT_{i-1} do
        if LQ_i + (d − F_{i-1} + (k − 1)c + 1 + D)t_m < LFF_{i-1,k} + τ then
            if F_{i-1} < d then
                F_i = F_{i-1} − (k − 1)c + 1;
            else
                if k = 1, then, F_i ← d − c + 1, else, F_i ← F_{i-1} − (k − 1)c + 1, endif;
            B_i ← Berth(F_i), flag ← 1, break;
    if flag = 0 then
        if LQ_i + (d + c − B_{i-1} + D)t_m < LB_{i-1} + τ then
            if B_{i-1} = c, then, B_i = F_i ← 1, else, F_i ← 0, B_i ← B_{i-1} + 1, endif;
        else
            F_i ← 0, B_i ← 1;
Function When-leave-buffer-berth():
    FT_i ← ceil(F_i/c);
    if FT_i = 0 then
        ES_i ← LQ_i + (c + d − B_i + 1 + D)t_m + S_i,
        LB_i ← max(0, LB_{i-1} + τ − ES_i) + ES_i;
    else if FT_i = FT_{i-1} then
        if (mod(F_i, c) = 1 and c ≠ 1) or c = 1 then
            For k = 1 : 1 : FT_i − 1, do LFF_{i,k} ← LFF_{i-1,k+1} + τ, endfor;
            LFF_{i,FT_i} ← LB_{i-1} + τ;
        else
            For k = 1 : 1 : FT_i, do LFF_{i,k} ← LFF_{i-1,k} + τ, endfor;
    else if FT_i > FT_{i-1} then
        For k = 1 : 1 : FT_{i-1}, do LFF_{i,k} ← LFF_{i-1,k} + τ,endfor;
        LFF_{i,FT_i} ← LB_{i-1} + τ;
    else
        if (mod(F_i, c) = 1 and c ≠ 1) or c = 1 then
            LFF_{i,FT_i} ← LB_{i-1} + τ;
            For k = FT_{i-1} : −1 : 1, do LFF_{i,k} ← LFF_{i-1,FT_{i-1}−FT_{i+k}} + τ, endfor;
            LFF_{i,FT_i} ← LB_{i-1} + τ;
        else
            For k = FT_i : −1 : 1, do LFF_{i,k} ← LFF_{i-1,FT_{i-1}−FT_{i+k}} + τ, endfor;
    ES_i ← LFF_{i,FT_i} + ct_m + S_i, LB_i ← max(0, LB_{i-1} + τ − ES_i) + ES_i;
```

F Tables of critical d to eliminate the negative effect of the signal on a near-side stop's capacity

Tables F.1a-d furnish the values of the critical d for various c, G/C, C_S and C and $\theta = 95\%$. Note that the values of C are normalized as multiples of μ_S. The practitioners can use interpolation between neighboring tabulated values to calculate the critical d if the relevant parameter values cannot be directly found in the tables.

Table F.1: Critical d to ensure a near-side stop's capacity is no less than 95% of the capacity of a corresponding isolated stop.

(a) $c = 1$

		C				
G/C	C_S	3	4	5	6	7
0.35	0.4	2	3	3	4	5
	0.6	2	3	4	4	5
	0.8	3	4	4	5	5
0.5	0.4	2	2	3	3	3
	0.6	2	2	3	3	4
	0.8	2	3	3	4	4
0.65	0.4	1	1	2	2	2
	0.6	1	2	2	2	2
	0.8	2	2	2	2	3

(b) $c = 2$

		C				
G/C	C_S	3	4	5	6	7
0.35	0.4	3	4	5	6	7
	0.6	3	4	5	6	7
	0.8	3	4	5	6	7
0.5	0.4	2	3	4	4	5
	0.6	2	3	3	4	5
	0.8	3	3	4	4	5
0.65	0.4	1	2	2	3	3
	0.6	1	2	2	3	3
	0.8	1	2	2	3	3

(c) $c = 3$

		C				
G/C	C_S	3	4	5	6	7
0.35	0.4	4	5	7	8	9
	0.6	4	5	6	7	8
	0.8	4	5	6	7	8
0.5	0.4	3	4	5	6	7
	0.6	3	4	4	5	6
	0.8	3	4	4	5	6
0.65	0.4	2	2	3	4	4
	0.6	2	2	3	3	4
	0.8	2	2	2	3	4

(d) $c = 4$

		C				
G/C	C_S	3	4	5	6	7
0.35	0.4	5	7	8	10	11
	0.6	5	6	7	9	10
	0.8	5	6	7	8	9
0.5	0.4	4	5	6	7	8
	0.6	3	4	5	6	7
	0.8	3	4	5	6	7
0.65	0.4	2	3	4	4	5
	0.6	2	3	3	4	5
	0.8	2	2	3	3	4

G Evidence and discussions of Observations 1 and 2

To see why Observation 1 is true, define C_A^s and C_D^s as the coefficients of variation in bus arrival and departure headways at stop $s \in \{1, 2, \ldots, N\}$, respectively. The C_A^s and C_D^s are formulated as:

$$C_A^s = E_{l\in\{1,2,\ldots,L\}}\left[\frac{\sqrt{V_{j\in\{1,2,\ldots\}}[a_{l,j+1}^s - a_{l,j}^s]}}{E_{j\in\{1,2,\ldots\}}[a_{l,j+1}^s - a_{l,j}^s]}\right], \tag{G.1}$$

$$C_D^s = E_{l\in\{1,2,\ldots,L\}}\left[\frac{\sqrt{V_{j\in\{1,2,\ldots\}}[d_{l,j+1}^s - d_{l,j}^s]}}{E_{j\in\{1,2,\ldots\}}[d_{l,j+1}^s - d_{l,j}^s]}\right]. \tag{G.2}$$

Note first that the headway regularization reduces C_A^1 to nearly 0. This renders a lower C_E^1 as compared to the do-nothing alternative, because C_E^s is positively correlated with C_A^s for any s. Thanks to the smaller C_E^1, the numbers of boarding patrons and the bus dwell times (which are dictated by the boarding numbers) at stop 1 are less varied too. This further engenders a smaller C_D^1 under headway regularization. Finally, C_A^2 also becomes smaller due to its positive correlation with C_D^1. The above reasoning will also show that C_A^s, C_E^s and C_D^s diminish for all stops in the corridor as a result of headway regularization.

The above is illustrated for the case of $\lambda = 600$ patrons/h/stop in Figure G.1. All other parameters take the values in Section 3.2.1. The dark curves display C_A^s, C_E^s, and C_D^s under headway regularization for $s \in \{1, 2, \ldots, 12\}$. The same metrics under the do-nothing alternative are shown via the grey curves. Note how the dark curves are significantly and consistently lower than the grey ones.

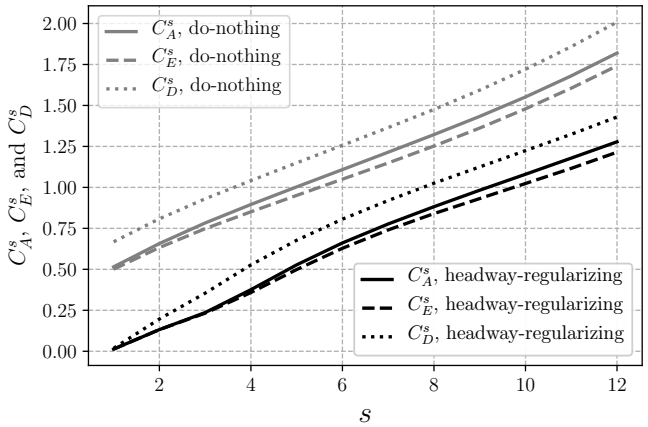

Figure G.1: Effects of headway regularization on C_A^s, C_E^s, and C_D^s.

Observation 2 is true since the average bus delay due to queueing at any stop s diminishes when the variation in bus headway, C_A^s, decreases (Gu et al., 2011). Moreover, a smaller C_E^s produces bus dwell times that are less varied, which further reduces the average bus delay (Gu et al., 2011, 2015).

References

Adamski, A., Turnau, A., 1998. Simulation support tool for real-time dispatching control in public transport. Transportation Research Part A: Policy and Practice 32 (2), 73–87.

Alonso, B., Moura, J. L., Ibeas, A., dell'Olio, L., 2013. Analytical model for calibrating delay at congested bus stops. Transportation Planning and Technology 36 (6), 520–528.

Anderson, P., Daganzo, C. F., 2020. Effect of transit signal priority on bus service reliability. Transportation Research Part B: Methodological 132, 2–14.

Andres, M., Nair, R., 2017. A predictive-control framework to address bus bunching. Transportation Research Part B: Methodological 104, 123–148.

Argote-Cabanero, J., Daganzo, C. F., Lynn, J. W., 2015. Dynamic control of complex transit systems. Transportation Research Part B: Methodological 81, 146–160.

Baker, R. J., Collura, J., Dale, J. J., Head, L., Hemily, B., Ivanovic, M., Jarzab, J., McCormick, D., Obenberger, J., Smith, L., et al., 2002. An overview of transit signal priority. Tech. rep., ITS America, Washington, DC.

Bartholdi III, J. J., Eisenstein, D. D., 2012. A self-coördinating bus route to resist bus bunching. Transportation Research Part B: Methodological 46 (4), 481–491.

Bian, B., Pinedo, M., Zhu, N., Ma, S., 2019. Performance analysis of overtaking maneuvers at bus stops with tandem berths. Transportation Science 53 (2), 597–618.

Bian, B., Zhu, N., Ling, S., Ma, S., 2015. Bus service time estimation model for a curbside bus stop. Transportation Research Part C: Emerging Technologies 57, 103–121.

Burinskiene, M., Gusaroviene, M., Gabruleviciute-Skebiene, K., 2014. The impact of public transport lanes on the operating speed of buses. In: Proceedings of 9th International Conference on Environmental Engineering, Vilnius, Lithuania.

Chandrasekar, P., Long Cheu, R., Chin, H. C., 2002. Simulation evaluation of route-based control of bus operations. Journal of transportation engineering 128 (6), 519–527.

Cominetti, R., Correa, J., 2001. Common-lines and passenger assignment in congested transit networks. Transportation science 35 (3), 250–267.

Cortés, C., Fernández, R., Burgos, V., 2007. Modeling passengers, buses and stops in traffic microsimulators. the mistransit approach on the paramics platform. In: 86th TRB Annual Meeting, Transportation Research Board.

Cortés, C. E., Burgos, V., Fernández, R., 2010a. Modelling passengers, buses and stops in traffic microsimulation: review and extensions. Journal of Advanced Transportation 44 (2), 72–88.

Cortés, C. E., Pagès, L., Jayakrishnan, R., 2005. Microsimulation of flexible transit system designs in realistic urban networks. Transportation Research Record 1923 (1), 153–163.

Cortés, C. E., Sáez, D., Milla, F., Núñez, A., Riquelme, M., 2010b. Hybrid predictive control for real-time optimization of public transport systems' operations based on evolutionary multi-objective optimization. Transportation Research Part C: Emerging Technologies 18 (5), 757–769.

Cvitanić, D., 2017. Joint impact of bus stop location and configuration on intersection performance. Promet-Traffic and Transportation 29 (4), 443–454.

Daganzo, C. F., 1994. The cell transmission model: A dynamic representation of highway traffic consistent with the hydrodynamic theory. Transportation Research Part B: Methodological 28 (4), 269–287.

Daganzo, C. F., 2009. A headway-based approach to eliminate bus bunching: Systematic analysis and comparisons. Transportation Research Part B: Methodological 43 (10), 913–921.

Daganzo, C. F., Pilachowski, J., 2011. Reducing bunching with bus-to-bus cooperation. Transportation Research Part B: Methodological 45 (1), 267–277.

Dai, Z., Liu, X. C., Chen, X., Ma, X., 2020. Joint optimization of scheduling and capacity for mixed traffic with autonomous and human-driven buses: A dynamic programming approach. Transportation Research Part C: Emerging Technologies 114, 598–619.

David, H., Nagaraja, H., 2004. Order Statistics. John Wiley & Sons, Inc., New Jersey, USA.

Delgado, F., Munoz, J. C., Giesen, R., 2012. How much can holding and/or limiting boarding improve transit performance? Transportation Research Part B: Methodological 46 (9), 1202–1217.

Delgado, F., Munoz, J. C., Giesen, R., Cipriano, A., 2009. Real-time control of buses in a transit corridor based on vehicle holding and boarding limits. Transportation Research Record 2090 (1), 59–67.

Diab, E. I., El-Geneidy, A. M., 2015. The farside story: Measuring the benefits of bus stop location on transit performance. Transportation Research Record: Journal of the Transportation Research Board (2538), 1–10.

Eberlein, X. J., Wilson, N. H., Bernstein, D., 2001. The holding problem with real–time information available. Transportation science 35 (1), 1–18.

El-Geneidy, A. M., Surprenant-Legault, J., 2010. Limited-stop bus service: an evaluation of an implementation strategy. Public Transport 2 (4), 291–306.

Estrada, M., Mensión, J., Aymamí, J. M., Torres, L., 2016. Bus control strategies in corridors with signalized intersections. Transportation Research Part C: Emerging Technologies 71, 500–520.

Fang, K., Samuel, Z., Wang, W., Said, D., Gladys, F., 2012. Integrated corridor management for urban transport: Concept and practices. Urban Transport of China 10 (3), 8–22.

Fernández, R., 2010. Modelling public transport stops by microscopic simulation. Transportation Research Part C: Emerging Technologies 18 (6), 856–868.

Fernández, R., Burgos, V., Cortés, C. E., 2007. Results of the microscopic modelling of traffic interactions at stops, junctions and roads for the design of bus rapid transit facilities. In: European Transport Conference 2007, The Netherlands, October 2007.

Fernández, R., Del Campo, M., Swett, C., 2008. Data collection and calibration of passenger service time models for the transantiago system. In: European Transport Conference 2008, The Netherlands, October 2008.

Fernández, R., Planzer, R., 2002. On the capacity of bus transit systems. Transport Reviews 22 (3), 267–293.

Fitzpatrick, K., Hall, K., Perdinson, D., Nowlin, L., 1996. Guidelines for the Location and Design of Bus Stops, Transit Cooperative Research Program Report 19. Transportation Research Board, Washington, D.C., USA.

Furth, P., SanClemente, J., 2006. Near side, far side, uphill, downhill: impact of bus stop location on bus delay. Transportation Research Record: Journal of the Transportation Research Board (1971), 66–73.

Ge, H., 2006. Traffic impacts of bus stops in urban area and related optimization techniques (in Chinese). Ph.D. thesis, Southeast University, China.

Germani, E., Szász, P. A., 1980. Comonor-a bus convoy system. In: 30th IEEE Vehicular Technology Conference. Vol. 30. IEEE, pp. 413–417.

Gibson, J., 1996. Effects of a downstream signalised junction on the capacity of a multiple berth bus-stop. In: Proceedings of the 24th PTRC European Transport Forum, London.

Gibson, J., Baeza, I., Willumsen, L., 1989. Bus-stops, congestion and congested bus-stops. Traffic engineering and control 30 (6), 291–302.

Global BRT Data, 2019.
URL `https://www.brtdata.org`

Greene, W. H., 2003. Econometric Analysis. Pearson Education, New Jersey, USA.

Gu, W., 2012. Models of bus queueing at isolated bus stops. Ph.D. thesis, University of California, Berkeley, USA.

Gu, W., Cassidy, M. J., 2013. Maximizing bus discharge flows from multi-berth stops by regulating exit maneuvers. Transportation Research Part B: Methodological 56, 254–264.

Gu, W., Cassidy, M. J., Gayah, V. V., Ouyang, Y., 2013. Mitigating negative impacts of near-side bus stops on cars. Transportation Research Part B: Methodological 47, 42–56.

Gu, W., Cassidy, M. J., Li, Y., 2012. On the capacity of highway checkpoints: Models for unconventional configurations. Transportation Research Part B: Methodological 46 (10), 1308–1321.

Gu, W., Cassidy, M. J., Li, Y., 2015. Models of bus queueing at curbside stops. Transportation Science 49 (2), 204–212.

Gu, W., Gayah, V. V., Cassidy, M. J., Saade, N., 2014. On the impacts of bus stops near signalized intersections: Models of car and bus delays. Transportation Research Part B: Methodological 68, 123–140.

Gu, W., Li, Y., Cassidy, M. J., Griswold, J. B., 2011. On the capacity of isolated, curbside bus stops. Transportation Research Part B: Methodological 45 (4), 714–723.

Gupta, S. S., 1960. Order statistics from the gamma distribution. Technometrics 2 (2), 243–262.

He, S., Dong, J., Liang, S., Yuan, P., 2019. An approach to improve the operational stability of a bus line by adjusting bus speeds on the dedicated bus lanes. Transportation Research Part C: Emerging Technologies 107, 54–69.

Hernández, D., Muñoz, J. C., Giesen, R., Delgado, F., 2015. Analysis of real-time control strategies in a corridor with multiple bus services. Transportation Research Part B: Methodological 78, 83–105.

Hickman, M. D., 2001. An analytic stochastic model for the transit vehicle holding problem. Transportation Science 35 (3), 215–237.

Hidalgo, D., Lleras, G., Hernández, E., 2013. Methodology for calculating passenger capacity in bus rapid transit systems: Application to the transmilenio system in bogotá, colombia. Research in Transportation Economics 39 (1), 139–142.

Hisham, F., Bunker, J. M., Bhaskar, A., 2018. Development of a modified bus stop capacity model. In: Transportation Research Board Annual Meeting, 97th, Washington, D.C., USA.

Jaiswal, S., Bunker, J. M., Ferreira, L., 2010. The influence of platform walking on BRT station bus dwell time estimation. Journal of Transportation Engineering 136 (12), 1173–1179.

Kittelson & Associates, Inc., 2013. Transit Capacity and Quality of Service Manual, 3rd Edition. Transit Cooperative Research Program Report 165, Transportation Research Board, Washington, D.C., USA.

Larson, R. C., Odoni, A. R., 1981. Urban Operations Research. Prentice-Hall, New Jersey, USA.

Laskaris, G., Cats, O., Jenelius, E., Rinaldi, M., Viti, F., 2018. Multiline holding based control for lines merging to a shared transit corridor. Transportmetrica B: Transport Dynamics, 1–34.

Levinson, H., St. Jacques, K., 1998. Bus lane capacity revisited. Transportation Research Record: Journal of the Transportation Research Board (1618), 189–199.

Li, J., Gupta, S. D., Zhang, L., Zhou, K., Zhang, W., 2012. Evaluate bus emissions generated near far-side and near-side stops and potential reductions by ITS: An empirical study. Transportation Research Part D: Transport and Environment 17 (1), 73–77.

Liu, H., Lu, X., Shladover, S. E., 2019. Traffic signal control by leveraging cooperative adaptive cruise control (CACC) vehicle platooning capabilities. Transportation Research Part C: Emerging Technologies 104, 390–407.

Lu, L., Su, Y., Yao, D., Li, L., Li, Z., 2010. Optimal design of bus stops that are shared by multiple lines of buses. In: Intelligent Transportation Systems (ITSC), 2010 13th International IEEE Conference on. IEEE, pp. 125–130.

Meirelles, A., 2000. A review of bus priority systems in brazil: from bus lanes to busway transit. In: Smart Urban Transport Conference, 2000, Brisbane, Queensland, Austrilia.

Menendez, M., 2006. An analysis of HOV lanes: Their impact on traffic. Ph.D. thesis, University of California, Berkeley, USA.

Mersky, A. C., Samaras, C., 2016. Fuel economy testing of autonomous vehicles. Transportation Research Part C: Emerging Technologies 65, 31–48.

Muñoz, J. C., Cortés, C. E., Giesen, R., Sáez, D., Delgado, F., Valencia, F., Cipriano, A., 2013. Comparison of dynamic control strategies for transit operations. Transportation Research Part C: Emerging Technologies 28, 101–113.

Navarro, M., Riquelme, I., Muñoz, J. C., Moya, J., 2017. Capacity of curbside bus stops located on bus corridors, considering level of service, overtaking lanes and a downstream traffic signal. In: Transportation Research Board Annual Meeting, 96th, Washington, D.C., USA.

Newell, G. F., 1965. Approximation methods for queues with application to the fixed-cycle traffic light. SIAM Review 7 (2), 223–240.

Newell, G. F., 1974. Control of pairing of vehicles on a public transportation route, two vehicles, one control point. Transportation Science 8 (3), 248–264.

Newell, G. F., 1993. A simplified theory of kinematic waves in highway traffic, part II: Queueing at freeway bottlenecks. Transportation Research Part B: Methodological 27 (4), 289–303.

Newell, G. F., Potts, R. B., 1964. Maintaining a bus schedule. In: Australian Road Research Board (ARRB) Conference, 2nd, 1964, Melbourne.

Nguyen, V. N., 2013. Bus prioritisation in motorcycle dependent cities. Ph.D. thesis, Darmstadt University of Technology, Germany.

Osuna, E., Newell, G., 1972. Control strategies for an idealized public transportation system. Transportation Science 6 (1), 52–72.

Papacostas, C., 1982. Capacity characteristics of downtown bus streets. Transportation Quarterly 36 (HS-033 743).

Prescott, P., 1974. Variances and covariances of order statistics from the gamma distribution. Biometrika 61 (3), 607–613.

Reilly, J., Aros-Vera, F., 2013. Estimating capacity of high volume bus rapid transit stations. In: 92nd Annual Meeting of Transportation Research Board, National Academics, Washington, DC.

Ross, S. M., 2014. Introduction to probability models, eleventh Edition. Academic Press, Cambridge, Massachusetts, USA.

Schmöcker, J.-D., Sun, W., Fonzone, A., Liu, R., 2016. Bus bunching along a corridor served by two lines. Transportation Research Part B: Methodological 93, 300–317.

Shen, M., Gu, W., Hu, S., Cheng, H., 2019. Capacity approximations for near-and far-side bus stops in dedicated bus lanes. Transportation Research Part B: Methodological 125, 94–120.

Shortle, J. F., Thompson, J. M., Gross, D., Harris, C. M., 2018. Fundamentals of queueing theory. John Wiley & Sons.

St. Jacques, K., Levinson, H. S., 1997. Operational analysis of bus lanes on arterials. Transit Cooperative Research Program Report 26, Transportation Research Board, Washington, D.C., USA.

Sun, A., Hickman, M., 2005. The real–time stop–skipping problem. Journal of Intelligent Transportation Systems 9 (2), 91–109.

Szász, P. A., Montans, L. C., Ferreira, E. O., 1978. COMONOR: ordinated bus convoy. Technical Paper 9, Companhia de Engenharia de Tráfego.

Takagi, H., 1988. Queuing analysis of polling models. ACM Computing Surveys (CSUR) 20 (1), 5–28.

Tan, H., Yang, X., 2014. A new capacity computing model of bus stop at upstream signalized intersection in peak. In: the 17th International IEEE Conference on Intelligent Transportation Systems.

Tan, J., Li, Z., Li, L., Zhang, Y., Lu, L., 2014. Berth assignment planning for multi-line bus stops. Journal of advanced transportation 48 (7), 750–765.

Terry, D. S., Thomas, G. J., 1971. Farside bus stops are better. Traffic Engineering 41 (6), 21–29.

Tirachini, A., 2014. The economics and engineering of bus stops: Spacing, design and congestion. Transportation Research Part A: Policy and Practice 59, 37–57.

Tirachini, A., Hensher, D. A., 2011. Bus congestion, optimal infrastructure investment and the choice of a fare collection system in dedicated bus corridors. Transportation Research Part B: Methodological 45 (5), 828–844.

TRB, 2000. Highway Capacity Manual. Transportation Research Board, Washington, D.C., USA.

van Oort, N., Boterman, J., van Nes, R., 2012. The impact of scheduling on service reliability: trip-time determination and holding points in long-headway services. Public Transport 4 (1), 39–56.

Vandebona, U., Richardson, A. J., 1986. Effect of checkpoint control strategies in a simulated transit operation. Transportation Research Part A: General 20 (6), 429–436.

Vazquez-Leal, H., Castaneda-Sheissa, R., Filobello-Nino, U., Sarmiento-Reyes, A., Sanchez Orea, J., 2012. High accurate simple approximation of normal distribution integral. Mathematical problems in engineering 2012.

Wang, C., Ye, Z., Fricker, J. D., Zhang, Y., Ukkusuri, S. V., 2018. Bus capacity estimation using stochastic queuing models for isolated bus stops in china. Transportation Research Record 2672 (8), 108–120.

Wang, C., Ye, Z., Wang, Y., Xu, Y., Wang, W., 2016. Modeling bus dwell time and time lost serving stop in china. Journal of Public Transportation 19 (3), 55–77.

Wu, W., Liu, R., Jin, W., 2017. Modelling bus bunching and holding control with vehicle overtaking and distributed passenger boarding behaviour. Transportation Research Part B: Methodological 104, 175–197.

Wu, X., Li, Z., Li, L., Su, Y., Lu, L., Tan, J., 2011. Berth assignment planning for multi-berth bus stops. In: Intelligent Transportation Systems (ITSC), 2011 14th International IEEE Conference on. IEEE, pp. 1519–1524.

Yabe, T., Nakamura, F., 2005. Study on the relationship between capacity, cost and operation alternatives of bus rapid transit. Journal of the Eastern Asia Society for Transportation Studies 6, 408–422.

Zhao, X., Gao, Z., Jia, B., 2007. The capacity drop caused by the combined effect of the intersection and the bus stop in a CA model. Physica A: Statistical Mechanics and its Applications 385 (2), 645–658.